Land cover change analysis of Big Creek conservation area with satellite remote sensing

by

Chen Shang

A thesis
presented to the University of Waterloo
in fulfillment of the
thesis requirement for the degree of
Master of Environmental Studies
in
Geography

Waterloo, Ontario, Canada, 2013

AUTHOR'S DECLARATION

I hereby declare that I am the sole author of this thesis. This is a true copy of the thesis, including any required final revisions, as accepted by my examiners.

I understand that my thesis may be made electronically available to the public.

Abstract

Due to the relatively complex land cover configuration and a series of significant ecological implications, the issue of land cover changes in the Big Creek area are of critical value to environmental conservation groups, policy makers, and relevant stakeholders. In consultation with the Carolinian Canada Coalition (CCC), the potential of IKONOS imagery as a high spatial resolution remote sensing product is assessed for significant habitat mapping, and a change detection methodology is developed and implemented for the Big Creek area that will be of value to decision makers and policy analysts. In order to take advantage of the synergistic strengths of multiple change detection techniques, a hybrid approach is adopted in this study, aiming to detect and stratify land cover changes over the time span from 2004 to 2012. On the basis of an assessment of the capability of differentiating changed from unchanged areas, the image differencing method based on Normalized Difference Vegetation Index (NDVI) was found to be the most accurate among the three change detection techniques employed in this study. As an attempt to incorporate local spatial autocorrelation information into the change detection analysis, the Getis statistic was used as a spatial filter in conjunction with the image differencing technique, and it showed great promise for improving the change/no change maps both qualitatively and quantitatively. In particular, the extreme Getis statistic proposed in this study demonstrated strong potential for automatically determining the optimal scale for spatial smoothing, which could greatly improve the efficiency and accuracy of change detection practices.

In addition, the performance of the post-classification comparison approach was found to be highly dependent on the intrinsic characteristics of the individual classified maps, rather than simply the accuracy scores of the classifications subject to the comparison. Therefore, it is

recommended that a benchmark approach be taken to compensate for this uncertainty of the post-classification comparison method, such that the negative impact of the misclassification errors in the individual classified maps could be reduced to an acceptable level.

The findings of this research will contribute to a better understanding of the usefulness of some widely used change detection techniques in a relatively complex physical environment with abundant vegetation cover. In addition, the application of the Getis statistic as a spatial filter is proven useful for suppressing potential "salt and pepper" effects in the context of change detection analysis, especially if high spatial resolution imagery is employed. With minor modifications, the workflow proposed in this study is likely to reliably fulfill the purpose of monitoring land cover dynamics in other environments as well. However, it should be noted that clear awareness of the characteristics of the study area and needs of information is a premise to the successful application of any change detection approach in different environments.

Acknowledgements

Upon completion of this thesis, I would first like to express my gratitude to my supervisor Dr. Ellsworth LeDrew for his guidance, support, and most importantly sharing his wisdom on not only the research questions I came up with but also the personal difficulties I encountered along the way. With his help over the past few years, I have been able to improve myself in ways that I could have never imagined. My sincere thanks also goes to my committee member Dr. Gordon Nelson for introducing me to the realm of Carolinian forest as well as his invaluable suggestions and feedback in various stages of my graduate research. I would also like to thank Brian Craig and a reader of my thesis Jarmo Jalava for their support and help on my questions pertaining to the physical environment of Long Point Region. Special thanks goes to the other reader of my thesis Dr. Richard Kelly for his insightful comments throughout my study at UW and all his remote sensing courses, from which I learnt a lot.

The field work in Norfolk County has been an invaluable experience for me, and I am grateful to all the people who made it possible. To Brad, I really appreciate your live demo on how to use the ancient ASD spectrometer. To Xuefeng, thank you so much for being my driver, body guard, and field assistant. Without your help, I could not have pulled it off. I would also like to extend my gratitude to Steve Xu from the Geospatial Center at UW for helping me acquire a variety of useful spatial datasets and Andrea Hebb from NCC for providing me with the NCC maps. My thank you goes to all the staff members in the department who made my graduate experience at UW an unforgettable one, especially Mike Lackner for his help with various software packages and Ms. Susie Castela for her administrative assistance.

I would also like to thank University of Waterloo, the Department of Geography and Environmental Management, Carolinian Canada Coalition, as well as the Natural Science and Engineering Research Council of Canada for the financial support I have received.

My gratitude extends to all my friends for their company during my striving and struggling in the past few years.

Lastly and most importantly, I am deeply indebted to my family, for their unconditional love, continuous support, and encouragement since I was a child. To them I dedicate this thesis.

Table of Contents

List of Figures

List of Tables

List of Abbreviations

ANSI	Area of Natural and Scientific Interest
ASD	Analytical Spectral Devices
CASI	Compact Airborne Spectrographic Imager
CCC	Carolinian Canada Coalition
CVA	Change Vector Analysis
ELC	Ecological Land Classification
ENVI	The ENvironment for Visualising Images
FLAASH	Fast Line-of-sight Atmospheric Analysis of Spectral Hypercubes
GCPs	Ground Control Points
GLCM	Grey Level Co-occurrence Matrix
HM	Histogram Matching
IR	Image Regression
KNN	K Nearest Neighbor
LAI	Leaf Area Index
LISA	Local Indicators of Spatial Association
LUCC	Land Use and Cover Change
MCS	Marker-Controlled watershed Segmentation
MGD	Maximum Getis Distance
NC	No-Change set
NCC	Nature Conservancy of Canada
NCIs	Neighborhood Correlation Images
NDVI	Normalized Difference Vegetation Index
NDWI	Normalized Difference Water Index

OBIA	Object-based Image Analysis
OCIs	Object Correlation Images
OSA	Object-Specific Analysis
OSU	Object-Specific Up-scaling
PCA	Principal Component Analysis
PCs	Principal Components
PIF	Pseudo Invariant Feature
PSF	Point Spread Function
RBF	Radial Basis Function
RCS	Radiometric Control Set
RMS	Root Mean Square
ROI	Region of Interest
SAR	Synthetic Aperture Radar
SVM	Support Vector Machine
TC	Tasselled Cap
ToA	Top of Atmosphere

Chapter 1

Introduction

1.1 Overview

In the context of urban planning and resource management, land use and cover change (LUCC) has always been of great importance to both scientists and decision makers. No matter whether caused by human activities or natural dynamics, land cover changes can affect the patterns of climate and biogeochemistry of the earth system in a global scale (Lambin and Strahler, 1994). Among various types of global resources, forest is essential in that human beings rely on it for air and water quality, timber, as well as other recreational purposes (Grossman and Forrester, 2001). In addition, forests are also involved in global bio-geochemical cycles, erosion reduction, and it provide habitat for a number of wildlife types (Wulder et al., 2004). Moreover, the research of forest biodiversity could contribute to the understanding of ecosystems, thus facilitating ecological assessments in the long run (Karsh et al., 2007). As an attempt at monitoring the LUCC dynamics at local, regional, and global scales, change detection analysis has drawn tremendous attention from the scientific and political community, shedding light on the development of sustainable resource management strategies (Gong, Sui, Ma, & Zhou, 2008).

Owing to its vastness of coverage and relatively high data availability, remote sensing has proved to be a useful technique in detecting land cover changes. For forested environments, the use of remote sensing images is especially necessary, due to their remoteness and extent. In the context of sustainable forest management, the knowledge of changes in forest is deemed critical. As a matter of fact, different forest changes can be found at a variety of spatial scales, varying from individual tree level, stand level, watershed level, until even larger scales. There are a series

of parameters that can be used to depict forest changes, such as duration, spatial extent, rate, and magnitude, upon which different types of change do not agree (Gong and Xu, 2003).

Under circumstances when onsite inspection is not feasible, analysis based on multitemporal satellite images are suitable for detecting and identifying land cover changes, such as the case with a closed forest. Depending on the level of preprocessing, feature space based on DN values, radiance, or reflectance is commonly considered as the source where information is extracted in remote sensing images, where the dimensions of the space represent various features used to describe the object of interest, and similar objects would reside closer to each other in the feature space and vice versa. However, this approach treats the individual pixels within a remotely sensed image separately without considering their interrelationship, which can be important at times. Due to the continuous nature of ground objects, the pixels that belong to the same feature are bound to be correlated, and this characteristic of remotely sensed data can be made good use of. In addition, the overlapping point spread function (PSF) of adjacent pixels implies the numerical correlation between their DN values, no matter whether they represent the same ground feature or not (Cracknell, 1998), which could be a source of uncertainty at times.

The spatial characteristics of remote sensing images have not been fully utilized in the development of change detection techniques. In order to capture the characteristics of inter-pixel relationships, the analysis of spatial association or geostatistical analysis is always considered as the key approach (Chica-Olmo & Abarca-Hernandez, 2000). If techniques that do not take contextual information into consideration are relied on for processing of remote sensing imagery, the "salt and pepper" effect cannot be suppressed, which is a problem commonly related with pixel-based approach (Yu et al., 2006). As a matter of fact, the "salt and pepper" effect is not only intrinsic to pixel-based processing techniques developed for single date remotely sensed

data, but also change detection approaches based on multidate imagery (Desclée, Bogaert, & Defourny, 2006). Therefore, it is worthwhile examining how measures of spatial correlation can be used in conjunction with remote sensing techniques to reduce the "salt and pepper" effect present in various research contexts, especially change detection analysis.

With respect to spatial association, there are two categories of metrics: global indicators of spatial association and local indicators of spatial association (Anselin, 1995). Given that an area of interest might not have a uniform pattern or variation, especially when the area becomes large, an assumption of spatial stationarity made by the global indicators of spatial association might not hold true under all circumstances, which gives rise to local indicators of spatial association (LISA). One particular member within the class of LISA is Getis Ord's Gi statistic (Getis & Ord, 1992), which accounts for local instabilities in overall spatial association (Anselin, 1995). Operating based on a user-defined distance parameter, the Getis statistic presents local spatial patterns that can be considered as hot spots, which contributes to the delineation of spatial homogeneity. With that in mind, the incorporation of the Getis statistic into existing change detection framework could potentially contribute to more accurate mapping of land cover changes.

1.2 Research Questions and Objectives

The main goal of this study is to detect and categorize land cover changes in Big Creek area, Norfolk, Ontario from 2004 to 2012 based on selected change detection algorithms. In addition, efforts are made to examine the performance of the individual techniques as well as their synergistic effects. Some of the key research questions in this study are listed as follows:

1) What is the most effective method in detecting land cover changes in the Big Creek area among the three change detection techniques adopted in this study?

2) How does the selection of change indicator influence the results of change detection?
3) How does the discrimination between positive and negative change contribute to the separability between changed and unchanged areas?
4) Does the application of the Getis statistic have the ability of improving change detection accuracy based on high spatial resolution imagery?
5) What is the relationship between the accuracy of post-classification comparison and that of the individual classified maps?
6) What is the spatial extent and nature of the land cover changes present in the Big Creek area from 2004 to 2012?

1.3 Thesis Structure

This thesis is organized into the following sections:

1) Chapter 1 introduces the context of this study, identifies the key research objectives, followed by the structure of this thesis.
2) Chapter 2 provides a review of the current literature on digital change detection techniques for LUCC applications based on remotely sensed data, with emphasis on high spatial resolution satellite imagery.
3) Chapter 3 delineates how characteristics of the study area, the data acquisition process, and discussion with environmental conservation groups contributes to the formulation of the proposed methodology.
4) Chapter 4 delivers a detailed description of the hybrid change detection approach proposed in this study for accurate mapping of land cover change.
5) Chapter 5 presents the results of the change detection analysis and discusses the findings of this research as well as uncertainties in the workflow, followed by a critical assessment

of possibilities for future improvements.

6) Chapter 6 provides a summary for this study and brief answers to the research questions. Contribution and limitations of this study is also evaluated, followed by a synthesis of recommendations for generalization of the proposed methodology.

Chapter 2

Literature Review

2.1 Introduction

Due to the relatively high expense of onsite inspection or the infeasibility of field campaigns under certain circumstances, change detection analysis based on multi-temporal satellite images are deemed suitable for investigating environmental change of the earth's surface. In addition, the large volume of historical remote sensing imagery proves to be an invaluable asset to environmental scientists and relevant decision makers. To make full use of historical remotely sensed data in conjunction with current remote sensing retrievals and analyze potential land use and cover change (LUCC), emphasis should be placed on the spatial temporal trends, as in the case with sea ice monitoring using hypertemporal remote sensing imagery (Piwowar & LeDrew, 1995), instead of simple cartographic representation of all the data available.

Despite the availability of remotely sensed data and the emerging change detection techniques, no conclusion has been drawn yet regarding the existence of a universal solution to all change detection applications. A number of change detection algorithms have been proposed to differentiate changed from unchanged landscapes and categorize multiple types of land cover changes in different contexts of environmental studies. Due to the varying emphases of the previous studies, the various types of data utilized, and various study areas from around the world, it poses a challenging question to identify the most appropriate approach towards a particular application based on current knowledge of change detection techniques (Lu, Mausel, Brondízio, & Moran, 2004). In order to present a comprehensive review of the literature

pertaining to this thesis, this chapter is divided into three sections. The first section aims to provide a synoptic summary of the current change detection techniques and discuss some critical aspects of change detection analysis, including data collection, preprocessing, accuracy assessment, etc. The second section evaluates several change detection techniques that are closely related to the methodology adopted in this thesis.

2.2 Digital Change Detection Techniques for Land Cover Changes Using Remotely Sensed Data

In order to provide a comprehensive assessment of the current digital change detection techniques and place them in the context of LUCC studies, this section is comprised of four subsections. The first section presents a classification system that categorizes the various change detection techniques into several generic classes, thus leading to better understanding of their differences and similarities. The second section emphasizes the influence of preprocessing procedures on the performance and reliability of the change detection approaches from geometric and radiometric perspectives of remote sensing imagery. The next section introduces the individual techniques along with their strengths and weaknesses in relative to one another. The last section touches upon the accuracy assessment measures employed to evaluate the performance of change detection techniques.

2.2.1 Taxonomy

According to the amount of input required in the analysis, change detection techniques can be divided into three categories: visual analysis, semi-automated, and automated. Although change detection cannot be practiced without any visual interpretation of the remotely sensed data, it should be noticed that the "visual analysis" method mentioned above refers to the type of

analysis where visual interpretation made by image interpreters is the main approach, followed by digitization of changed areas (Lu et al., 2004). As for the difference between semi-automated and automated approaches, the former normally demands collection of training data, while the latter is mainly of unsupervised nature despite the necessity for interpretation and labeling of the results. According to the output from the existing studies, change detection methods can be roughly perceived as either qualitative or quantitative. The former category seeks to distinguish between changed and unchanged land covers, whereas the latter one further stratifies different types of changes on the basis of change/no change discrimination, thus providing direction of changes.

Furthermore, the existing change detection techniques can be divided into two groups considering the amount of remotely sensed data utilized in the analysis, namely bi-temporal and temporal trajectory approaches (Coppin, Jonckheere, Nackaerts, Muys, & Lambin, 2004). As their names suggest, the bi-temporal analysis makes use of two remote sensing images acquired at two different epochs of time over the identical geographic area, while the temporal trajectory analysis can be deemed as an extension of the bi-temporal one in the temporal space, such that profiles of the study area can be established based on multiple observations acquired at different points of time. As the profile corresponds to the temporal trend of a particular variable of interest, it is capable of characterizing the area of interest, which is the rationale for temporal trajectory analysis (Lambin & Strahler, 1994). When it comes to the taxonomy of change detection algorithms based on their intrinsic properties, it has evolved to a certain degree as new sensor systems and techniques have emerged during the past two decades (Singh, 1989, Lu et al., 2004, Gong et al., 2008). Furthermore, the level of detail regarding the individual change detection methods considered in the taxonomy has an impact on the results. For example, image

differencing, image ratioing, and change vector analysis (CVA) can all be included in the broad category of image algebra, despite the fact that they compare the multi-date remote sensing images in different ways.

2.2.2 Preprocessing

In order to ensure the validity of change detection results and maximize the performance of various change detection techniques, preprocessing procedures are performed prior to the commencement of change detection algorithms. Depending upon its purpose, preprocessing procedures can be categorized as either geometric or radiometric processing. As remarked by Toutin (2003), the requirements for geometric correction of remote sensing images have changed dramatically as more advanced sensors are put into use. In occasions where data from different sources are utilized, highly accurate geometric processing is particularly important, thus ortho-rectification of multi-source images is required with the aid of DEM.

To ensure the validity of the extracted information, radiometric image processing should be performed prior to the commencement of change detection analysis, owing to the fact that unprocessed "raw" images are exposed to a variety of errors, including internal, external, systematic, and random errors. In order to reduce or eliminate these errors, a series of radiometric processing techniques have been developed: sensor radiometric rectification, surface reflectance calculation according to atmospheric corrections, radiometric normalization for multi-temporal or multi-scene analysis, and special correction targeted at terrain related errors (Peddle et al., 2003).

Relative radiometric normalization is another crucial aspect of preprocessing, which aims to reduce the radiometric inconsistencies between multi-temporal images caused by different acquisition conditions. As concluded by Yang and Lo (2000), there are mainly five types of

relative radiometric normalization methods: pseudo-invariant features (PIF), radiometric control set (RCS), image regression (IR), no-change set (NC) determined from scattergrams, and histogram matching (HM). For all of these image normalization approaches, some mathematical function between subject and reference images needs to be established. Based on a series of comparisons, Yang and Lo (2000) found that those algorithms making use of a large sample size are able to achieve good overall accuracy, but they are likely to reduce radiometric resolution and coefficient of variation of the images. PIF and RCS are reported to be capable of preserving the amount of spectral change between multi-temporal images to a greater degree, which means they can better support the change detection analysis. Lastly, performance of relative radiometric normalization is proven to be prone to variations in the following factors: land use/cover distribution, local topography, land-water proportion, resemblance between subject and reference images, as well as sample size. According to the above factors, the most suitable relative radiometric normalization method should be chosen for each study, so as to maximize the performance of change detection algorithm to be employed subsequently (Yang and Lo, 2000).

In addition to the procedures mentioned above, it is worth noting that the selection of appropriate remotely sensed data plays an important role in ensuring the validity of those preprocessing techniques, ranging from geometric correction, image co-registration, radiometric processing, to relative normalization (Lu et al., 2004). Due to the fact that different sensor systems tend to feature different spatial, spectral, and radiometric resolutions, it is advisable to use a single data source consistently for a particular change detection study. As a matter of fact, varying orbits possessed by different platforms can influence the look angle of the remote sensing images. Therefore, extra caution should be exerted if comparisons are made between various sources of remotely sensed imagery, under circumstances where the utilization of

multiple data sources is advantageous or unavoidable. Lastly, images acquired at anniversary dates of different years are recommended for change detection analysis, in order to minimize a series of extraneous effects, including sun illumination conditions, seasonal variability, and phenological fluctuations (Lu et al., 2004).

2.2.3 Digital change detection techniques

Considering the limited space in this chapter and the nature of this thesis as a bi-temporal analysis, techniques developed for time trajectory analysis are not included in this review, thus the emphasis of this paper will be placed on bi-temporal analysis. The various techniques reported in current literature for bi-temporal analysis can be roughly divided into eight categories, including classification method, image differencing, image ratioing, transformation, change vector analysis, image regression, model method, and object-based approach. As for the algorithms considered as hybrid methods in some review articles (Coppin et al., 2004; Lu et al., 2004), they normally incorporate more than one established change detection methods, thereby combining the advantages of the individual methods. Since the hybrid methods do not refer to a specific type of algorithm of the same origin, they are deemed as derivatives or variations of the classical methods, thus excluded from the taxonomy described above.

The classification method mainly includes two streams: post-classification comparison and composite analysis. The post-classification approach entails separate classifications of remote sensing images acquired at different time points over the study area and presents the change detection results in a change matrix, which is similar to the confusion matrix used for accuracy assessment of single classification. This method is easy to carry out and less dependent on the quality of preprocessing procedures; however, the errors of the individual classifications might accumulate in the change detection results. Despite the straightforwardness of this method, post-

classification comparison method is still actively engaged in the field, and some of its recent developments involve the usage of multiple remote sensing data sources (Alphan, Doygun, & Unlukaplan, 2009; Serra, Pons, & Sauri, 2003). Composite analysis, or direct classification method, seeks to classify different types of land cover changes based on a stack of the original multispectral images, and this process is commonly referred to as multi-date clustering. It should be noted that this method necessitates researchers' familiarity with the study area; otherwise, the labeling of classes could be erroneous (Coppin et al., 2004).

As its name suggests, image differencing entails subtraction of a spectral band or a designated index of the date two image from that of the date one image, where the selection of change indicator depends on the emphasis of the individual applications. Since it relies on a single variable of interest derived from the remotely sensed data for change detection purpose, the accuracy of the results are closely related to the selection of change indicator, and it is not capable of producing quantitative change information (Lu et al., 2004). Some of the recent efforts aiming at the exploitation of image differencing method focus on the reliable and accurate thresholding of the difference image (Bruzzone, 2000).

Similar to the image differencing method, image ratioing extracts change information according to a single change indicator derived from the remote sensing imagery, and it operates on a pixel by pixel basis. According to Lu, Mausel, Brondízio, and Moran (2004), it is able to reduce the influence of topography, shadow, and illumination conditions. Despite the simplicity of its implementation, recent development or application of image ratioing algorithm has been lacking.

Although intuitive procedures such as image differencing and image ratioing have been applied in the context of change detection analysis, more complex algorithms are employed in

this field as well, such as transformation. Some of the commonly seen transformation algorithms include principle components analysis (Fung & LeDrew 1987; Gong, 1993) and Tasselled Cap (TC) transformation (Fung, 1990; Healey, Cohen, Yang, & Krankina, 2005). While principal component analysis (PCA) necessitates careful intrepretation of the relationship between the individual principle components (PCs) and possible changes of interest, the wetness, brightness, and greenness indices derived from TC transformation have direct physical meanings. In addition, PCA is highly scene dependent, and possible changes depicted in lower PCs might not be exhaustive. On the other hand, TC transformation is scene independent, due to its nature as a phyiscal based method (Coppin et al., 2004).

Change vector analysis (CVA) was firstly proposed by Malila (1980) for forest change detection as an unsupervised analytical approach that could produce both qualitative and quantitative change information. It includes two components that may contribute to change detection analysis: change magnitude and change angles, which respectively relates to intensity and direction of land cover changes. Despite some adaptation of CVA approach that operates in multi-temporal space (Lambin and Strahler, 1994), continuous development has been aimed at its application in bi-temporal change detection analysis, such as the incorporation of spherical analysis (Allen & Kupfer, 2000), the isolation of change vectors as an independent variable (Nackaerts et al., 2005), and automated procedures searching for optimum change/no change threshold based on change magnitude (Chen et al., 2003) etc. In order to fully explore the potential of CVA, more attention needs to be paid to its implementation issues and applications.

Compared with the methods introduced above, image regression is a less popular technique in the context of change detection analysis. First is the regression of date one image against the other image. Afterwards, the synthetic image derived from the regression is subtracted from the

date one image. The bias obtained after the subtraction can be considered as the deviation between the two images, taking the differences of the mean and the variance between the two original images into consideration. After applying a thresholding method towards the residuals, the real changes can be picked out. The advantage of the image regression method lies in its capability of reducing the impact of varying sun angles and atmospheric disparity in the change detection analysis, and it is considered marginally more accurate than image differencing approach in certain applications (Singh, 1989).

The model method is actually an abstract category of change detection algorithms, instead of a specific concept. According to Lu et al. (2004), some of the well-developed models suitable for change detection analysis include the Li-Strahler reflectance model (Li & Strahler, 1992), spectral mixture model, and biophysical parameter estimation. Despite the advancement and complexity of the individual models, they are originally proposed for single image processing. Based on the information separately retrieved from multi-temporal remote sensing images, comparisons are made and changes of the variables of interest can be made note of. Besides, these model methods more or less depend on ancillary data sources apart from remotely sensed data. Therefore, data availability could be a potential obstacle to the application of those models.

As for the object-based method, they are mostly the recently proposed change detection algorithms inspired by the concept of object oriented classification. Hall and Hay (2003) proposed a change detection framework entailing object-specific analysis (OSA), object-specific up-scaling (OSU), marker-controlled watershed segmentation (MCS), and image differencing procedures, and applied it in a forest environment. This methodology is able to highlight and depict landscape changes through multiple scales in an automatic fashion, meanwhile reducing noise within the remotely sensed data. With the help of a GIS database, object-based

classification change detection framework can also be established by comparing the objects stored in the database and classified objects derived from remote sensing imagery using maximum likelihood classification. As a matter of fact, the supervised classification depends on the GIS database in terms of not only the comparison between pre-stored objects and the classified objects in the n-dimensional feature space, but also the selection of training data (Walter, 2004). That is to say, this approach is less applicable for applications where historical data are insufficient, and the accuracy of the change detection analysis is highly influenced by the data quality in the GIS database.

Based on a region-merging segmentation algorithm, Desclée, Bogaert, and Defourny (2006) proposed an object-based change detection method and applied it to a forested region with success. After the multi-date remote sensing imagery is segmented according to spatial, spectral, and temporal characteristics, the objects representing potential changes are highlighted using an iterative trimming procedure, followed by a chi-square test. Based on the significance test, the abnormal objects can be identified, corresponding to real changes. The proposed method outperforms the pixel-based change detection technique (implemented as RGB-NDVI) over the same source of reference, although its generalizability over other landscapes and the ability of categorizing multiple land cover changes remains to be explored. Unlike the methods mentioned above, which are suited to remotely sensed data derived from visible to near-infrared portion of the spectrum, progress has also been made in the change detection algorithms designed for synthetic aperture radar (SAR) imagery. The synergy between pixel-based and feature based methods are stressed by Gamba, Acqua, and Lisini (2006): after linear features are extracted and compared between multi-date SAR images, the results are used to confirm change detection results achieved with the pixel-based approach, where image fusion technique comes into play.

Besides its accuracy, the proposed method is considered immune to misregistration errors and varying viewing angle of the sensor.

Taking advantage of the similarity between the images subjected to the bi-temporal change detection analysis, Chen, Hay, Carvalho, and Wulder (2012) analyzed the feasibility of adding object correlation images (OCIs) and neighbourhood correlation images (NCIs) in the object-based change classification. Compared with the object-based change classification without additional features, the use of correlation images proves helpful to the increase of change detection accuracy. In addition, the NCIs are able to improve the accuracy of pixel-based change classification as well. Although it is proved through this case study that object-based change detection outperforms pixel-based change detection technique, this conclusion might be applicable only to the particular implementation of change classification, and the utility of correlation images in other change detection algorithms remains to be tested. Detailed discussion of the advantages and challenges of object-based change detection techniques can be found in Chen et al. (2012). Table 2.1 shows a brief summary of the various digital change detection techniques mentioned above.

Table 2.1 Summary of digital change detection techniques

Methods	Intrinsic properties	Advantages	Disadvantages	Examples
Classification method	Comparison of independent land cover classifications or clustering of stacked multidate remote sensing images	Allows for less strict preprocessing; Requires minimal adaptation to different change detection scenarios	Results prone to misclassification errors in the individual classifications; Demands researchers' familiarity with the study area	Land cover change (Alphan, Doygun, & Unlukaplan, 2009); Agricultural change (Serra, Pons, & Sauri, 2003)
Image differencing	Subtraction of one spectral band or composite index between two multidate remote sensing images	Easy to implement; Intuitive structure that makes the trial and error approach feasible	Quantitative change information unavailable; Accuracy is highly dependent on the selection of change indicator	Expansion of invasive species (Pu et al., 2008); Forest damage (Wang & Xu, 2010)
Image ratioing	Change/no change differentiation based on the ratio between a spectral band or composite index derived from each image	Reduces the influence of topography, shadow, and illumination conditions	Quantitative change information unavailable; Accuracy is highly dependent on the selection of change indicator	Land cover change (Afify, 2011)
Transformation	Manipulation of the multidate imagery for direct extraction of changed features or better physical interpretation	Reduces data dimensionality	Does not offer exhaustive depiction of various types of changes	Land cover change (Fung & LeDrew, 1987); Forest disturbance (Healey et al., 2005)
Change vector analysis	Capture change related information in magnitude and direction of the change vectors	Produces both quantitative and qualitative change information according to multiple change indicators	Change detection results dependent on the relevancy of the selected change indicators and the representation of change vectors	Forest change (Malila, 1980; Nackaerts et al., 2005); Land cover change (Chen et al., 2003)
Image regression	Regression analysis between the multidate images followed by image differencing	Suppresses the effect of varying sun angles and atmospheric disparity	Accuracy may vary according to the proportion of changed areas in each particular case	Land cover change (Ridd & Liu, 1998)
Model method	Physical or empirical models applied on single date images followed by comparison of extracted information	Consideration of physical aspects of LUCC dynamics	Heavy requirement for ancillary data	Forest structural change (Zeng et al., 2008); vegetation change (Elmore et al., 2000)
Object-based approach	Presents changed and unchanged patches of land as image objects	Specifically designed to derive information from high spatial resolution imagery	Does not feature high accuracy for low resolution imagery	Forest change (Hall & Hay, 2003); land cover change (Chen et al., 2012)

2.2.4 Accuracy assessment

As with single image classification and any other remote sensing derived estimates, accuracy assessment plays a fundamental role in change detection studies as well. With the help of accuracy assessment procedures, users of any change detection product, or remote sensing products in general, are able to understand the uncertainties contained in the results. Since remote sensing applications aim to approximate the reality, field measurements are generally used as reference data, to which the remote sensing estimates are compared. However, the collection of ground truth data can be problematic for change detection analysis, due to the large temporal scale associated with most of the change detection applications (Coppin et al., 2004). A critical issue regarding ground truth data collection is sampling design, where multiple aspects of the sampling process need to be dealt with caution, including sampling strategy, sample size, and spatial autocorrelation, etc. With the aid of field measurements, the accuracy of change detection studies can be evaluated in the form of error matrix, which is a quality estimation framework originally designed for single image classification.

2.3 Assessment of potential change detection techniques for Southern Ontario ecosystems

This section presents several case studies employing similar techniques as those of the present study, so as to place the proposed methodology in a proper context. There are three main techniques introduced below, including image differencing, post-classification comparison, and the Getis statistic for remote sensing applications.

2.3.1 Image differencing

Aiming at examining the expansion of saltcedar, an invasive species, found at Lovelock, Nevada, a change detection study was conducted using multitemporal Compact Airborne Spectrographic Imager (CASI) hyperspectral instrument (Pu et al., 2008). In order to accurately detect the change of saltcedar cover, two change detection methods were employed in this project: NDVI differencing and post-classification comparison approach. Since the remotely sensed data used in the analysis have approximately 40 bands (the exact numbers of bands vary due to the different specifications of the images), data compression techniques were utilized prior to the deployment of the individual change detection techniques. For the post-classification comparison approach, PCA was first performed on the original hyperspectral dataset. Subsequently, two groups of principal components were selected, each containing five principal components, representing the majority of information from visible and near infrared portion of the spectrum respectively. Afterwards, these ten bands were used as input features into a maximum likelihood classifier, followed by the generalization of six to eight output classes to three more general land cover types: farmland, saltcedar, and bare/wildland (Pu et al., 2008). Based on the individual classified maps, the construction of change matrix was undertaken according to the routine of post-classification comparison method.

Since the main objective of this application was to compare the two change detection techniques, rather than to select the optimal change indicator for saltcedar, only NDVI was subjected to image differencing procedure. It should be noted that NDVI images were derived from predefined bands that were considered the most representative of red and near infrared channels among all the candidate hyperspectral bands. For the purpose of relative normalization between the images subjected to change detection analysis, a linear regression model was

developed based on some unchanged areas among the multidate CASI imagery. More specifically, data from the date two image was regressed against that from the date one image, followed by the subtraction of predicted date two from real date two image.

Prior to the determination of thresholds to be applied on the NDVI difference image, an assumption was made that changes related with NDVI increase might not be radiometrically symmetrical to the ones related with NDVI decrease, which was validated by examining the histogram of the difference image. Therefore, the determination of change/no change threshold for areas with increased and decreased NDVI values were adjusted according to their individual mean and standard deviations. As for the multiplier associated with the standard deviations, it was kept the same for both the NDVI increase and decrease scenarios, and derived through of a series of trials based on validation samples: the one with the highest kappa coefficient was considered the most appropriate (Pu et al., 2008).

In order to make results obtained by the post-classification comparison approach comparable to that of the NDVI differencing method, the change matrix was simplified to only include three categories: no change, saltcedar increase, and saltcedar decrease. The accuracy assessment indicated that NDVI differencing technique outperformed the other, since it had a higher kappa value. Although the change/no change maps produced with the two change detection approaches suggested similar trends regarding the spatial temporal variation of saltcedar, the one corresponding to post-classification comparison was of lower quality, due to the varying accuracies of the individual classifications (Pu et al., 2008). Despite the fact that NDVI differencing was not able to provide detailed "from to" information compared with the post-classification comparison approach, its ease of implementation and effectiveness in

detecting saltcedar related changes made it an preferable change detection technique (Pu et al., 2008).

2.3.2 Post-classification comparison

With two IKONOS multispectral images, Newman, Knudby, and LeDrew (2007) employed a post-classification comparison algorithm to assess the change of coral cover over time. Since coral was the main object of interest in this study, the classification scheme of the individual classifications was established based on the various concentration levels of live coral at the study area, ranging from superabundant where the percentage of live coral is extremely high to deep water where live coral is unobservable. The comparison of the two classified images enabled quantitative estimation of live coral prevalence within each management zone. It should be noted that the estimates of live coral cover were aggregated from a probabilistic point of view, which relied on the relatively large spatial extent of the individual management zones and the ground confirmation of the coral cover (Newman, Knudby, & LeDrew, 2007). Owing to such characteristic of the change detection approach, the spatial variation of live coral changes was only presented at the inter management zone level.

2.3.3 The use of the Getis statistic in remote sensing studies

Originally introduced by Getis and Ord (1992) and adapted by Wulder and Boots (1998) for use in remote sensing community, the Getis statistic has proved to be a useful measure of local spatial clustering of objects of interest (Seixas, 2000). As an early attempt at employing the Getis statistic in forestry management, Wulder and Boots (2001) compared the color coded map based on the Getis statistic with the result of supervised classification that utilizes multispectral bands of TM imagery, which were found to be similar. It is also noted that fuzzy boundaries of land

patches are found in the Getis statistic results, and that the Getis values are of variable or object resolution (Wulder & Boots, 2001).

In a recent ecological modeling study, the Getis statistic is used to facilitate the sensitivity analysis of a calibrated physiological model (3PG) (Wulder, White, Coops, Nelson, & Boots, 2007). By altering two of the critical model input parameters (soil water holding capacity and soil fertility rating) in a forest growth model, different results are obtained for the leaf area index (LAI) and stand volume, which are two main outputs of the model. Difference maps are generated to highlight the discrepancy between the model outputs from the benchmark and the test group, and the Getis statistic can be derived for the series of difference maps. After multiple comparisons are performed, the cumulative hotspots might represent the areas that are particularly sensitive to the variations in the selected model inputs. In other words, the spatial autocorrelation measure can aid the interpretation of model outputs, and shed light on the further modification of the model for better prediction capabilities.

Rather than applying it to single date images, LeDrew, Holden, Wulder, Derksen, and Newman (2004) designed a change detection method based on the Getis statistic for coral reefs using SPOT imagery. As an nonparametric approach, both the changes of the maximum Getis statistic for the individual pixels over the image pair and the window size associated with maximum level of local spatial autocorrelation found at the study area are used as a proxy for object or land cover homogeneity. More specifically, regions of interest (ROIs) are collected for potential contaminated coral reef sites as well as open water area as the null case of change. Afterwards, the temporal variation of each pixel in each ROI in terms of the maximum Getis distance (MGD) over time is summarized by a cumulative histogram of changed pixels. Given that stressed coral reef is assumed much more homogeneous than healthy coral reef, locations

where the maximum window size alters substantially through time will be diagnosed as changed. Unlike conventional pixel-based change detection method, the proposed approach relying on a particular measure of local spatial association is deemed immune to changes in water column effects and atmospheric conditions where the spatial operator is applied (LeDrew, Holden, Wulder, Derksen, & Newman, 2004).

2.4 Discussion and Conclusion

Although a number of comparative studies have been conducted in an effort to gain insight into the performance of the individual change detection techniques, conclusions drawn from those studies might be valid only to the specific applications themselves. As a matter of fact, the performance of a particular algorithm can be easily affected by its implementation. For example, the reason why an image differencing method fails to detect land cover changes of interest may be attributed to the insensitivity of the selected change indicator. In addition, the characteristics of the remotely sensed data employed for the change detection application as well as the particularities of the study area can be sources of uncertainties when it comes to evaluating the performance of a specific change detection technique. Due to these factors mentioned above, contradictory findings regarding change detection algorithms are not rare in the current literature. Therefore, consideration of the study area and the remote sensing imagery should be taken in the selection of appropriate change detection techniques. Besides, the most effective approach might differ according to the variable of interest, owing to the variation of spatial scale, contextual information, as well as spectral signatures between distinct land cover types. After multiple algorithms are chosen as candidates, comparative analysis proves useful, through which the most accurate results can be obtained.

A clear trend concerning the development of change detection techniques is the increasing use of statistical procedures, which could potentially increase the accuracy of the results. In addition, the utilization of increased amount of information relevant to the variable of interest might contribute to more accurate and reliable change detection analysis. If the discrimination between change and unchanged areas or different types of changes can be made from multiple perspectives, the mechanism of human vision system is simulated, thus the robustness of the change detection algorithm can be enhanced. As more advanced remote sensing instruments are put into use, object-based change detection concepts are proposed to make full use of the finer spatial resolution relative to that of the conventional sensors, such as TM. Although multi-date change classification appears to be a popular approach towards object-based change detection analysis, it might be less applicable to pixel-based paradigm. That being said, the use of textual and contextual information can be helpful when applied in pixel-based change detection techniques as well. Furthermore, the variation and continuity of signals in the temporal domain might lead to increased change detection accuracy, if multi-temporal remotely sensed data are available.

According to the review of literature, the performance of image differencing technique is largely dependent on the selection of change indicator. Similarly, the spatial variable on which the Getis statistic is calculated greatly influences its capability of depicting hotspots in the spatial domain. Besides, the window size or lag distance used to configure the computation of the Getis statistic is critical as well. By calculating the statistic at different scales, the maximum Getis value and the corresponding window size can be determined, which contain critical information about the spatial structure of variables under investigation. Since the Getis statistic has the advantage of reducing some interfering effects that are present to the entire image, such as

atmospheric conditions, it is considered useful for reducing noises in change detection practices. Due to the fact that noise tends to follow a random distribution in space, it is not supposed to be highly correlated with the spatial variable of interest. Therefore, this characteristic of the Getis statistic might be useful in suppressing the salt and pepper effect in single date image processing as well as change detection analysis.

Unlike the image differencing technique, the post-classification comparison approach provides not only qualitative but also quantitative change information. In addition, it is relatively easy to implement, despite the various endeavours made to improve the accuracy of the single date classifications. With a carefully designed classification scheme for the study area, transitions between the individual types of land cover can be revealed, thus contributing to the categorization of land cover changes. Since high spatial resolution multitemporal remote sensing images are used in the present study, it is essential to exploit the spatial information contained in the dataset and assess its interplay with the change detection techniques as well as the influence it has on accuracy of the change detection application. Due to its popularity in the context of change detection analysis, the results obtained from post-classification comparison can be considered as a benchmark to evaluate the strengths and weaknesses of the proposed methodology.

Chapter 3

Research Design

3.1 Study Area

The Long Point Region has undergone land modifications since the settlement of the early First Nations inhabitants. Marked by extensive deforestation, the land cover change activities in the region peaked between 1850s and 1960s, as the local farmers tried to convert the landscape to facilitate their agricultural productions. According to Long Point Region Conservation Authority (2008), the Long Pont Region witnessed the drastic declination of forest cover from more than 70 percent to below 15 percent during this period. Due to a series of reforestation and restoration endeavors, the Long Point Region has recovered approximately five percent of forest cover, reaching the 20 percent level as of now. As can be seen from Figure 3.1, there are several small urban centers in the region, while the rest of the landscape is mainly rural land, characterized by forests, agricultural fields, and wetlands.

As a significant component of the Long Point Region, wetlands play an irreplaceable role in the ecological and hydrological processes in the area, which varies from surface and ground water protection to biodiversity conservation (Long Point Region Conservation Authority, 2008). As a part of the Deciduous Forest Region of Canada, the Long Point region is home to a critical forest ecosystem as well. In addition to the common deciduous tree species such as oak, ash, and maple, the region also sustains a range of endangered species such as cucumber tree, black oak, and tulip tree, making it an integral part of the Carolinian zone (Long Point Region Conservation Authority, 2008).

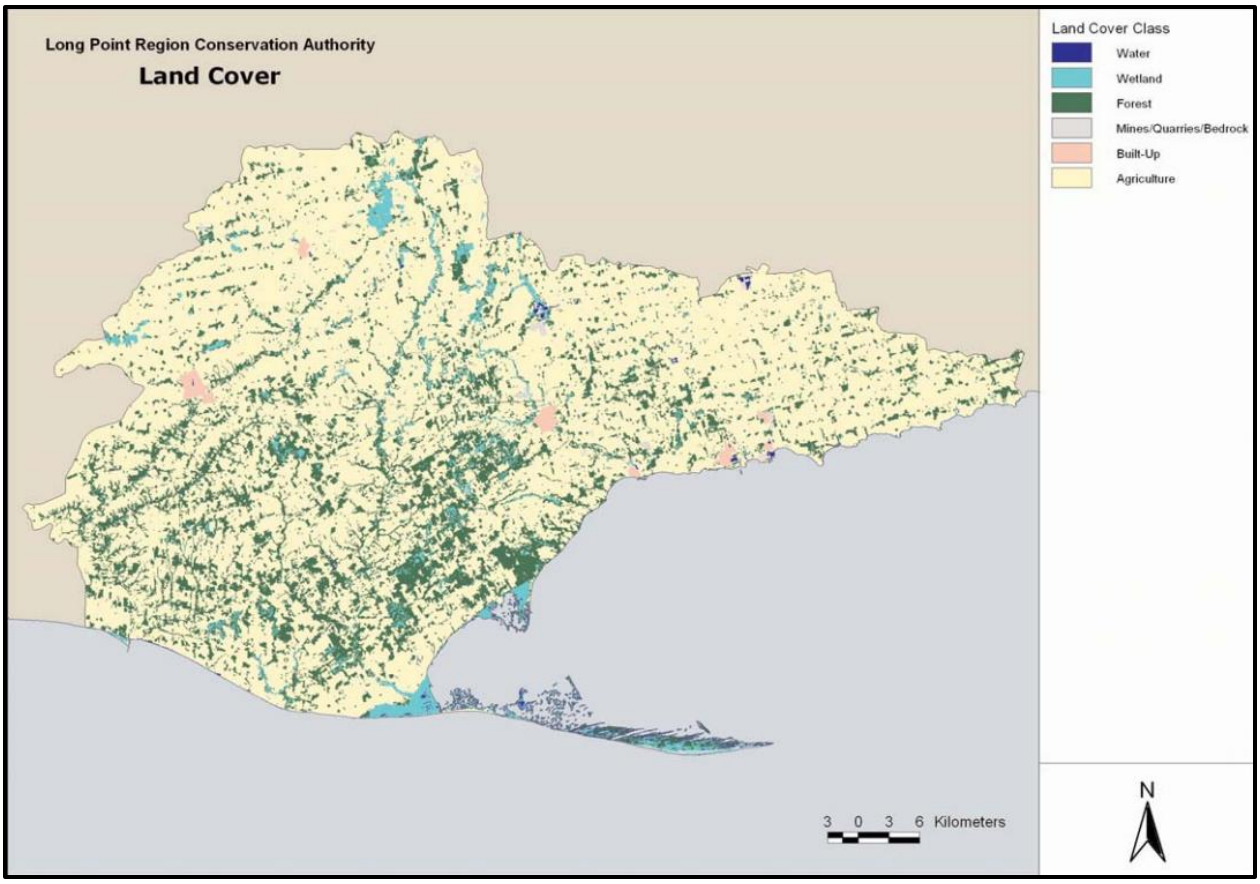

(Long Point Region Conservation Authority, 2008)

Figure 3.1 Land cover map of the Long Point Region

Spreading from Toronto, Lake Huron, to Lake Erie, the Carolinian zone only occupies approximately 0.25% of Canada's total territory, yet it supports nearly one third of the country's rare species as well as over one quarter of the country's human population. However, such a unique region is under severe threat, due to severe fragmentation problems (Johnson, 2007). In 1984, 38 sites were identified as critical natural areas by Carolinian Canada Coalition (2013b), and conservation endeavors have been aimed at securing these sites. Considering data availability issues and the objective of this study, the Big Creek conservation area is selected as the study area, which is part of Norfolk County, Ontario. Just northern to the Long Point peninsula, it covers one of the 38 Carolinian Canada signature sites, called "Big Creek Valley - South Walsingham Sand Ridges" (Carolinian Canada Coalition, 2013b). Figure 3.2 shows a map

of Carolinian Ecozone and its location in North America, covered by a true color composite of the IKONOS image used for this study.

Identified as an “Area of Natural and Scientific Interest" (ANSI), the Big Creek conservation area covers sand plain forest and the surrounded river valley complex, making it one of the significant critical forest ecosystems, without which a number of plant and animal lives would be found further south (Carolinian Canada Coalition, 2013b). Since this area is managed by public, private, and non-profit landowners, the bulk of the conservative practices in the area are accomplished by the land owners, mainly including reforestation activities. In a broad theme, such endeavors could contribute to the carbon sequestration as a strategy adopted to cope with climate change. In addition, it is expected that the reforestation activities could help restore the habitat for various species, among which many are endangered. Another aim of the conservative measures is to reconnect the highly fragmented forests, such that the population of plant and animals can be maintained at a reasonable level (Carolinian Canada Coalition, 2013b). According to the big picture project (Jalava, et al., 2000), in which a rough estimation of the forest loss was conducted, the Carolinian landscape had experienced as much as 69% (from 80 to 11%) of degradation, and only 0.07% of the forest is in old growth condition. In this study, land cover changes associated with Carolinian forest will be investigated, which not only includes the amount but also the location of the changes.

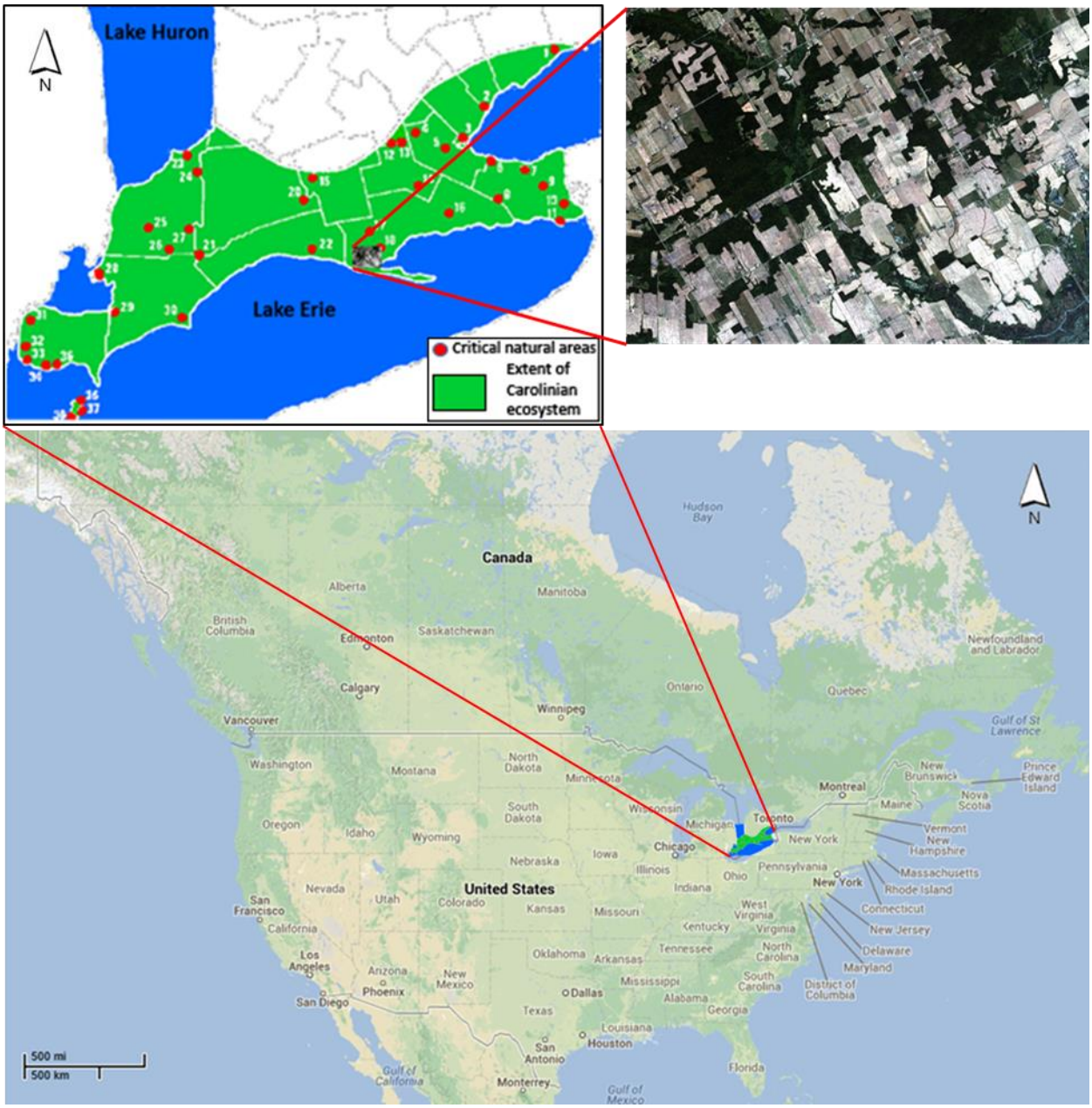

(Adapted from Carolinian Canada Coalition, 2013b)
(Google Map, 2013)

Figure 3.2 Map of Carolinian ecosystem covered with IKONOS image delineating the study area, shown in the context of North America

3.2 Data Acquisition

3.2.1 Satellite imagery

Since the main objective of the present study is to analyze land cover changes using remote sensing imagery, consideration of sensor configuration was made at the planning stage of the study. Once the spatial and temporal scope of the project is finalized, availability of relevant remotely sensed data can be queried at online data portals. Considering the purpose of identifying land cover changes through time, it is preferable to make use of remote sensing observations dating back to 1990s, when some of the recent restoration projects are conducted at Norfolk County (Carolinian Canada Coalition, 2013c). However, many of the remote sensing instruments that feature high spatial resolution did not become available until recently, such as GeoEye-1 (2008), WorldView-1 (2007), and WorldView-2 (2009). Therefore, the potential instruments that can be used for the present study are IKONOS and QuickBird, which provide temporal coverage of approximately 10 years (LAND INFO Worldwide Mapping, LLC, 2013). Considering its reasonable price and larger image archive compared with QuickBird, IKONOS imagery is deemed more suitable for this research.

The primary reason why IKONOS imagery is favoured over the more traditional remote sensing datasets is attributed to its designation as high spatial resolution imagery, which could contribute to the detection of changes that can only be discovered at fine spatial scales. In addition, the high spatial resolution of IKONOS is deemed useful in extracting texture measures for the ground objects of interest, thus facilitating the discrimination between different types of cover. Details revealed by this high resolution product could be amenable to spatial analysis, which focuses on the scale issues of remote sensing, instead of the spectral ones. Therefore, it is

probable that IKONOS imagery had the potential for facilitating more accurate change detection analysis compared with more conventional remote sensing products, such as TM and SPOT.

IKONOS was launched in 1999 and has been used for various geospatial applications for over 13 years (GeoEye, 2006). It is the first commercial remote sensing satellite that reached the spatial resolution of one meter. Operating at an altitude of 681 kilometers, it moves along a sun synchronous orbit and has an image swath of 11.3 kilometers at nadir and 13.8 kilometers off-nadir. Capable of covering the majority of the earth surface within a relatively short period of time, IKONOS features a revisit time of approximately three days. With a radiometric resolution of 11 bit, the images delivered in Geotiff format have a dynamic range of 0 to 2047. As can be seen from Table 3.1, the four multispectral bands of IKONOS cover the blue, green, red, and near infrared region of the solar spectrum respectively, featuring a spatial resolution of four meters. With a higher spatial resolution measured at one meter, the panchromatic band measures the overall reflectance from the spectrum ranging from green to near infrared (GeoEye, 2006).

Table 3.1 Specifications of IKONOS imagery

Channel	Spectral range (μm)	Dynamic range (bit)	Spatial resolution (m)
Band 1 (blue)	0.445 – 0.516	11	4
Band 2 (green)	0.506 – 0.595	11	4
Band 3 (red)	0.632 – 0.698	11	4
Band 4 (near infrared)	0.757 – 0.853	11	4
Panchromatic	0.526 – 0.929	11	1

Adapted from GeoEye (2006).

The detailed acquisition parameters retrieved from the metadata of the multitemporal IKONOS imagery are summarized in Table 3.2. It is worth noting that two cloud free images are required for the purposes of this study. That being said, the other acquisition parameters vary from one image to the other, which indicates the image acquisition condition between the two images differs to a certain extent. Although extraneous effects induced by fluctuating variables such as sun elevation and acquisition elevation can be reduced by radiometric processing for optical sensors (Chander et al., 2009), there is an apparent discrepancy between the two images: the acquisition dates are approximately one month apart, with the 2004 image obtained in early June, while the 2012 image obtained in early August. Ideally, change detection analysis would benefit from the employment of multitemporal remote sensing images collected at anniversary dates of different years, but this particular image pair is the best among the ones that are available, considering the strict cloud coverage criterion.

Table 3.2 Acquisition parameters of the multitemporal IKONOS imagery used in this study

Key parameters	2004 image	2012 image
Nominal Collection Azimuth	346.4347 degrees	283.6338 degrees
Nominal Collection Elevation	83.11150 degrees	67.36409 degrees
Sun Angle Azimuth	145.0137 degrees	151.9435 degrees
Sun Angle Elevation	67.23167 degrees	62.09115 degrees
Acquisition Date/Time	2004-07-03 16:31 GMT	2012-08-04 16:35 GMT
Percent Cloud Cover	0	0

(GeoEye, 2013)

3.2.2 Ancillary data

After the appropriate imagery is chosen for this project, factors pertaining to the collection of reference data should be considered. Reference data obtained through field campaigns serve two main purposes in remote sensing applications: the ground for selection of training and testing sites for automated procedures and their evaluation as well as the reference for radiometric processing of the imagery. It is possible to conduct ground observations before the acquisition of remotely sensed data, guided by current knowledge of the study area. However, there might be changes occurring between the date of field campaign and the image acquisition date, especially the subtle ones, which gives rise to the need for synchronous collection of ground data (Justice & Townshend, 1981). This methodology is particularly desirable if the object of investigation is highly variable in a short period of time.

As a matter of fact, ideal synchronous ground observations are difficult to undertake, owing to the varying weather condition at the study area and uncertainties of the actual image acquisition date within the contracted time window of acquisition. Therefore, ground measurements are considered acceptably useful if the temporal discrepancy between the field campaign and the satellite imagery acquisition is within a few days. In addition, it is beneficial to make use of existing geospatial dataset of the study area, such that the sampling design could be facilitated. Based on the 2004 archive IKONOS image, an unsupervised classification was performed to generate a classified map with 15 land cover classes. As an attempt to confirm these classes, one example from each class was used as a ground reference point. For the ease of access, all the sample sites were picked along the local roads, following a normal opportunistic sampling strategy.

In order to establish an up-to-date functional spectral library for the study area, spectral measurements were made at all the sample sites, except for the above canopy forest and water body class, which are generally not accessible by foot. The main instrument employed for the field investigation was an Analytical Spectral Devices (ASD) spectrometer, covering 340nm to 1070nm portion of the spectrum, with a spectral resolution of 1.4nm. In addition to the spectral measurement, photos were taken for each sample site to provide a record of the landscape. To account for uncertainty in the satellite overhead schedule, redundant measurements were made through three field campaigns, which covers the timeframe from late July to mid-August. Despite the spectral measurements made over a range of land cover types, they did not meet the requirement of the empirical line method for atmospheric correction (Karpouzli & Malthus, 2003), due to the absence of deep water bodies or black asphalt in the study area. Since no spectral profile was collected for the forest class, the land cover classifications for 2004 and 2012 image did not make direct use of the ASD measurements. Nevertheless, the ground spectral measurements were used to link the spectral response recorded in the image and the ground condition, which contributes to the support of the visual interpretation of the multidate remote sensing imagery.

3.3 Consultation with Environmental Conservation Groups

With a keen interest in LUCC dynamics in the Big Creek area, Carolinian Canada Coalition (CCC) has provided continuous support and help for the current study, which contributed greatly to the formulation of the research objectives. Due to the nature of the big picture project as a comprehensive conservation plan, an essential goal of this study is to examine the land cover changes from 2004 to 2012, which are closely related to the monitoring of restoration projects and connectivity of the ecosystem at large. Since forest is able to provide habitat for a range of

wildlife types (Brooks et al., 2002), it plays a critical role in protecting biodiversity; therefore, forest related changes are of particular importance in this study. According to an ecological land classification (ELC) from Nature Conservancy of Canada (NCC), there is a high level of spatial mixture between swamp and forest. However, they prove to be undistinguishable based on visual interpretation of the multitemporal satellite imagery.

Preliminary investigation of these two classes was conducted using the Jeffries-Matusita and Transformed Divergence measures (Swain & Davis, 1978) embedded in ENVI (Exelis Visual Information Solutions, 2013a), which aim to estimate the spectral separability between any given pair of classes from a statistical point of view. The separability values derived from both of these two indices have a theoretical range of zero to two, and a value greater than 1.9 means the selected pair of classes can be well differentiated. In the case of the forest and swamp pair, the separability values were approximately 0.2 for both the Jeffries-Matusita and Transformed Divergence measures regardless of whether the spectral separability analysis was performed on the 2004 or 2012 image, indicating extremely low separability between these two classes based on the four multispectral bands of IKONOS imagery. As a matter of fact, it was suspected that the ELC from NCC might not be a reliable ancillary data source for the present study. Subsequently, forest and swamp are considered as a single class, forest, in the following analysis. Assuming that the spatial distribution of forest and swamp delineated in the ELC is valid, it is less likely to be detected from long range remote sensing systems, unless Light Detection and Ranging (LiDAR) or hyperspectral instruments are used.

In addition, the discussion with the representatives from CCC greatly facilitated the design of classification scheme for this study. Although the majority of the study area is covered by forest and agricultural fields, a few classes with relatively small coverage were deemed of

significant ecological value as well, such as pasture and plantation. The possibility of dividing forest into deciduous, coniferous, and mixed subclasses was also discussed, yet the feasibility was relatively low with IKONOS being the only data source, due to their complex spatial structure and intra-class variations. After a series of explorations were undertaken, the methodology was designed for this study. Figure 3.3 shows a number of factors that have made the proposed methodology a well-informed one. The detailed methodology denoted by the big ellipse in the middle of this chart entails the critical processing steps pertaining to the technical aspect of this study, which will be discussed in detail in Chapter 4.

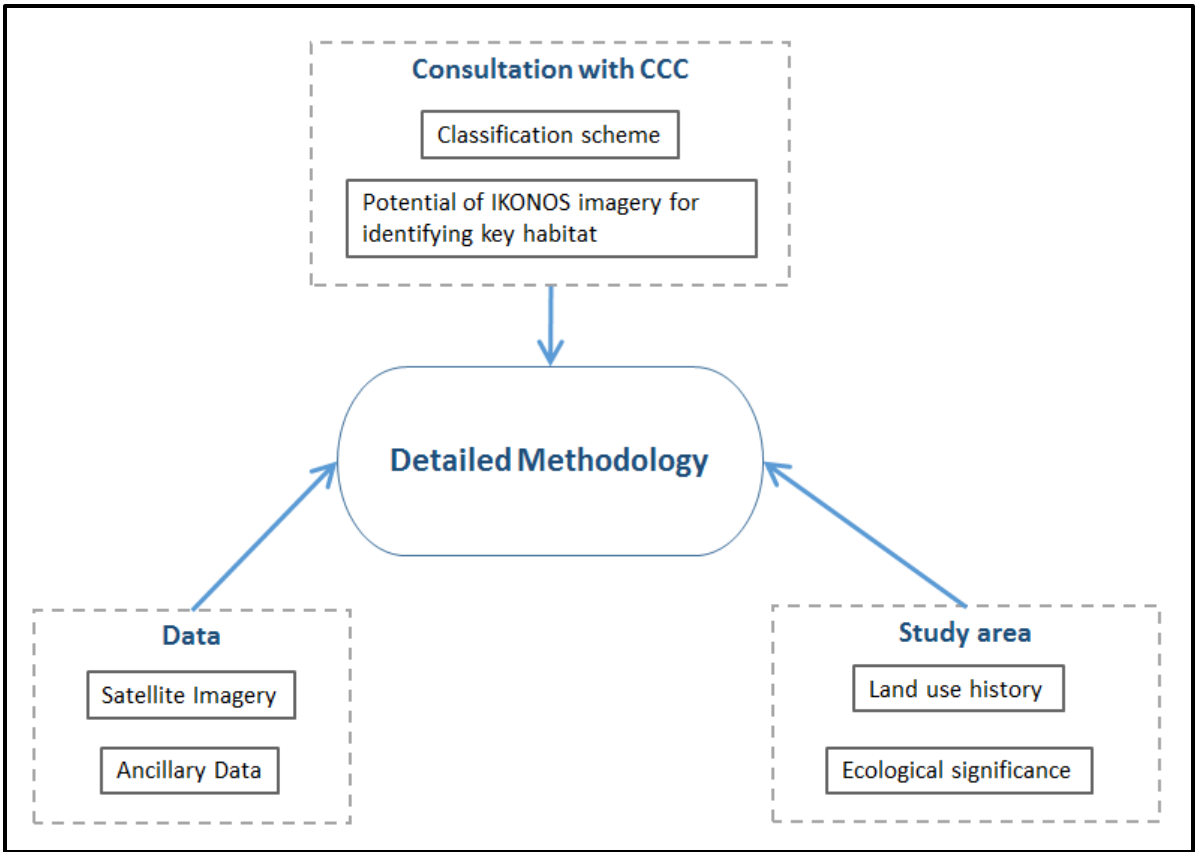

Figure 3.3 Various factors contributing to the research design

Chapter 4

Methodology

4.1 Overview of the Proposed Methodology

Since a binary change/no change map does not provide information on the spatio-temporal dynamics of each type of cover, especially the ones that conservation groups like CCC are interested in, this study aims to deliver both qualitative and quantitative change information. Due to its ease of application and the capability of deriving quantitative change information from individual classified maps, the post-classification comparison approach is considered suitable for this study (Lu, et al., 2004). Considering the fact that the study area is highly vegetated, post-classification comparison has a unique advantage: it allows for certain level of generalization for land cover classes with relatively significant intra-class spectral variability, which is not unusual for vegetated classes, such as forest and agricultural fields.

If the intra-class variability is well captured in the training samples, phenological fluctuations or species discrepancies within each vegetated class can be taken into consideration in the classification analysis, such that changes of little significance from land cover point of view may be suppressed. Nevertheless, the tolerance of intra-class variability may result in lower inter-class separability, especially for the ones that have intrinsically similar spectral characteristics, such as agricultural fields, pasture, and orchard. This may in turn compromise the performance of the land cover classifications, and the classification errors would further propagate into the post-classification comparison phase of the workflow, leading to less accurate quantitative change information. As a matter of fact, false change alarms are particularly prone to misclassification errors in the classified maps subject to the post-classification comparison

approach. In light of this drawback of the post-classification comparison approach, improving the quality of the individual land cover classifications is deemed a critical path to the successful employment of this particular change detection method (Singh, 1989).

On the contrary, if image algebra based change detection techniques are utilized, any pixel that has not undergone substantial spectral change is very unlikely to be determined as changed, regardless of which land cover class it belongs to. Essentially, it is impossible for change detection algorithms involving direct comparison of the multidate remote sensing images to raise false alarms caused by misclassification of various types of land cover, which is the case with the post-classification comparison approach. In addition, the interesting changes would appear as relatively homogeneous patches in change indicator images such as a difference image or band ratio. Accordingly, it is not unusual to observe successfully detected changed areas corresponding to relatively compact patches in the change indicator images.

However, change results obtained from image algebra based change detection algorithms are less immune to intra-class spectral variations, sometimes termed as land modifications (Petit, et al., 2001), in the multitemporal feature space. This could induce false alarms that are avoidable by the post-classification comparison approach. Under circumstances where two types of land cover with similar spectral signatures constitute changes of interest, accurate change detection is especially challenging, since inter-class contrast might not be as distinctive as intra-class variations in the feature space. Therefore, a simple threshold might not be sufficient to separate changed from unchanged pixels, regardless of the essence of the thresholding mechanism. This drawback of the image algebra based techniques gives rise to the pursuit of a change indicator less prone to the problem associated with conflicting intra-class variability and inter-class contrast.

In order to take advantage of both the image algebra and classification based approaches, hybrid change detection method has been proposed, leading to more accurate and informative change detection analysis than what can be achieved with either of these two techniques alone (Petit, et al., 2001). In particular, change mask can be extracted from binary change/no change maps generated by image algebra based method and applied to change maps derived from the post-classification comparison approach. As an attempt to improve the spatial homogeneity of the change/no change maps in the present study, the Getis statistic (Getis & Ord, 1992) is employed in conjunction with the image differencing technique as a spatial filter, such that local spatial association characteristics can be taken into consideration.

A flowchart introducing the proposed methodology can be found in Figure 4.1, while the pertinent technical details are presented in the subsequent sections of this chapter. The first stage of the workflow necessitated the preprocessing of the raw multitemporal IKONOS imagery, including radiometric calibration and image registration. When it comes to the change detection approach, a two-stream strategy was followed, which involved change/no change discrimination and change type categorization. In order to reach the goal of change/no change discrimination, image differencing technique and change vector analysis were employed, followed by a spatial filtering procedure based on the application of the Getis statistic. Afterwards, both pixel and object-based classification techniques are examined, as an effort to improve the accuracy of the post-classification comparison method. For both groups, a variety of factors are taken account of, such as input features, classification parameters, training sample size, and filtering options. Rather than exploring only the qualitative change information, post-classification comparison method aims to further divide the changed areas into different classes, based on the nature of the changes. To determine the best classification pair for change detection, the change/no change

maps derived from post-classification comparison approach are compared with each other as well as that from image differencing and CVA, which in turn ensures the accuracy of both change/no change discrimination and change type categorization. It should be noted that accuracy assessment conducted at various stages of this study are not included in this flowchart.

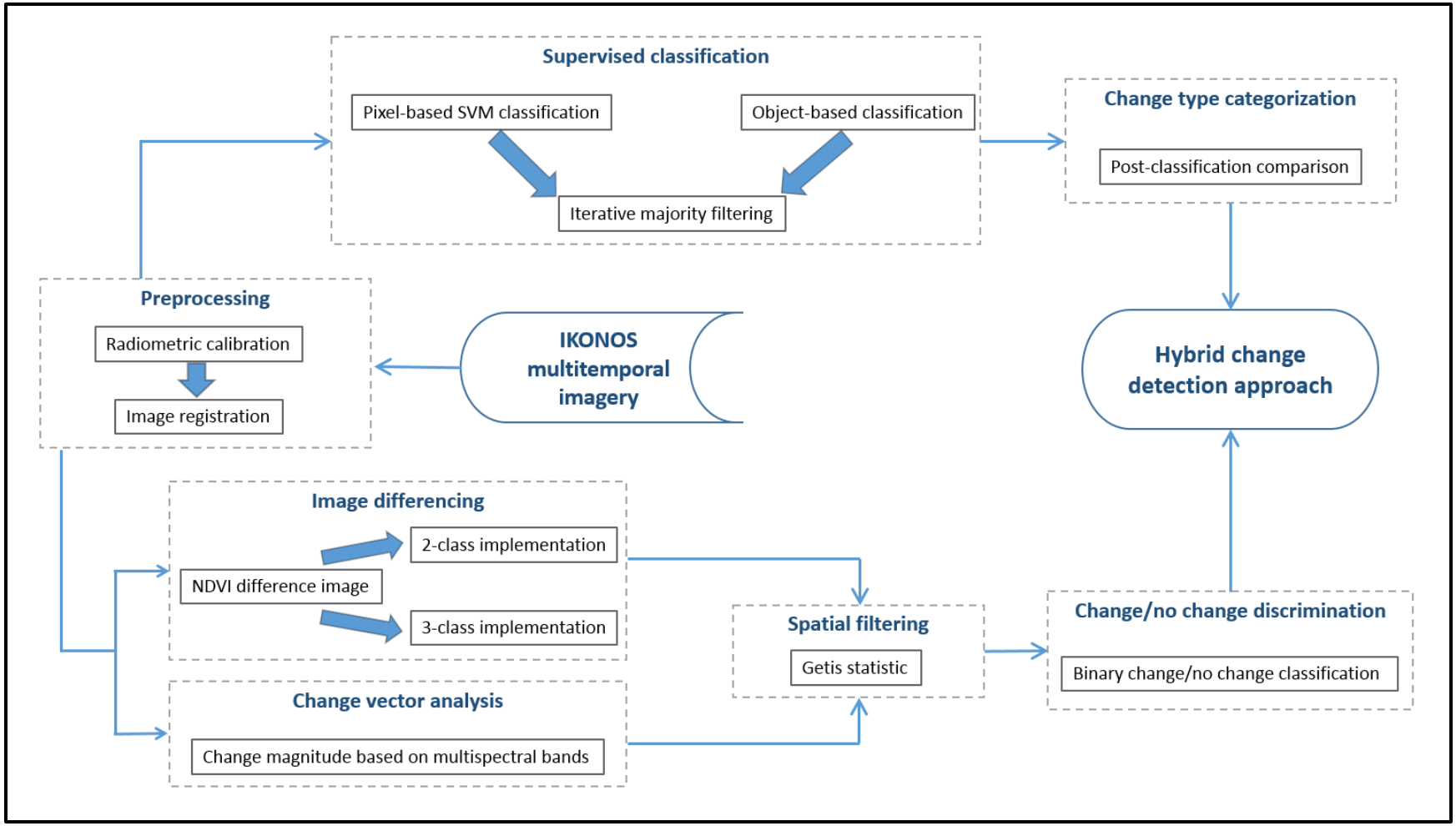

Figure 4.1 Flowchart of the proposed methodology

4.2 Preprocessing

In order to ensure the accuracy of the results derived from this study, a series of preprocessing steps were undertaken, including image coregistration and radiometric calibration of the multitemporal remote sensing imagery. Before any operation was applied to the multispectral images, the images were converted from raw DN values to top of atmosphere (ToA) reflectance using post-launch gain and offset parameters based on an add-on built for ENVI (The ENvironment for Visualising Images), retrieved from ENVI code library (Exelis Visual Information Solutions, 2013b). After the conversion, the 11-bit images have a new range from zero to one. In order to eliminate the atmospheric scattering effect from the datasets, either absolute atmospheric correction or relative radiometric normalization technique should be applied (Song, Woodcock, & Seto, 2001).

As a typical example of absolute atmospheric correction method, Fast Line-of-sight Atmospheric Analysis of Spectral Hypercubes (FLAASH) embedded in ENVI (Exelis Visual Information Solutions, 2013d) supports the correction of a wide range of imagery collected by various multispectral and hyperspectral sensors in different viewing geometries. Rather than relying on the interpolation of radiation transfer parameters derived from pre-calculated model outputs, FLAASH makes use of the MODTRAN4 radiation transfer code, which gives it an edge over many competing atmospheric correction packages. In addition, it takes account of the adjacency effect of atmospheric scattering, thus contributing to more reliable and accurate atmospheric correction (Exelis Visual Information Solutions, 2013d). Therefore, FLAASH was considered appropriate for this study. To parameterize FLAASH, the atmospheric model and aerosol model were manually set as “Mid-Latitude Summer” and “Rural” respectively, while the

rest of the required parameters were extracted from the image metadata. Despite the careful tuning of the model, a certain portion of the corrected images obtained negative reflectance values, which compromised the usability of FLAASH in this study. Similar to the case with absolute atmospheric correction, pseudo invariant feature (PIF), a popular relative radiometric normalization technique, failed to deliver normalized images in correct range, no matter whether the PIFs were selected using the conventional approach (Schott et al., 1988) or the automatic implementation (Du, Teillet, & Cihlar, 2002). Therefore, the IKONOS images measured in ToA reflectances only and not corrected for the atmosphere were used for subsequent processing.

After the radiometric processing was completed, coregistration of the multitemporal imagery was conducted in ENVI (Exelis Visual Information Solutions, 2013d), with 2004 image being the reference image and 2012 image being the slave image. For the sake of a good match throughout the whole image, 48 ground control points (GCPs) were collected. As shown in Figure 4.2, the GCPs were evenly distributed throughout the entire scene, and the majority of them were located at intersections of the local road network. The coregistration was based on first-order polynomial and nearest-neighbour resampling, such that the spectral characteristics of the slave image remained intact after the operation. Visual inspection of the registered multitemporal imagery indicated improved image match after the coregistration, which was confirmed by a relatively small root mean square (RMS) error of 0.41 pixel. After the acceptable results from coregistration was acknowledged, the image pair was stacked and clipped according to the minimum spatial extent among the two images, thus ensuring that they cover exactly the same area with valid measurements. After all the preprocessing steps were accomplished, the emphasis of this study shifted to the classification stage of the workflow.

Figure 4.2 Distribution of GCPs in the 2012 IKONOS image

4.3 Supervised classifications

As an indispensable component of the post-classification comparison approach, land cover classification was considered of great importance to this study. Due to its capability of classifying pixels into a group of predefined categories, supervised classification techniques were employed, instead of the unsupervised clustering methods. For both images used in this study, a series of experiments were made, which could be divided into two broad categories: pixel-based and object-based.

4.3.1 Pixel-based classification

Owing to its widely reported superior performance compared to conventional machine learning algorithms, such as minimum distance classifier and maximum likelihood classifier, support vector machine (SVM) has gained popularity over other approaches in recent years (Mountrakis et al., 2011). In addition to the performance consideration, SVM falls into the category of a nonparametric classifier, which means it does not assume any specific probability distribution of the remotely sensed data (Keuchel et al., 2003). Considering the fact that a normal distribution might be invalid for certain imagery and classification schemes, SVM was deemed suitable for this study, especially if large number of training samples are not available (Mountrakis et al., 2011).

After preliminary visualization of the multitemporal imagery, a classification scheme consisting of eight land cover classes was determined, including forest, fallow, water body, agriculture, plantation, orchard, asphalt, and pasture. Due to the 32-day deviation of image acquisition date from the anniversary date, different phenological states of the crops were observed from the multitemporal satellite images: only a small amount of vegetation are present at the agricultural fields in the 2004 image, while the majority of the agricultural fields appear to be vegetated in the 2012 image. This can be seen from the false colour images in Figure 4.3, where vegetation is highlighted in shades of magenta and background soil with little vegetation has a blue cast. Upon further interpretation of the 2012 IKONOS image, two types of agricultural fields were found, with slightly different levels of vegetation present. Figure 4.4 shows a comparison between the two types of agricultural fields found in the 2012 image, where the areas of interest are highlighted in green rectangles. In addition to the different tones in the standard false color composites, the varying grey levels in the Normalized Difference Vegetation Index

(NDVI) (Rouse et al., 1974) images also indicate their spectral discrepancy and variation in homogeneity. In order to reduce potential classification errors induced by the intra-class variability, these two types of agriculture were treated as two independent classes in the various land cover classifications performed on the 2012 image. For the sake of consistency between the 2004 and 2012 classifications, they were combined into a single class for any comparison to be made between images in the subsequent analysis.

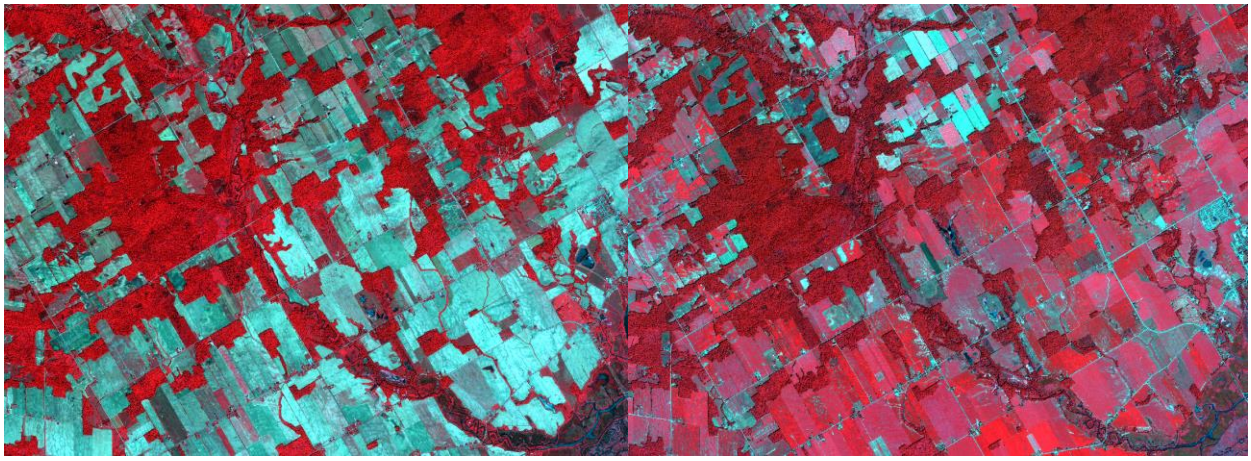

Figure 4.3 Phenological discrepancy between the 2004 (left) and 2012 (right) IKONOS image

To ensure the accuracy and robustness of the supervised classifications, the collection of training samples was guided by the stratified random sampling strategy for both images. Considering the dominance of vegetation in the study area, NDVI was employed as an additional input feature to the pixel-based classifications, which could potentially contribute to the discrimination between different types of vegetated land cover. In addition, the normalized difference water index (NDWI) (McFeeters, 1996), albeit less popular than NDVI in remote sensing community, might be useful in the delineation of wetlands in the study area. Therefore, NDWI was employed as another spectral input feature to be added to the classification system apart from NDVI. That being said, the usefulness of these two spectral indices are merely an

assumption, which needs to be confirmed by the classification analysis to be performed accordingly. The equation used to derive NDWI is given as follows:

$$NDWI = \frac{\rho_{GREEN} - \rho_{NIR}}{\rho_{GREEN} + \rho_{NIR}} \quad (4.1)$$

where ρ_{GREEN} and ρ_{NIR} represents the reflectance from green and near infrared band of a sensor respectively.

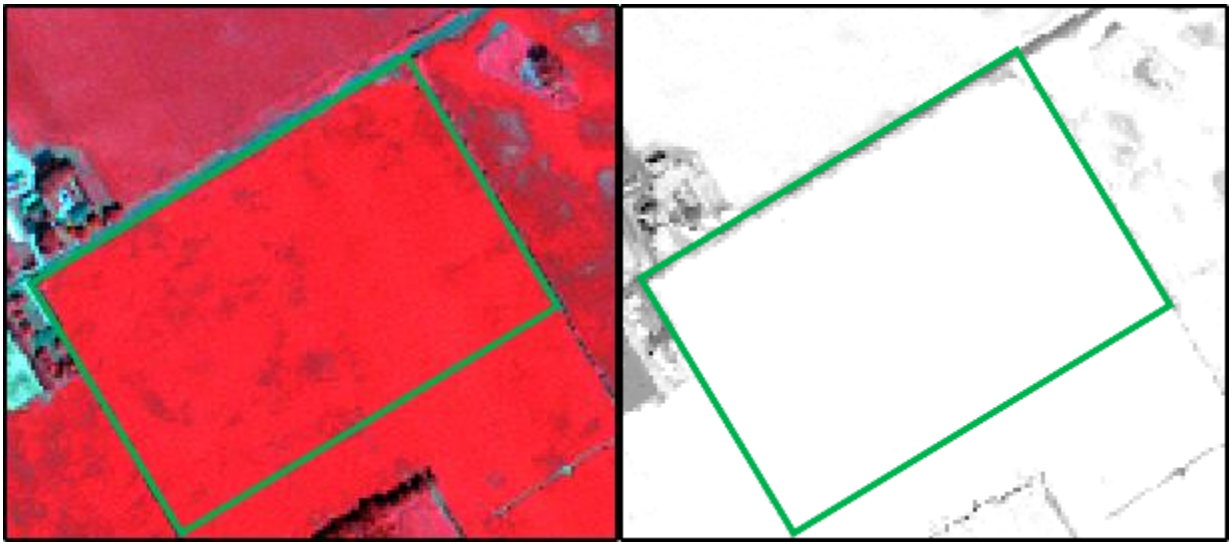

(a) Type 1 agriculture in standard false color composite (b) Type 1 agriculture in NDVI image

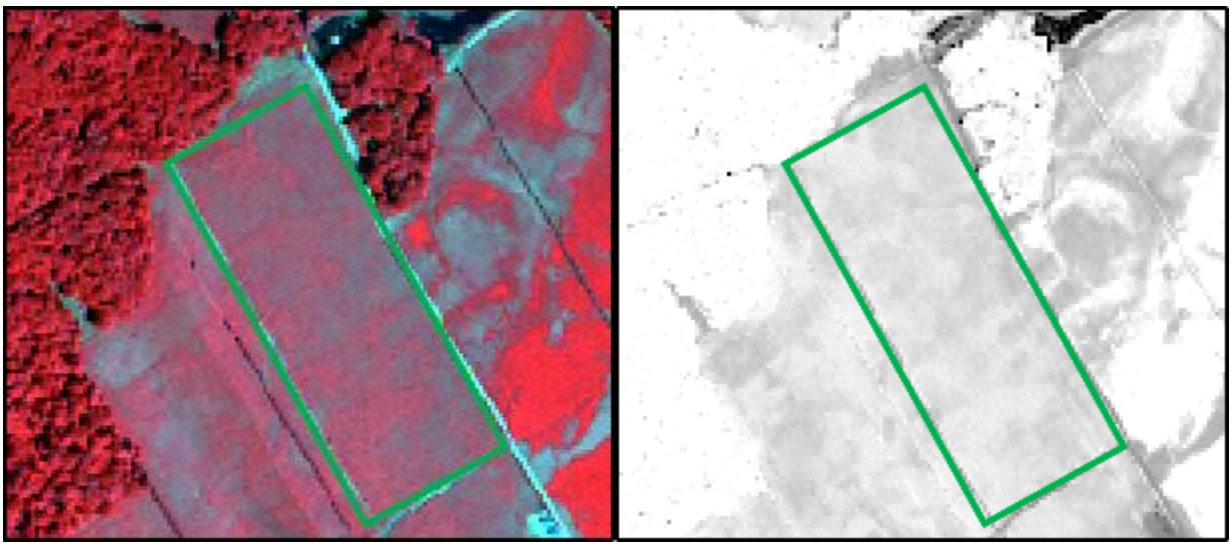

(c) Type 2 agriculture in standard false color composite (d) Type 2 agriculture in NDVI image

Figure 4.4 Two types of agricultural fields in the 2012 image

An intrinsic drawback of pixel-based classifications is the lack of spatial information incorporated into the decision making system (Atkinson & Lewis, 2000). In order to exploit the rich spatial information available from the IKONOS imagery, texture measures are taken into consideration, in addition to the four multispectral bands and two spectral indices mentioned above. Categorized as texture filter in ENVI (Exelis Visual Information Solutions, 2013e), the occurrence matrix (Anys et al., 1994) and the Grey Level Co-occurrence Matrix (GLCM) approach (Haralick, Shanmugam, & Dinstein, 1973) were examined. The indices calculated from the occurrence matrix include data range, mean, variance, entropy, and skewness, which are computed based on a moving window of specified size. Different from the occurrence matrix, co-occurrence matrix is calculated by considering two joint windows with a lag in predetermined distance and direction, and the texture indices include mean, variance, homogeneity, contrast, dissimilarity, entropy, second moment, and correlation. In order to obtain comprehensive understanding of the usefulness of texture measures, both texture filters were applied to the four multispectral bands of IKONOS as well as the two spectral indices mentioned above.

The main decision regarding the parameter characteristics required to perform occurrence matrix analysis is the size of the moving window, while the parameterization of co-occurrence matrix is more complex, which includes not only the size of the moving window, but also co-occurrence shift and greyscale quantization level. To start with, experiments with both matrices were made with two different sizes of moving window: 3 by 3 and 5 by 5, whereas the default setting for the additional parameters in the co-occurrence matrix was adopted, which means the co-occurrence shift and greyscale quantization level was set as (1,1) and 64 respectively.

According to visual interpretation of the various texture measures derived from both methods, it was found that the signal-to-noise ratio of the texture images became higher if the

size of the moving windows was increased from 3 by 3 to 5 by 5. Given the requirements of the classification scheme, selection of the individual texture measures was based upon their potential for improving the separability between different types of cover. For example, the variance image of band 1 was deemed suitable for highlighting linear features, such as the local roads, since it showed significant contrast between those linear features and the background. The roads were especially well delineated with a 5 by 5 moving window applied. Furthermore, NDWI variance image exhibited promise in depicting streams, indicated by the great dissimilarity between streams and their surroundings observed in the texture image. Besides the extraction of linear structures, characterization of the spatially dominant classes was also of critical importance. In particular, the skewness image of NDWI and second moment image of NDVI were considered useful in mapping fallow land, owing to their capability of separating fallow from agricultural fields to a certain degree. Although agricultural and fallow fields can be well differentiated by the distinctive inclination of "red edge" associated with vegetation, the employment of these texture features could potentially increase their spatial homogeneity, thus reducing the "salt and pepper" effect in the classified map.

Furthermore, data range and contrast image of band 3 were able to present residential areas in a homogeneous fashion, which may contribute to higher classification accuracy for the impervious class. Lastly, the entropy image of band 4 derived from the occurrence matrix highlighted disparity between vegetated and non-vegetated areas, despite the presence of speckles in the forests, potentially as a result of gaps between closed canopies. It should be noted that the usefulness of the texture features are evaluated in a relative sense, which means the ones mentioned above are considered more useful than the other features derived from the occurrence and co-occurrence matrices. In addition, it is possible that the use of these texture features may

not necessarily lead to more accurate classifications as expected, since visual assessment of the individual texture images and supervised classification are independent processes.

Based on the observations mentioned above, classification analysis of the IKONOS images were divided into five groups, each with a different set of input features, listed in Table 4.1, where 'raw' means the four multispectral channels of IKONOS, while b1 and b3 represents band 1 and band 3 respectively. The first two groups contain only the spectral features; therefore, the comparison between these two groups would unveil the usefulness of the two vegetation indices in improving the classification accuracy. According to the visual interpretation of the individual texture images, variance of band 1 and data range of band 3 were considered the most useful texture features among all the other candidates. Consequently, group 3 and group 4 were established by adding these two texture features to group 1 and group 2 respectively. Group 5 consists of six spectral input features (multispectral bands, NDVI, and NDWI) and all the texture features that were deemed useful, including band 1 variance, NDWI variance, NDWI skewness, NDVI second moment, band 4 entropy, band 3 data range, and band 3 contrast. As a result, the total number of features in the group 5 classification adds up to 13.

Table 4.1 Composition of each feature group for pixel-based classifications

Feature groups	Group 1	Group 2	Group 3	Group 4	Group 5
Included features	Raw	Raw+NDVI+NDWI	Raw+Variance b1+Data range b3	Raw+NDVI+NDWI+ Variance b1+Data range b3	Raw+ all texture

In order to perform supervised classifications, the SVM classifier implemented in ENVI (Exelis Visual Information Solutions, 2013g) was employed. This adopts the pairwise comparison strategy to perform multi-class classification. It is also referred to as the "one against

one" approach (Pal & Mather, 2005), aiming to classify each pixel into one of the two classes until all possible 2-class combinations are exhausted, followed by a majority voting to determine the final membership of the pixel. Compared with the "one against the rest" alternative, the training process for "one against one" is less time consuming and better at handling large dataset (Samadzadegan et al., 2010). Therefore, the SVM classifier in ENVI was considered suitable for this study.

According to Hsu, Chang, and Lin (2010), the RBF (Radial Basis Function) kernel of SVM is the first choice among all the available options, due to its generality and relative ease of configuration. Owing to the fact that the number of features used as input to the SVM classifier is relatively limited, which does not exceed 13 in any case, the RBF kernel is a feasible solution. As for the kernel parameters selected for the classifier, the set of default values were adopted, which means Gamma was the reciprocal of the number of features, penalty parameter was 100.00, and pyramid level was 0. According to ENVI HELP (2013), the Gamma parameter is a positive floating point value used to configure the kernel function, while the penalty parameter is a positive floating point value that specifies the extent of tolerance for training errors (higher values force rigid margins and create models that might not generalize well, and vice versa). The pyramid level parameter is used to set the number of hierarchical processing levels in the process of SVM training and classification: if it is zero, the image will be processed at full resolution only; otherwise, the image will be classified at a lower resolution and reclassified at a higher resolution if the probability threshold is not met.

After the parameterization strategy for SVM was determined, a series of classifications were performed for both 2004 and 2012 IKONOS images based on the feature groups in Table 3.1. In order to evaluate the quality of the classified maps, the error matrix approach was taken,

which requires the use of testing samples to determine the accuracy of the thematic maps of interest. Following a multinomial distribution, the following equation was used to determine the number of testing samples (Congalton & Green, 2009):

$$n = \frac{B\Pi_i(1-\Pi_i)}{{b_i}^2} \quad (4.2)$$

where n is the total number of pixels required for the accuracy assessment, Π_i represents the fractional percentage of the class with the coverage of closest to 50% of the study area among all the k classes, b_i is the expected level of precision, B is derived from chi-square table with one degree of freedom and 1-α/k, and α is the desired confidence interval.

Since the class proportion was not known *a priori*, the "worst case scenario" was applied, which means Πi was set as 50%. Therefore, to calculate the number of samples required in each class, with a confidence interval of 95% and anticipated precision of 5%, the following calculation was carried out:

$$n = \frac{B\Pi_i(1-\Pi_i)}{{b_i}^2} = \frac{7.568 \times 0.5(1-0.5)}{0.05^2} \approx 757$$

After the total number of ground reference pixels was divided by the number of classes, the average number of samples per class was determined to be approximately 95. Due to the fluctuating coverage of the individual land cover classes, the actual number of testing samples for each class varied from 91 to 101, which did not deviate much from the calculated standard.

To reduce the "salt and pepper" effect present in many pixel-based classifications, the majority filter was used. As an attempt to explore its potential for improving the classification results, an iterative filtering approach was taken: for a given window size, the majority filter was

successively applied to the classified map, until the decrease of overall accuracy was observed (determined from confusion matrix). Since the majority filter with different window sizes conduct spatial aggregation of classified maps at different scales, two options were sought, including 3 by 3 and 5 by 5 moving windows. Due to the large number of candidate classifications, this iterative filtering operation was only applied to the classification based on original multispectral bands of IKONOS and the classification featuring the highest overall accuracy, such that the experiments did not become unnecessarily labour-intensive.

4.3.2 Object-based classification

With the development of advanced optical sensors, an increasing number of high spatial resolution imaging satellites were put into use in the recent decade. As a result, the objects of interest are more likely to be comprised of more than one pixel, which is the opposite case of that with medium or low resolution imagery. As an approach dedicated to classifying remotely sensed data in a spatial explicit manner, object-based image analysis (OBIA) has gained popularity as a result (Blaschke, 2010). In order to perform an OBIA, a fundamental technique called segmentation is used prior to any classification procedure. It aims to group adjacent pixels in an image into spatially and spectrally homogeneous objects of comparable size to the objects of interest, which are treated as basic entities in the classification process afterwards (Hay, 2001). According to Kartikeyan et al. (1998), image segmentation methods can be classified into two broad categories: local behavior-based and global behavior-based techniques. The former approaches the problem by focusing on the local variation of spectral signatures, while the latter performs the segmentation by analyzing the image characteristics from a holistic point of view. The local behavior-based segmentation algorithms can be further divided into two classes: region extraction and edge detection (Fu & Mui, 1981). The region extraction techniques present image

objects as homogeneous patches through one of the three approaches, including region dividing, region growing, and hybrid approach. The edge detection methods aim to identify the boundaries between adjacent objects by maximizing the spectral variation around the edges (Yu et al., 2006). After the segmentation is completed, various classifiers can be used to classify the individual objects into a group of predefine classes, which is similar to the pixel-based classification process, except that the basic classification units are objects rather than pixels.

The feature extraction module in ENVI 5.0 (Exelis Visual Information Solutions, 2013g) was used as the object-based classifier in this study. It implements an edge detection and an intensity based approach toward the segmentation problem, followed by either rule based or example based classification. The rule based classifier essentially acts as an expert system where the knowledge about the spectral, spatial, and textural characteristics of the individual classes need to be provided explicitly by an expert. The example based classifier relies on the examples of each class specified by the user, which are similar to the regions of interest (ROI) in pixel-based supervised classifications. Due to the fact that the performance of rule based classifier is subject to users' judgements to a great degree, it was considered less suitable than the example based classifier for this study.

The intensity based segmentation is more suitable for images with slight gradients such as DEM (Exelis Visual Information Solutions, 2013g), which is not the case with multispectral satellite imagery; therefore, the edge detection option was adopted in this study. The scale level associated with the edge detection segmentation determines the size of the image segments. The strategy followed to evaluate the optimal scale parameter was to maximize the scale level on condition that each segment include only one type of cover. For the merge setting, two merging algorithms are available: Full Lambda Schedule and Fast Lambda (Exelis Visual Information

Solutions, 2013g). They both aim to further increase the size of the homogeneous image objects after the edge based segmentation, based on the spectral and spatial information of the image objects. However, due to the fact that the latter option is a simplified version of the former, the Full Lambda Schedule was adopted as the merging algorithm.

Similar to the criterion used to determine the optimal scale parameter, the merge level was also selected to maximize the size of the image objects without having to combine multiple image segments that belong to different classes. As for the texture kernel size, it determines the size of the moving window within which the texture measures are computed. Through a trial and error process, the five by five window was found to be better at capturing local spectral variations of the image than the three by three window. Due to the limited time allocated for this study, experiments were not made with other window sizes for the segmentation. When it comes to the input features fed to the object-based classification, two groups of features were used: the first group includes the four multispectral bands of IKONOS imagery, while the second group was comprised of the original multispectral bands and NDVI as well, which could potentially contribute to the improvement of classification accuracy.

As can be seen from the segmentation parameters listed in Table 4.2, the scale and merge level for the 2004 and 2012 multispectral images are quite similar, due to relatively stable image structure of the unchanged areas. As for the variations in the segmentation parameters, they are likely to be the result of varying spatial homogeneity over time, possibly caused by phenological discrepancy and land cover changes. Furthermore, the employment of NDVI as an additional input feature did not result in much change in the segmentation parameters, since it is essentially a derivative from the original multispectral imagery.

Table 4.2 Segmentation parameter settings for the object-based classifications

Segmentation Parameters		Segment Setting		Merge Setting		Texture Kernel Size
		Algorithm	Scale Level	Algorithm	Merge Level	
2004 image	Without NDVI	Edge	42	Full Lambda Schedule	92	5
	With NDVI	Edge	42	Full Lambda Schedule	93	5
2012 image	Without NDVI	Edge	43.5	Full Lambda Schedule	87.5	5
	With NDVI	Edge	43.5	Full Lambda Schedule	87.5	5

What followed the segmentation procedure was the classification, based on K Nearest Neighbour (KNN) technique. There are two alternative classifiers implemented in ENVI (Exelis Visual Information Solutions, 2013g), which are PCA and SVM respectively, but they turned out to be less accurate than the KNN method upon initial testing. As a nonparametric supervised classifier (McDermid et al., 2005), KNN takes account of a number of characteristics of the individual image objects when it performs the classification, such as spectral, spatial, and textural features. Besides the training samples, it requires the K parameter as a user input, which specifies the number of nearest neighbours of each image object in the multidimensional feature space that contribute to the classification. Since K is an odd number, the membership of each image object is determined by the most popular votes given by the K neighbours. In order to achieve the best classification performance from KNN, a benchmark approach was employed that involves a series of different K parameters, ranging from one to seven. Due to the fact that the size of the training sample could also affect the quality of the classified maps, two sets of

training samples were collected for the classifications, with the large ROI group containing almost twice as many samples as the small ROI group. As an attempt to understand how the influence of the majority filter varies from pixel-based to object-based classifications, the iterative filtering operation was also performed for the object classification that features the highest accuracy among its peers. It should be noted that the accuracy assessment of the object-based classifications was conducted the same way as that for the pixel-based classifications, since the classified maps were considered equivalent as mapping product.

4.4 Change/no change discrimination

Due to the multitude of available change detection methods with various levels of reported accuracy, the CVA and image differencing techniques are selected to derive qualitative change information for the study area. The main reason why they are adopted in this study is attributed to their relatively simple structure and ease of configuration, thus contributing to the application of the Getis statistic as a spatial filter as well as the interpretation and evaluation of associated results. In addition, the comparison between CVA and NDVI based image differencing could shed light on whether the multitude of input channels or a single sensitive change indicator is more appropriate for this study. Furthermore, the two different implementations of image differencing serve the purpose of examining how change detection analysis can be influenced by taking possible discrepancy between positive and negative changes into consideration.

4.4.1 Change vector analysis

Originally proposed by Malila (1980) for forest change detection, change vector analysis (CVA) appeared as an unsupervised change detection method that could produce both qualitative and quantitative results. Like most of the other digital change detection methods, change vector

analysis takes advantage of the changes of spectral features as the results of land cover changes. Unlike the case with any method that involves classification of remotely sensed data, where the input of training data is mandatory, CVA can be used independently of any training process. According to the individual researcher's configuration, CVA can take any number of change indicators as input that are deemed useful to the detection of land cover changes. In other words, it is designed to make better use of the information contained in the multidimensional feature space of remotely sensed data, compared with some less sophisticated change detection algorithms such as image differencing and image ratioing. Nevertheless, it remains to be explored whether this more sophisticated technique could lead to higher accuracy in change detection studies.

Due to the small number of bands available in IKONOS imagery (only four) compared to hyperspectral imagery, the potential for image transformations is relatively limited. Horne (2003) derived the Tasselled Cap transformation coefficients for IKONOS imagery, but the interpretation of the output features are different from that of the Landsat TM, due to the lack of information from the mid-infrared portion of the spectrum. Therefore, the original multispectral channels of IKONOS were used as change indicators, and the change magnitude was calculated using the following equation:

$$\text{Magnitude} = \sqrt{{b_1}^2 + {b_2}^2 + {b_3}^2 + {b_4}^2} \qquad (4.3),$$

where b_1, b_2, b_3, and b_4 stands for the difference image associated with the blue, green, red, and near-infrared band respectively.

Without any prior knowledge about the types of land cover change, it would be relatively difficult to conduct change type categorization based on the change angles derived from CVA,

no matter whether supervised or unsupervised method were employed. Therefore, only the change magnitude was used as part of the change/no change classification. As for the algorithm used in conjunction with the CVA to produce the binary classification, supervised classifier SVM was favoured over the empirical thresholding approach because one is able to avoid the trial and error process yet also handle the learning of the image interpreter's knowledge based on the selected training sites. Since there was only one input feature for this binary change/no change classification, the RBF kernel of the SVM classifier was considered appropriate (Hsu, et al., 2010). The default settings for the kernel parameters were adopted: Gamma was the reciprocal of the number of features, penalty parameter was 100.00, and pyramid level was 0. For the sake of fair comparison, the SVM classifier with the RBF kernel and the corresponding default setting was used consistently for the change/no change classification in the subsequent analysis as well, such that the emphasis of this study could be placed on the usefulness of the individual change indicators.

When it comes to the collection of training samples for the differentiation between changed and unchanged pixels, three classes were taken account of: unchanged, positive change, and negative change. For CVA and 2-class implementation of the image differencing method, the training samples associated with the positive and negative change were combined together, while they were kept separated otherwise. Accordingly, efforts were made to include pixels representing various types of changes in the positive and negative change class, thus the spectral variability within each group could be captured. Similarly, pixels representing different types of unchanged land covers were collected as training samples for the unchanged class, so as to account for the potential subtle differences between various unchanged pixels in terms of their spectral characteristics.

4.4.2 Image differencing

Considering the dominance of vegetation in the study area, NDVI was selected as the most promising change indicator to be used in conjunction with image differencing technique. After all, the determination of forest, plantation, and pasture related changes are of great interest to conservation practitioners and relevant policy makers. The image differencing was performed by subtracting the 2004 NDVI image from the 2012 NDVI image. In order to examine how the results of change/no change discrimination respond to the separation of positive and negative changes in the classification process, two different implementations of the image differencing technique were made. The first one aims to classify the difference image into two classes: changed and unchanged, while the second one has a 3-class classification scheme: unchanged, positive change, and negative change.

For the 2-class implementation, the absolute value of the NDVI difference image was used as input to the SVM classifier, which is essentially equivalent to the change magnitude in CVA with NDVI being the only change indicator, where smaller values represent minimal change in NDVI and vice versa. On the contrary, for the 3-class implementation, the original NDVI difference image was classified directly by SVM. It should also be noted that the positive and negative change class were combined subsequently for consistent performance evaluation of the various change indicators, since a binary change/no change map is the deliverable of the change/no change discrimination step.

4.4.3 The Getis Statistic used as a spatial filter for change detection

4.4.3.1 Derivation and formulation of the Getis statistic

As an early benchmark of spatial association, initial implementation of global spatial autocorrelation measures, such as Moran's I, were derived for an entire image, which assumes

spatial dependence or stationarity (Getis & Ord, 1992). In order to examine local spatial patterns, however, local indicators of spatial association need to be used as complementary information. They express local clusters of dependence that remains undetected otherwise. The Getis statistic is first defined by the following equation:

$$G_i(d) = \sum_{j=1}^{n} w_{ij}(d)x_j / \sum_{j=1}^{n} x_j, \qquad \text{j not equal to i,} \tag{4.4}$$

where d is the lag distance used to determine the size of the moving window, w_{ij}(d) is a spatial weights matrix where cells within the moving window have the value of one while cells outside the window are assigned the value of zero, n represents the number of cells within the study area, and x_j stands for the spatial variable of interest. It should be noted that at the time when this method was first introduced, it was not intended for remote sensing applications but rather analysis of spatial patterns for medical studies of HIV. Therefore, the term "n" in the equation is interpreted as the number of cells or regions within the area of interest, which are represented by a single variable of interest stored as point form data. Another version of the Getis statistic is denoted by symbol $G_i^*(d)$, and the only difference between them is that $G_i^*(d)$ includes the central pixel of the moving window into the summation as numerator of the definition equation, while $G_i(d)$ does not (Getis & Ord, 1992).

In the context of remote sensing applications, the notion of $G_i^*(d)$ is used in favour of $G_i(d)$, because it derives the statistic based on the window with user-defined dimensions (Wulder & Boots, 1998). Nevertheless, the most commonly used form of the Getis statistic in remote sensing literature is the standardized version of $G_i^*(d)$, which is defined by the following equation:

$$G_i^*(d) = \frac{\sum_j w_{ij}(d)x_j - W_i^*\bar{x}}{s\left[\frac{W_i^*(n-W_i^*)}{n-1}\right]^{\frac{1}{2}}} \quad (4.5)$$

where d is the lag distance used to determine the size of the moving window, $w_{ij}(d)$ is a symmetric spatial weights matrix where pixels within the moving window have the value of one whereas other pixels in the image are assigned the value of zero, x_j is used to express the spatial variable of interest, $\bar{x}$ is the mean of the entire image, n is the number of pixels within the image, W_i^*represents the number of pixels within the moving window, and s is the global standard deviation. After the standardization, large negative values of G_i^* represent clustered pixels with low values, while large positive values of G_i^* represent clustered pixels with high values (Ord & Getis, 1995).

According to Getis and Ord (1992), a key property of the Getis statistic is that it is scale-invariant, but not location invariant. That is to say, if the variable of interest is multiplied by a non-zero coefficient to create a new variable, the same Getis score will be obtained for each cell as the previous variable. Nonetheless, if a certain non-zero number is added to the variable of interest, different results for the Getis statistic will occur. The null hypothesis behind the Getis statistic is that the set of x values within d of location i is a random sample retrieved without replacement from the set of all x values. In addition, it is worth mentioning that it is designed for variables with natural origin, and transformation like log functions might create erroneous results. The statistical significance level of the statistic for the vicinity of a certain pixel relies on its deviation from the global mean. If the window size is too large, the data points around the individual grid cells become highly clustered, which lowers the relative significance of the numerator in the Getis equation. In other words, as the expectation for the Getis statistic

increases along with the increased size of the moving window, the local clustering effect is neutralized. Due to the incorporation of a moving window in the definition of the Getis statistic, the statistic value of neighbouring cells are unavoidably correlated, since they share a fair number of cells in their vicinities (Getis & Ord, 1992).

4.4.3.2 Application of the Getis statistic on change indicators

Due to the intrinsic property of the Getis statistic as a tool capable of presenting relatively homogeneous "hotspots" within remote sensing imagery, it is interesting to examine how it could change the characteristics of the difference image and the accuracy of change/no change discrimination as a result. Therefore, the Getis statistic was calculated for the change magnitude derived from CVA as well as the NDVI difference image, including both the 2-class and 3-class implementations. In order to assess the influence of varying window sizes on the application of the Getis statistic in the context of change detection, the binary change/no change classification was performed on the Getis images derived from an assortment of window sizes, ranging from three by three to nine by nine.

As an attempt to investigate the possibility of determining the optimal window size in an automatic fashion for change detection applications, the concept of the maximum Getis image (LeDrew, Holden, Wulder, Derksen, & Newman, 2004), which literally extracts the maximum Getis values over a group of Getis images calculated with varying window sizes, was implemented and used to produce change/no change maps. Since G_i^* values with a large magnitude represents clustered pixels with high or low values in the original images, G_i^* values that deviate furthest from zero represent an extreme state of pixels, which could potentially lead to improved separability of pixels located on the two tails of the distribution. In light of this idea, the extreme Getis value for each pixel across multiple window sizes were selected to compose

the extreme Getis image, which was also classified by SVM for the three groups of image features. To be specific, for any pixel whose G_i^* values are positive across the Getis image stack, the maximum Getis value will be selected to form the extreme Getis image, while for the rest of the pixels in the image, the minimum Getis value across the Getis image stack will be selected instead. Thus, the separability between pixels towards the tails of the histogram and those near the peak can be enhanced.

Compared with the conventional definition of the maximum Getis image, the extreme Getis image was deemed more likely to improve the accuracy of change detection applications. In order to assess the usefulness of the extreme Getis statistic, it was applied on the CVA change magnitude image, the 2-class NDVI difference image, and the 3-class NDVI difference image. Therefore, a total of seven binary classifications were performed on each of these three change indicators, including one based on the original feature, four based on the Getis images derived from different window sizes, one based on the maximum Getis image, and the last one based on the extreme Getis image.

4.4.4 Accuracy assessment of change/no change discrimination

As a quality control procedure, accuracy assessment is of critical value to this study, since the reliability of the accuracy measures directly influences the understanding of the performance of the proposed methodology. Considering the deliverable of the change/no change discrimination analysis to be a binary map, the accuracy assessment approach proposed by Ginevan (1979) for binomial distribution was deemed a feasible solution. Based on a predetermined lookup table, it takes four parameters to determine the number of testing samples required for the accuracy assessment, which are Q_1, α, Q_2, and β. Q_1 and α represents the anticipated higher accuracy bound and the associated confidence interval respectively, while Q_2

and β stands for the anticipated lower accuracy bound and the corresponding confidence interval. In this study, we take a one in a hundred risk (Q_2) of accepting a classification with an overall accuracy lower than 85% (β) and a one in a thousand risk (Q_1) of rejecting a classification with an overall accuracy higher than 95% (α); therefore, 239 ground reference points are required to populate the error matrix with 23 of them allowed to be misclassified. The number of ground reference points per class was further increased to 120 to make them even. Similar to the case with training sample collection for the binary change/no change classification, the variability within both the changed and unchanged class was taken into consideration when testing samples were selected, such that the reliability of the accuracy assessment could be ensured. The overall accuracy and kappa coefficient were calculated based on the confusion matrix corresponding to each binary classification, which were used to assess the performance of each candidate.

4.5 Change type categorization

In order to derive quantitative change information from the study area, which is not available from either CVA change magnitude or image differencing, post-classification comparison was conducted to depict transitions from one type of cover to another. However, the post-classification comparison approach was not used as an independent method towards the change detection analysis. Instead, its performance in differentiating between changed and unchanged areas was compared to the best result derived from the change/no change discrimination phase of this study. Since there are eight types of land cover in the classification scheme designed for this study, it is difficult to evaluate the performance of post-classification comparison with a complete change error matrix, which necessitates eight types of unchanged and 56 types of changed samples to populate (Congalton & Green, 2009). Therefore, this comparison not only allows for the accuracy assessment of the post classification approach, but

also sheds light on how it can be used in conjunction with change detection techniques aimed at change/no change differentiation.

Due to the large number of classified maps derived from the supervised classification stage of this research, the post-classification comparison was established on several representatives from the pool of candidates. The first comparison was made between the two classified maps that feature the highest overall accuracy in 2004 and 2012 respectively. The second pair of images used for the comparison was the most accurate classification from the object-based group for 2004 and 2012 image respectively. The third pair was constituted by the most accurate object-based classifications without the use of any majority filter. The fourth pair was comprised of the most accurate classifications from the pixel-based group. Similar to the case with the third pair, the fifth pair consisted of the most accurate pixel-based classifications without the application of any majority filter. The sixth and seventh pair respectively corresponded to the classifications based on original multispectral bands of IKONOS imagery with and without the use of majority filter. Thus, insights could be obtained on the quality of the individual classifications from change detection perspective, rather than from a single date mapping point of view.

After the seven pairs of classifications were selected for post-classification comparison, the accuracy assessment of the produced binary maps was conducted in the same way as the other change/no change discrimination products. It was assumed that the classification pair associated with the most accurate change/no change map would also produce the most accurate information regarding transitions between various types of land cover. Afterwards, a change mask was generated based on the binary map that features the highest overall accuracy, no matter whether it was derived from CVA, image differencing, or post-classification comparison. The most useful

pair of classifications was then used to categorize the changed pixels into a variety of transition classes, providing the quantitative change information.

4.6 Summary of the procedural choices leading to the best practice

As with many research projects, the final methodology varies from that first adopted as lessons are learned and procedures are tested. In order to summarize the various procedural choices made during the course of this study that have led to the most accurate results, an updated flowchart is presented in Figure 4.5. This is to be compared to the initial methodology presented in Figure 4.1 and includes the results of exploratory testing and modifications as appropriate.

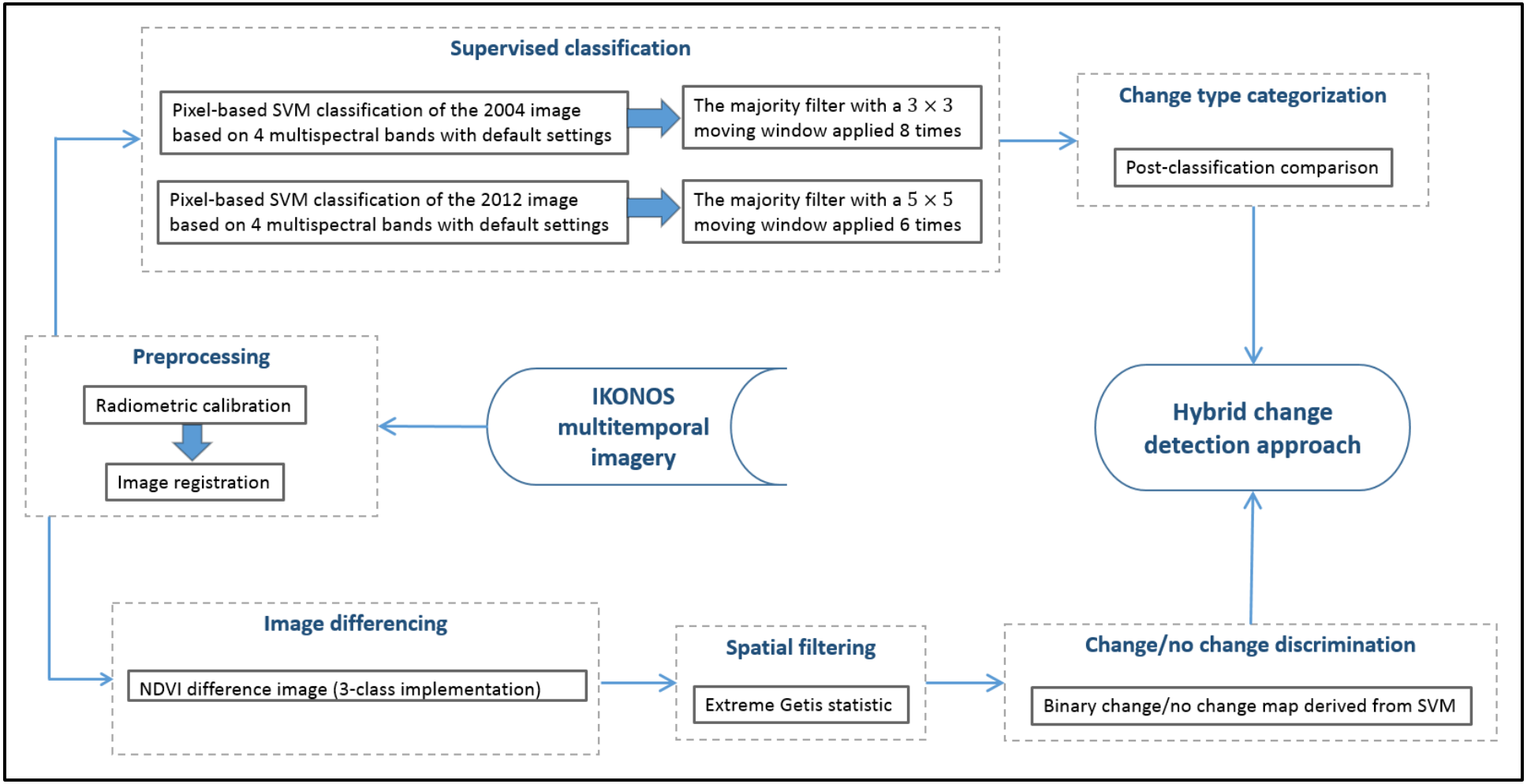

Figure 4.5 Updated flowchart delineating the decision in each step that resulted in the best practice

Chapter 5

Results and Discussion

In this chapter we present the major findings of this study as well as discussion of the strengths, weaknesses, and uncertainties of the various analyses performed in this study, which can be divided into four sections: supervised classifications, change/no change discrimination, post-classification comparison, and land cover change interpretation. The first section covers classification results generated from pixel-based and object-based classification techniques. The second section mainly includes binary change maps generated from CVA, image differencing, as well as the derivatives based on the Getis statistic. The third section features a performance assessment of the post-classification comparison approach based on different classification pairs, thus shedding light on some intrinsic problems associated with the post-classification comparison method. The last section focuses on the interpretation and assessment of land cover changes occurring in the Big Creek area from 2004 to 2012 according to the change maps and transition matrix as final deliverables of this study.

5.1 Supervised Classifications

5.1.1 Pixel-based classification

Despite the sound theory behind SVM, its effectiveness in land cover classification tends to vary from one case to another. With a classification scheme entailing several classes with similar spectral signatures, it would be particularly challenging to sustain a relatively high accuracy with SVM or any other modern classifiers adopted in the remote sensing community. Figure 5.1 shows an example of SVM classification based on the multispectral bands of the 2004 IKONOS image. In the top right corner of the image, some of the agricultural fields are misclassified as

orchard and pasture. In addition to the fact that these three classes all fall into the category of vegetation from species point of view, their aggregated spectral characteristics at four-meter resolution could result in even more confounding spectral manifestations than what is measured with handheld spectrometers in near range. For example, different spacing between the individual plants in a field, the status of the soil background as well as recent moisture conditions could lead to varying spectral properties of the same type of cover, even within the same study area. In addition, the phenological variation of vegetation might contribute to fluctuating level of separability between distinct types of vegetation. Owing to the relatively sparse spacing between trees in a plantation site, which is comparable to the four-meter resolution of IKONOS, the plantation structures show great intra-class variability in terms of its spectral properties, ranging from bare soil to trees. Without the incorporation of any texture measure in a pixel-based classification, it would be particularly difficult to avoid the misclassification associated with plantations.

Although the plantation sites depicted in red in the classified map are differentiated from forest, a number of pixels representing shadow areas in the forest are also misclassified as plantation, exemplifying the "salt and pepper" effect in the current classification. As can be seen from the standard false color composite image in Figure 5.1, the plantation sites generally have darker tone than the surrounding forest, which are spectrally similar to canopy gaps in the forest stand. Therefore, it would be challenging to discriminate between canopy gaps and plantation without considering their spatial characteristics, which essentially calls for the employment of object-based classification. Due to the various problems associated with this classification, it has a relatively low overall accuracy and kappa coefficient, which are only 79.0% and 0.76 respectively. Similar to the case with the 2004 IKONOS image, the SVM classification based on

the raw multispectral bands of the 2012 image does not have very good reliability, indicated by its overall accuracy of 80.5% and kappa coefficient of 0.78.

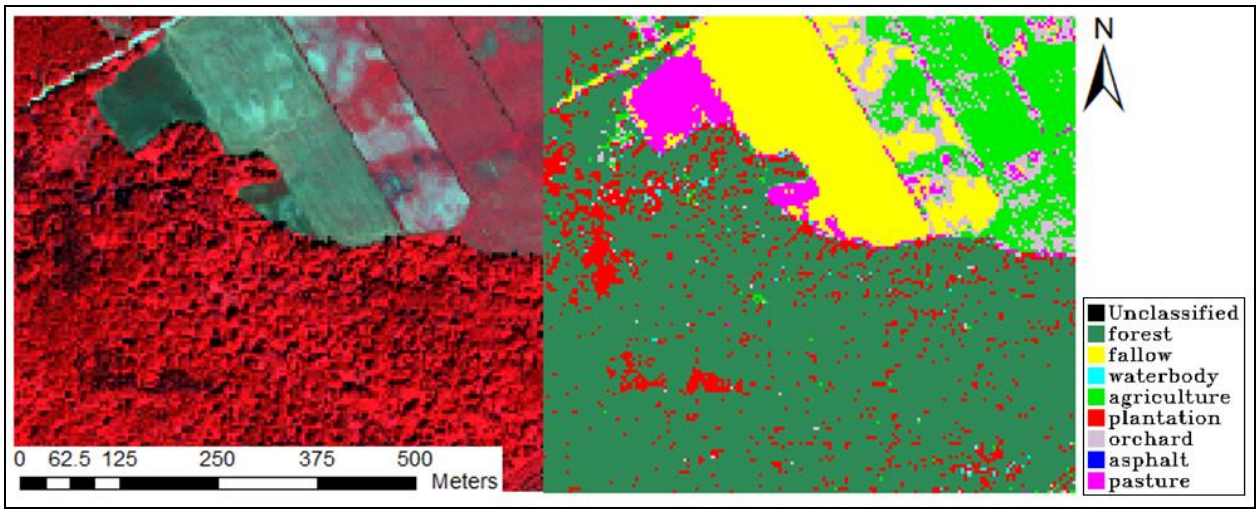

(a) IKONOS standard false color composite (b) SVM classification

Figure 5.1 Illustration of problems with SVM based on multispectral bands of IKONOS

According to data presented in Table 5.1, the addition of NDVI and NDWI into the feature group does not improve the overall accuracy of the SVM classification performed on the 2004 image, since the feature group consisting of raw multispectral bands, NDVI and NDWI and the one that only contains multispectral bands result in the same overall accuracy and kappa coefficient. The reason why the addition of NDVI and NDWI does not lead to more accurate classification could be attributed to the lack of additional discrimination power for the current classification scheme, especially between the several vegetated classes suffering from relatively high misclassification rates. On the other hand, the employment of texture features does prove useful for the classification of the 2004 image. Compared with the original feature group, the group with the textural supplement of band 1 variance and band 3 data range has increased the overall accuracy and kappa coefficient of the classified map to 84.2% and 0.82 respectively. The classification with the highest overall accuracy for the 2004 image is based on the feature group consisting of four multispectral bands and all the texture bands, featuring an overall accuracy of

84.6% and a kappa coefficient of 0.82. As for the group comprised of multispectral bands, NDVI, NDWI, as well as the two selected texture bands, it has an overall accuracy of 83.9% and a kappa coefficient of 0.82, which is also more accurate than the results obtained by the two feature groups without any texture band. However, it has the lowest accuracy among the three groups equipped with texture features, which indicates the minimal contribution of the two spectral indices.

Table 5.1 Accuracy of the 2004 pixel-based classifications

Pixel-based 2004 classifications	Raw	Raw + NDVI + NDWI	Raw + Variance b1 + Data range b3	Raw + NDVI + NDWI + 2 texture	Raw + all texture
Overall accuracy	79.0%	79.0%	84.2%	83.9%	**84.6%**
Kappa coefficient	0.76	0.76	0.82	0.82	**0.82**
Rank	4	4	2	3	**1**

In Table 5.2 we present a more detailed examination of the two classifications based on raw feature group and the one containing multispectral bands and all the texture bands respectively. For forest, fallow, water body, and plantation, the two classified maps generally have comparable user's accuracy and producer's accuracy, indicating stable performance of SVM over these classes regardless of the use of texture features. Due to their unique spectral signatures, it is very likely that the spectral information in the raw IKONOS image alone is sufficient to identify them with a relatively high accuracy. By contrast, classification of the other classes in the classification scheme benefits from the addition of texture measures to a certain degree, with various levels of increase in user's and producer's accuracy. Although the user's accuracy of the asphalt class records a decrease from 93.5% to 92.2%, the change is minimal

compared with the increase of its producer's accuracy from 86.0% to 94%, which indicates the improved ability of the classifier to assign asphalt pixels into the corresponding class.

Table 5.2 Performance of SVM based on two selected feature groups for the 2004 image

Class-specific accuracy scores	Multispectral bands only		Multispectral bands and all texture features	
	Producer's accuracy	User's accuracy	Producer's accuracy	User's accuracy
Forest	88.1%	79.5%	87.1%	80.0%
Fallow	96.0%	95.1%	94.0%	95.9%
Water body	93.1%	91.3%	93.1%	97.9%
Agriculture	79.2%	55.2%	83.2%	73.0%
Plantation	97.0%	94.2%	97.0%	94.2%
Orchard	31.7%	43.8%	64.4%	61.9%
Asphalt	86.0%	93.5%	94.0%	92.2%
Pasture	61.4%	81.6%	64.4%	85.5%

Similar to the case with the classifications performed on the 2004 IKONOS image, the addition of texture measures in the input feature group derived from the 2012 image results in consistent improvement of the overall accuracy by approximately 7%, which can be seen from Table 5.3. Nevertheless, the feature group consisting of raw spectral bands and all texture features does not lead to the most accurate classification of the 2012 image. On the contrary, the other two groups comprising the texture information boasts the highest accuracy among the five feature group candidates, with an overall accuracy of 87.4% and a kappa coefficient of 0.86. In comparison to the group with two additional spectral indices, the feature group consisting of multispectral bands of IKONOS and two texture features are deemed of higher quality, since it has relatively stable performance in the classification of both 2004 and 2012 images. In addition, the fewer number of input features also means higher efficiency in the classification process.

Therefore, the classification based on four multispectral bands and two texture measures are considered as the best practice for the 2012 image. As a matter of fact, the use of NDVI and NDWI has reduced the overall accuracy from 80.5% to 80.1% and the kappa coefficient from 0.78 to 0.77 in the classifications of the 2012 image based solely on spectral information, which implies their negative impact on the classification. Considering the comparable performance of these two spectral feature groups in the case of the 2004 image classification, it is suspected that NDVI and NDWI are not useful for SVM classifications of a typical rural scene in Southern Ontario based on IKONOS images, unless their contribution to the classifications was limited by the selected kernel and hyperparameters associated with SVM. That being said, they might be valuable in land cover classifications of images with coarser spatial resolution, based on a different classifier, or for a different environment, a conjecture which would require more experimentation to validate.

Table 5.3 Accuracy of the 2012 pixel-based classifications

Pixel-based 2012 classifications	Raw	Raw + NDVI + NDWI	Raw + Variance b1 + Data range b3	Raw + NDVI + NDWI + 2 texture	Raw + all texture
Overall accuracy	80.5%	80.1%	**87.4%**	**87.4%**	86.9%
Kappa coefficient	0.78	0.77	**0.86**	**0.86**	0.85
Rank	4	5	**1**	**1**	3

According to Table 5.4, the addition of texture features into the input feature set is able to improve the producer's accuracy and user's accuracy in most cases, especially for classes that suffer from low accuracy in the original classification, such as orchard and asphalt. As for the occasional drop of producer's accuracy or user's accuracy for certain classes, it is accompanied

by the decrease of commission or omission errors with greater magnitude. For example, the producer's accuracy of fallow decreased from 94.0% to 91.0% after the texture features were incorporated into the input feature set, but the corresponding commission errors were reduced from 17.5% to 3.2%. This observation is consistent with the trend identified from the 2004 classifications, which confirms the enhanced performance of SVM resulting from the employment of texture features. This improvement can be essentially attributed to the supplementary information fed to the classifier, which functionally increases the separability between classes which are originally difficult to differentiate. For example, the significant improvement of asphalt's user's accuracy in the 2012 image could be associated with the contrast between roads and their surroundings captured by the variance image of band 1, which is unavailable in spectral features alone. In addition, the hypothesis that the use of data range of band 3 could contribute to more accurate mapping of impervious surface is partially validated not only by the improved user's accuracy of asphalt in both the 2004 and 2012 classifications, but also the relatively compact and homogeneous presentation of the residential areas in the classified maps shown in Figure 5.2.

Considering the significant influence of land cover classifications on the performance of the post-classification comparison approach, efforts should be made to explore the full potential of the classifier of choice, which necessitates the selection of the most useful features for the classification. As a technique that is gaining popularity in the remote sensing community in the recent decade, the random forest approach proposed by Breiman (2001) has a unique capability for assessment of the relative contribution of each feature involved in a random forest classification, which can be used as either a classifier or a standalone feature selection method. Instead of having to rely on an image interpreter's visual examination of the potential input

features, random forest has the advantage of performing feature selection automatically and objectively in an efficient manner, which is especially valuable under circumstances where a large number of input features are dealt with. In addition, visual interpretation of an image focuses on the characteristics of the image itself, thus remaining independent of the classification to be performed afterwards. Therefore, it would be difficult to attribute a certain portion of observed performance boost to a specific input feature if a group of features are added into the feature group all at once. Although random forest does not qualify as a physical based feature selection model, it is deemed a promising technique capable of quantitatively assessing the usefulness of various potential input features for the classification of remote sensing imagery. Accordingly, it could essentially lead to more accurate single date classifications, thus contributing to the improved accuracy of post-classification comparison in a change detection context.

Table 5.4 Performance of SVM based on two selected feature groups for the 2012 image

Class-specific accuracy scores	Multispectral bands only		Multispectral bands and two texture features	
	Producer's accuracy	User's accuracy	Producer's accuracy	User's accuracy
Forest	80.2%	80.2%	85.2%	84.3%
Fallow	94.0%	82.5%	91.0%	96.8%
Water body	100.0%	90.2%	95.1%	95.1%
Agriculture	91.0%	67.9%	96.0%	80.0%
Plantation	88.0%	79.3%	90.0%	84.9%
Orchard	35.2%	80.0%	69.2%	80.8%
Asphalt	75.3%	97.4%	95.1%	95.1%
Pasture	76.2%	73.3%	76.2%	82.8%

Upon visual interpretation of the two best classified maps derived respectively from the 2004 and 2012 IKONOS image in Figure 5.2, phenological discrepancy between the agricultural fields can be identified, which occupies a large portion of the scene. With only a few exceptions, almost all the agricultural fields went through the transition from fallow in 2004 to vegetated in 2012, due to the extensive crop coverage. In addition, the spatial distribution of the major land covers in the study area can be determined from the classified maps, such as residential areas depicted in blue and forest depicted in sea green. A drawback worth noting from the two classified maps is the presence of the "salt and pepper" effect, despite the fact that these two classifications feature the highest overall accuracy among all the classifications performed for each date. Consequently, it would be relatively difficult to extract homogeneous patches of changed land by overlaying these two classified maps on top of each other, which gives rise to the subsequent step in the analysis.

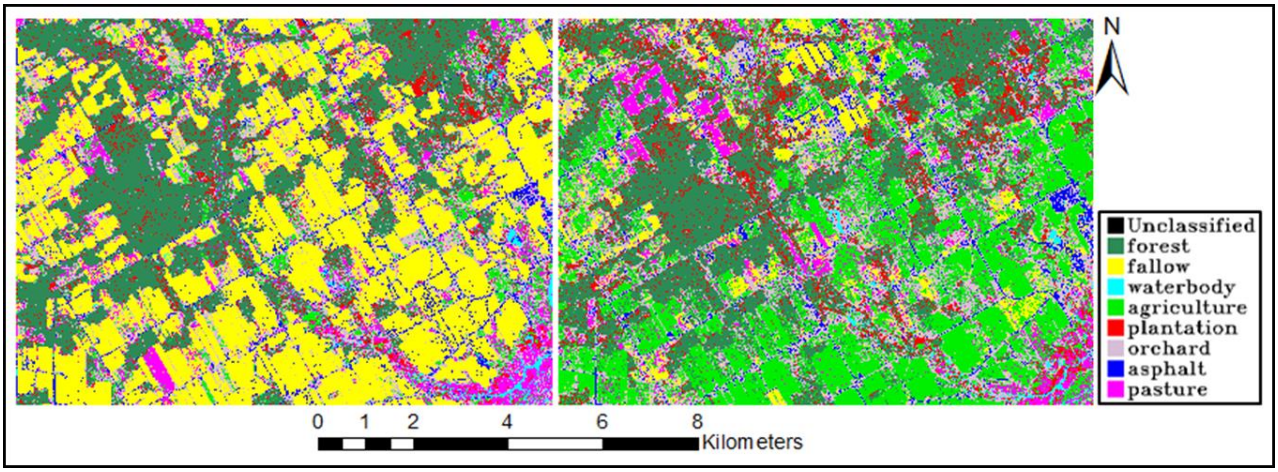

(a) 2004 best classification (b) 2012 best classification

Figure 5.2 Comparison of the best classified maps for the 2004 and 2012 IKONOS image

5.1.2 Object-based classification

An essential step involved in any object-based classification approach is the segmentation, which influences the quality of the classified map to a great extent. Figure 5.3 gives an example

of how the scale and merge level determines the segmentation results. After the scale parameter is specified, the image is first divided into a number of segments according to the spectral, textural, and spatial characteristics of the individual pixels. Due to great level of intra-class variability, forest appears highly fragmented with a scale parameter of 42. On the contrary, the adjacent fallow land remains relatively compact, owing to its low intra-class variability. Through a trial and error process, the scale parameter of 42 was considered as the most appropriate for the segmentation of the 2004 IKONOS image, since it is the maximum scale parameter without combining pixels belonging to different classes into a single segment. The spatially adjacent image segments are grouped together after the merge parameter is set, presenting the final image objects subject to the subsequent classification procedure. With a merge level of 93, the previous forest segments are partially combined, such that plantation sites within the forest stand can be differentiated. However, there are still small image objects within the forest stand, which represent gaps between closed canopies. As for fallow land, it looks more homogeneous after the merge level was specified as 93, since the small image segments within the patch were grouped into the surrounding segments to form a larger image object, which can be seen from Figure 5.3.

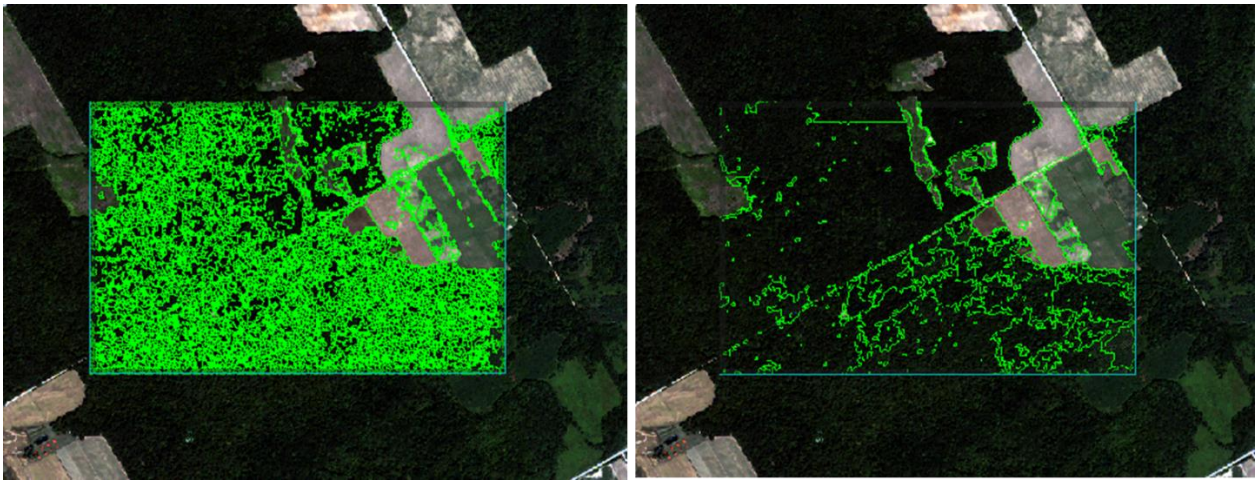

(a) Scale Level: 42, Merge level: 0 (b) Scale Level: 42, Merge level: 93

Figure 5.3 Illustration of segmentation process based on a subset of the 2004 IKONOS image

Similar to the case with pixel-based classifications, a benchmark approach was adopted to compare the performance of object-based classification produced with different settings. As can be seen from Table 5.5, a total of 32 object-based classifications were performed for the 2004 image based on different input features, various sizes of training samples, as well as miscellaneous number of nearest neighbours for the KNN classifier. Through the comparison of accuracy scores between the four columns ranging from KNN1 to KNN7 in Table 5.5, the number of nearest neighbours associated with the most accurate classification in each row can be determined, with the corresponding overall accuracy highlighted in bold. Among the classifications with the input of NDVI, the highest overall accuracy scores achieved within the large ROI and small ROI group are 88.2% and 90.6% respectively (highlighted in bold), while the counterpart scores among the classifications without NDVI as an additional feature are 86.0% and 88.8% respectively.

Based on the limited number of experiments conducted in this study, a universally optimal nearest neighbour was not found for object-based KNN classifications, since the optimal nearest neighbour varies from one to seven according to different input features and training samples. As more nearest neighbours are taken into consideration, the decision made by the KNN classifier becomes more dependent on the number of training samples collected for each class. Essentially, if the number of nearest neighbours was specified as the total number of objects in the image, all the image objects would be assigned to the class with the most training samples. Nevertheless, if only one nearest neighbour was used to determine the membership of each object, the results would be extremely prone to the errors induced by mislabelled training samples or large intra-class variability. Therefore, the determination of the optimal number of nearest neighbours for KNN classification involves a trade-off between making the classifier unnecessarily sensitive to

the variations within the training samples and blurring the boundaries separating different classes in the feature space. With the ability of finding the most appropriate K parameter based on a series of experiments, a benchmark approach is deemed suitable for this task. Since object-based classifications aim to assign the membership of the individual objects rather pixels in an image, the classification process is relatively quick, thus justifying the use of a benchmark approach.

Compared with the accuracy of the pixel-based SVM classification for the 2004 image, the object-based approach has shown superior performance: the most accurate classification in Table 5.5 has an overall accuracy of 90.6% (highlighted in red) and a kappa coefficient of 0.89. Considering the highest overall accuracy of 84.6% among the pixel-based 2004 classifications, almost all the object-based classifications performed on the 2004 image are more accurate than that, with the only exception being the classification with an overall accuracy of 84.5%, which is based on large training sample, original spectral bands of IKONOS, and a K parameter of only one.

Figure 5.4 presents a more graphical view of the performance of the individual object-based classifications of the 2004 image. It is obvious that the group based on the large training sample and the raw multispectral bands of IKONOS is the least accurate compared with the other three groups. In addition, the overall higher accuracy of classifications taking advantage of NDVI as an additional feature indicates the potential contribution of NDVI in object classifications, which is not the case with the pixel-based classifications. This discrepancy may be attributed to the distinctive classification units between these two classification paradigms: pixel-based classifications assign membership to the individual pixels, while object-based classifications deal with the image objects. Even if texture measures were extracted from the multispectral imagery as an attempt to incorporate local spatial autocorrelation information into the classification,

pixel-based classifiers would still treat each pixel as discrete points in the multidimensional feature space. On the contrary, the spectral, textural, and spatial metrics used as input features in object-based classifications are derived from the individual image objects. Therefore, the numerical signature (including spectral, textural, and spatial characteristics) of an object is determined collectively by the pixels contained in it, which is different from the numerical signature of most pixels in this object. Accordingly, NDVI could be very appropriate for differentiation between various types of vegetated covers in object classifications, although it did not bring extra discrimination power to the pixel-based SVM classifications in this study. In addition, the usefulness of a specific feature might be well related to the classifier under investigation. Since SVM and KNN was selected respectively for the pixel-based and object-based classifications in this study, they may have different levels of sensitivity to NDVI, which could also account for the fluctuating contribution of NDVI in pixel-based and object-based classifications employed in this study.

Another trend that can be identified from Figure 5.4 is the negative impact of larger training sample size on the classification accuracy, suggesting that the use of a relatively small training sample size would be appropriate for the 2012 image. Although a larger number of training samples would secure the accurate allocation of more objects selected as training samples, it may reduce the separability of objects belonging to different classes in the feature space, which would lower the overall performance of the classifier. For example, if water bodies highly influenced by sun glint were selected as training samples, these unrepresentative samples would possess a similar spectral signature to that of asphalt. As a result, real asphalt objects would be more likely to be classified as water bodies, since they might be closer to these unrepresentative water samples than the training samples collected for the asphalt class in the feature space. Therefore,

the overall accuracy of the classification might be compromised if unrepresentative objects were collected as training samples to enforce their allocations, especially if a relatively small K parameter was adopted. Considering the fact that the two classifications based on large ROI achieved their highest accuracy with a K parameter of five and seven respectively with and without NDVI in the feature group, uncertainties induced from the training samples are very likely to be the cause of decreased overall accuracy associated with the increased number of training samples in the experiment, which would bias the classifier to the greatest extent with a small K parameter.

According to this inference based on the results of the 2004 classifications, training samples selected from the 2012 image were maintained around the same quantity as the small sample collected for the 2004 classification, while no experiment was made with larger sample sizes. Table 5.6 shows the accuracy scores of the object-based classifications performed on the 2012 image. The most accurate classification features an overall accuracy of 88.8% (highlighted in red) and a kappa coefficient of 0.87, exhibiting better performance than its pixel-based counterpart, which has an overall accuracy of 87.4%. In addition, the optimal numbers of nearest neighbours do not coincide for the classification groups with and without the addition of NDVI. In terms of the general performance of the two groups, classifications making use of NDVI have higher overall accuracy and kappa coefficient in most cases, which confirms the usefulness of NDVI in object-based classification based on KNN classifier.

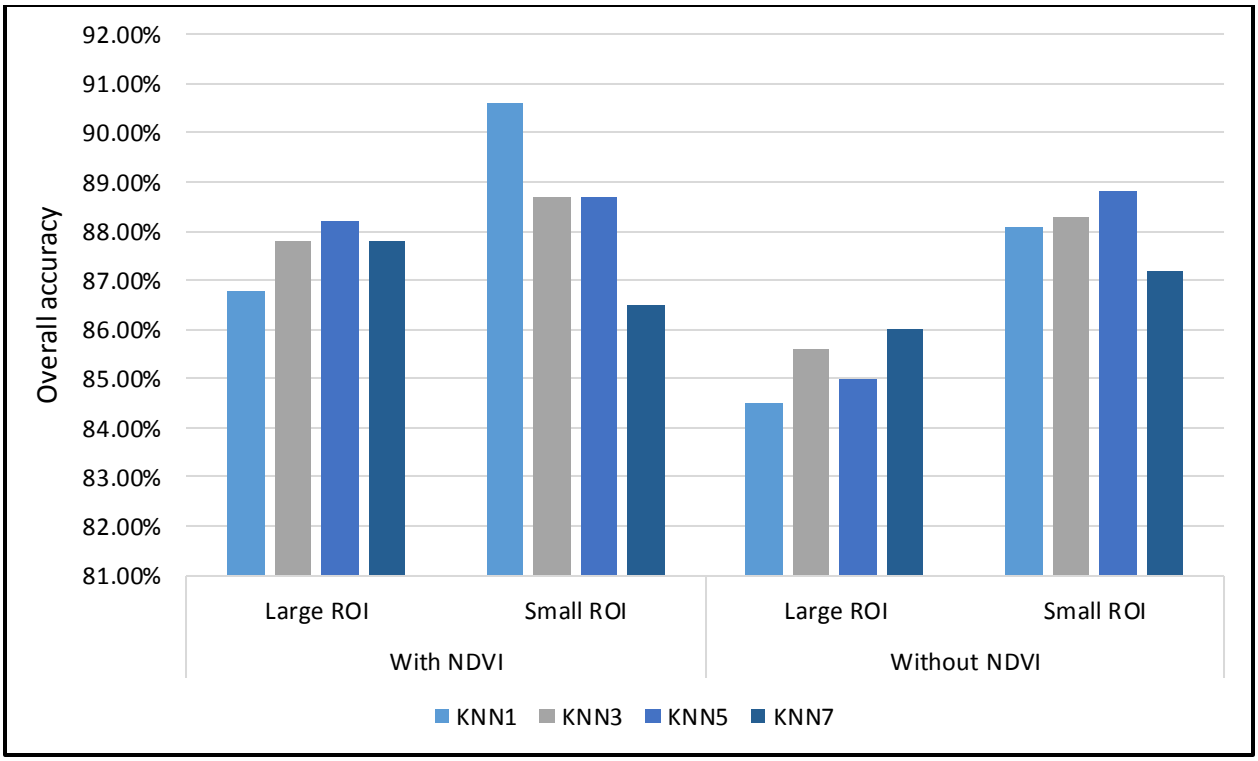

Figure 5.4 Performance comparison between the 2004 object-based classifications

Compared with pixel-based classifications of IKONOS imagery, the superior performance of object-based classifications not only leads to higher accuracy scores, but also much more homogeneous visual presentation of the classified maps. Figure 5.5 shows a series of classified maps derived from pixel and object-based classification approaches. Despite the similar spatial patterns depicted in the two types of classifications for each date, the object-based classifications are apparently less prone to the "salt and pepper" effect, thus leading to more accurate representation of highly textured ground objects, such as plantation sites. This result is to be expected, since the segmentation process involved in object classifications is essentially designed to eliminate the "salt and pepper" effect in pixel-based classifications. Although object-based classification exhibits superior performance in this study, it is worth noting that the classification results are largely dependent on the segmentation process. If the image was oversegmented, the "salt and pepper" effect might still be present in the classified map. On the other hand, if the

image was undersegmented, spatially adjacent objects belonging to different classes might be categorized into a single class, resulting in misclassification errors. Therefore, it is suggested that segmentation parameters are selected with caution.

Table 5.5 Accuracy of the 2004 object-based classifications

Quality of 2004 classified maps		KNN1		KNN3		KNN5		KNN7	
		Overall accuracy	Kappa coefficient	Overall accuracy	Kappa coefficient	Overall accuracy	Kappa coefficient	Overall accuracy	Overall accuracy
With NDVI	Large ROI	86.8%	0.85	87.8%	0.86	**88.2%**	0.87	87.8%	0.86
	Small ROI	**90.6%**	0.89	88.7%	0.87	88.7%	0.87	86.5%	0.85
Without NDVI	Large ROI	84.5%	0.82	85.6%	0.84	85.0%	0.86	**86.0%**	0.84
	Small ROI	88.1%	0.86	88.3%	0.87	**88.8%**	0.87	87.2%	0.85

Table 5.6 Accuracy of the 2012 object-based classifications

Quality of 2012 classified maps	KNN1		KNN3		KNN5		KNN7	
	Overall accuracy	Kappa coefficient	Overall accuracy	Kappa coefficient	Overall accuracy	Kappa coefficient	Overall accuracy	Kappa coefficient
With NDVI	85.8%	0.84	**88.8%**	0.87	88.3%	0.87	86.9%	0.85
Without NDVI	85.8%	0.84	86.3%	0.84	**86.8%**	0.85	83.8%	0.81

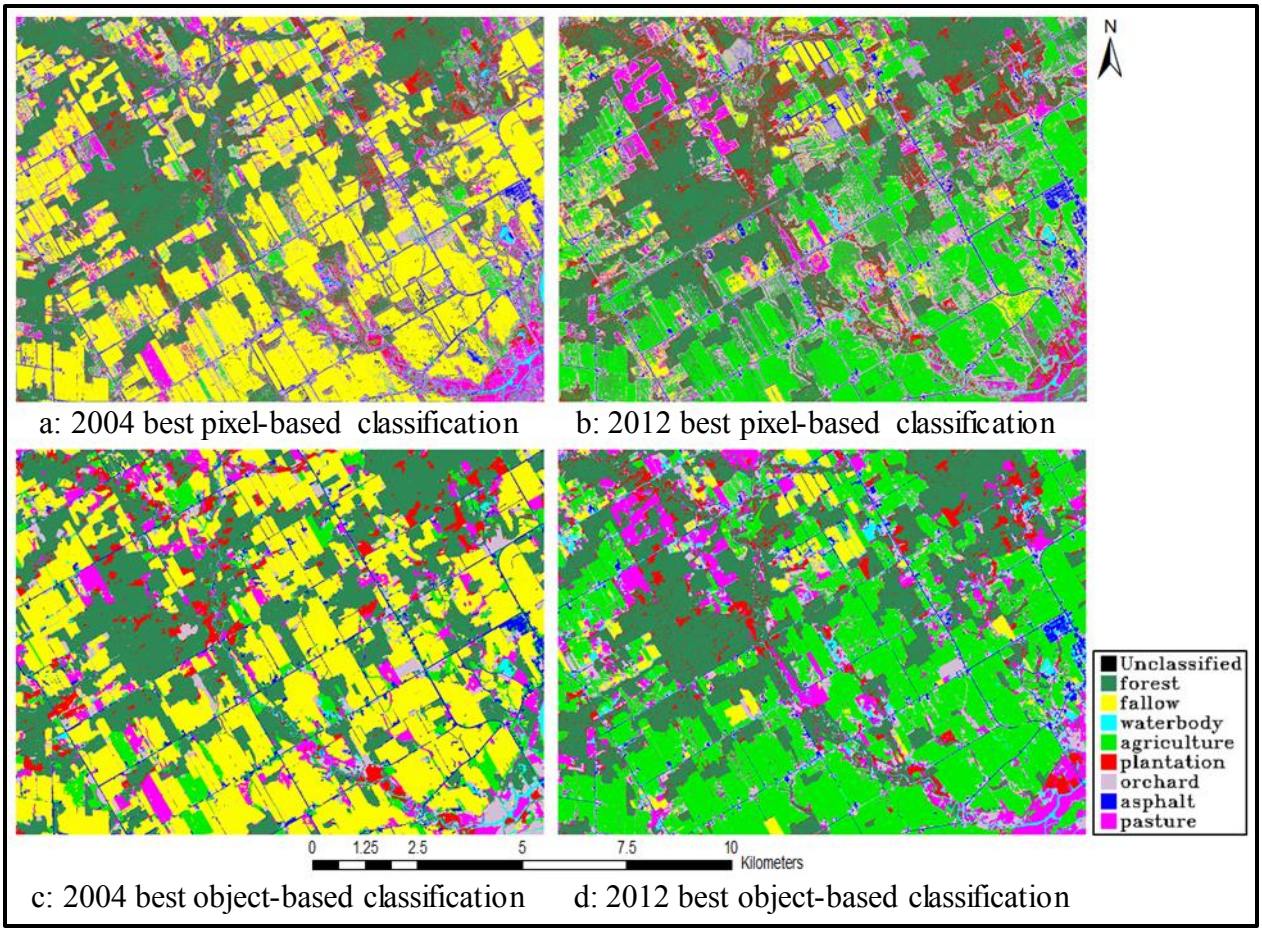

Figure 5.5 Comparison between the pixel-based and object-based classifications

5.1.3 Iterative majority filtering

In order to reduce the "salt and pepper" effect present in the pixel-based classifications performed on both the 2004 and 2012 IKONOS images, the majority filter was applied iteratively to the classified maps. The classification based on raw multispectral bands and the most accurate classification for both dates were subject to this procedure, so as to shed light on any potential discrepancy between their responses to the iterative majority filtering operation. In addition, the same operation was conducted on the best object-based classification derived from the previous analysis, which essentially serves as a control group. Table 5.7 shows that the most accurate filtered 2004 classification has an overall accuracy of 91.2% and a kappa coefficient of 0.90 (highlighted in red), which was obtained by applying the majority filter with a three by three

moving window five times on the object-based classification. Compared with the unfiltered object-based classification, the overall accuracy of the filtered one is only increased by 0.6%, which indicates marginal improvement. As for the pixel-based raw group, the iterative majority filtering approach was able to improve its overall accuracy from 79.0% to up to 82.9% and kappa coefficient from 0.76 to 0.80 (highlighted in bold), which are still lower than the accuracy scores derived from the other two groups. The performance boost brought to the best pixel-based classification for the 2004 image measures from 84.6% to 88.0% in overall accuracy and from 0.82 to 0.86 in kappa coefficient.

The bar chart in Figure 5.6 presents the influence of the iterative majority filtering procedure on the 2004 classifications in a more intuitive fashion. Within the two pixel-based classification groups, it can be seen that the initial accuracy improvement is relatively significant upon the application of the majority filter, regardless of the size of the moving window, while the succeeding application of the majority filter does not results in as much change. As a matter of fact, the overall accuracy of the filtered classifications can be considered essentially as fluctuations around that of the first filtered map derived from either the three by three or five by five kernel. In addition, no trend can be identified in terms of which window size is more suitable for improving the classification results based on the experiments conducted in this study. As for the object-based group, the changes brought by the successive application of the majority filters are almost negligible compared with the two pixel-based groups, which is due to the lack of serious "salt and pepper" effect in the object classification.

Table 5.7 Performance of the iterative majority filter on the 2004 classifications

Quality of selected 2004 classifications	2004 pixel-based raw		2004 pixel-based best practice		2004 OO	
	Overall accuracy	Kappa coefficient	Overall accuracy	Kappa coefficient	Overall accuracy	Kappa coefficient
Without the majority filter	79.0%	0.76	84.6%	0.82	90.6%	0.89
3 × 3 1st	81.5%	0.79	87.6%	0.86	90.8%	0.90
3 × 3 2ed	82.0%	0.79	87.6%	0.86	90.9%	0.90
3 × 3 3rd	82.4%	0.80	87.6%	0.86	90.9%	0.90
3 × 3 4th	82.3%	0.80	87.7%	0.86	91.1%	0.90
3 × 3 5th	82.3%	0.80	87.2%	0.85	**91.2%**	**0.90**
3 × 3 6th	82.4%	0.80	87.3%	0.86	91.2%	0.90
3 × 3 7th	82.8%	0.80	87.3%	0.86	91.2%	0.90
3 × 3 8th	**82.9%**	**0.80**	87.3%	0.86	91.2%	0.90
3 × 3 9th	82.9%	0.80	87.3%	0.86	91.2%	0.90
5 × 5 1st	82.1%	0.80	**88.0%**	**0.86**	90.7%	0.89
5 × 5 2ed	81.8%	0.79	87.0%	0.85	90.9%	0.90
5 × 5 3rd	82.5%	0.80	86.4%	0.84	90.9%	0.90
5 × 5 4th	82.0%	0.79	85.6%	0.84	90.8%	0.90

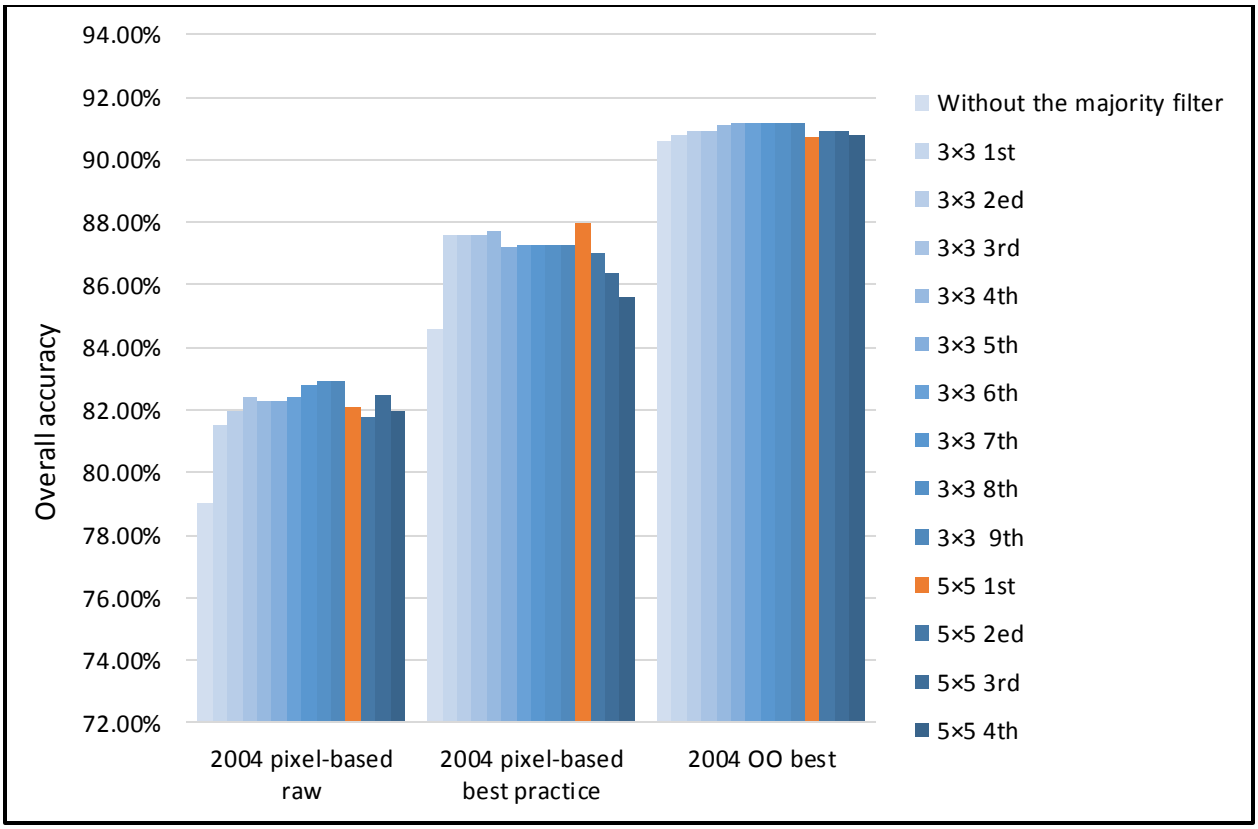

Figure 5.6 Influence of the iterative majority filtering procedure on different 2004 classifications

Table 5.8 lists the accuracy scores derived from the successive application of the majority filters on the 2012 classifications, with the highest score in each Column highlighted in bold. The most accurate filtered classification in the table has an overall accuracy of 93.7% and a kappa coefficient of 0.93 (highlighted in red), which is obtained by applying the three by three majority filter four times on the best pixel-based 2012 classification. Compared with the unfiltered classification, which has an overall accuracy of 87.4% and a kappa coefficient of 0.86, the application of the iterative majority filtering procedure has improved these two metrics by 6.3% and 0.07 respectively. Similar to the case with the 2004 classifications, the iterative majority filter procedure was able to improve the quality of the 2012 pixel-based raw classification to a certain degree as well, marked by the change of overall accuracy from 80.5% to 86.9% and kappa coefficient from 0.78 to 0.85. When it comes to the object-based classification of the 2012

image, minimal improvement was observed after the majority filters were applied: the overall accuracy was increased from 88.8% to 89.7%, while the kappa coefficient was increased from 0.87 to 0.88.

Figure 5.7 presents the results of the iterative majority filtering on the 2012 classifications in the form of bar chart. The variation of accuracy scores within the object-based group is negligible, which is opposite to the case of the two pixel-based groups. In addition, an interesting fact was found from this chart: despite the various levels of change brought by the majority filters to the 2004 classifications, it did not change the relative rank between the three classification groups; however, all the filtered classifications in the 2012 best pixel-based group obtained higher accuracy than the classifications in the object-based group, which features the highest performance among the three unfiltered classifications. This indicates the significant potential of the majority filter for improving accuracy of pixel-based classifications.

Although the two pixel-based classifications reached the highest accuracy based on majority filters with different window sizes, accuracy associated with the five by five window is consistently higher than that of the three by three window after the majority filter is applied once, which is observed from the case of both 2004 and 2012 classifications. Therefore, the five by five moving window would be more suitable for improving the pixel-based classifications derived from IKONOS imagery used in this study if the majority filter were to be applied only once. Nevertheless, this conclusion is empirically based on the accuracy scores observed in this study, which does not have much generality to research involving different classifiers, imagery, or physical environment. To shed light on the optimal window size for the majority filter, variogram analysis may be required in the future to determine the scale of local spatial association for each type of cover under investigation.

Table 5.8 Performance of the iterative majority filter on the 2012 classifications

Quality of selected 2012 classifications	2012 pixel-based raw		2012 pixel-based best practice		2012 OO	
	Overall accuracy	Kappa coefficient	Overall accuracy	Kappa coefficient	Overall accuracy	Kappa coefficient
Without the majority filter	80.5%	0.78	87.4%	0.86	88.8%	0.87
3 × 3 1st	84.0%	0.82	92.1%	0.91	89.2%	0.88
3 × 3 2ed	83.9%	0.82	92.7%	0.92	89.2%	0.88
3 × 3 3rd	84.4%	0.82	93.2%	0.92	89.3%	0.88
3 × 3 4th	85.2%	0.83	**93.7%**	**0.93**	89.3%	0.88
3 × 3 5th	85.3%	0.83	93.6%	0.93	89.6%	0.88
3 × 3 6th	85.5%	0.83	93.6%	0.93	**89.7%**	**0.88**
3 × 3 7th	85.5%	0.83	93.6%	0.93	89.7%	0.88
3 × 3 8th	85.5%	0.83	93.5%	0.93	89.7%	0.88
5 × 5 1st	85.4%	0.83	92.7%	0.92	89.4%	0.88
5 × 5 2ed	85.8%	0.84	92.6%	0.92	89.6%	0.88
5 × 5 3rd	86.3%	0.84	92.6%	0.92	89.3%	0.88
5 × 5 4th	86.4%	0.84	92.5%	0.91	89.1%	0.87
5 × 5 5th	86.8%	0.85	91.9%	0.91	88.9%	0.87
5 × 5 6th	**86.9%**	**0.85**	90.8%	0.90	89.1%	0.87
5 × 5 7th	86.9%	0.85	90.7%	0.89	88.9%	0.87

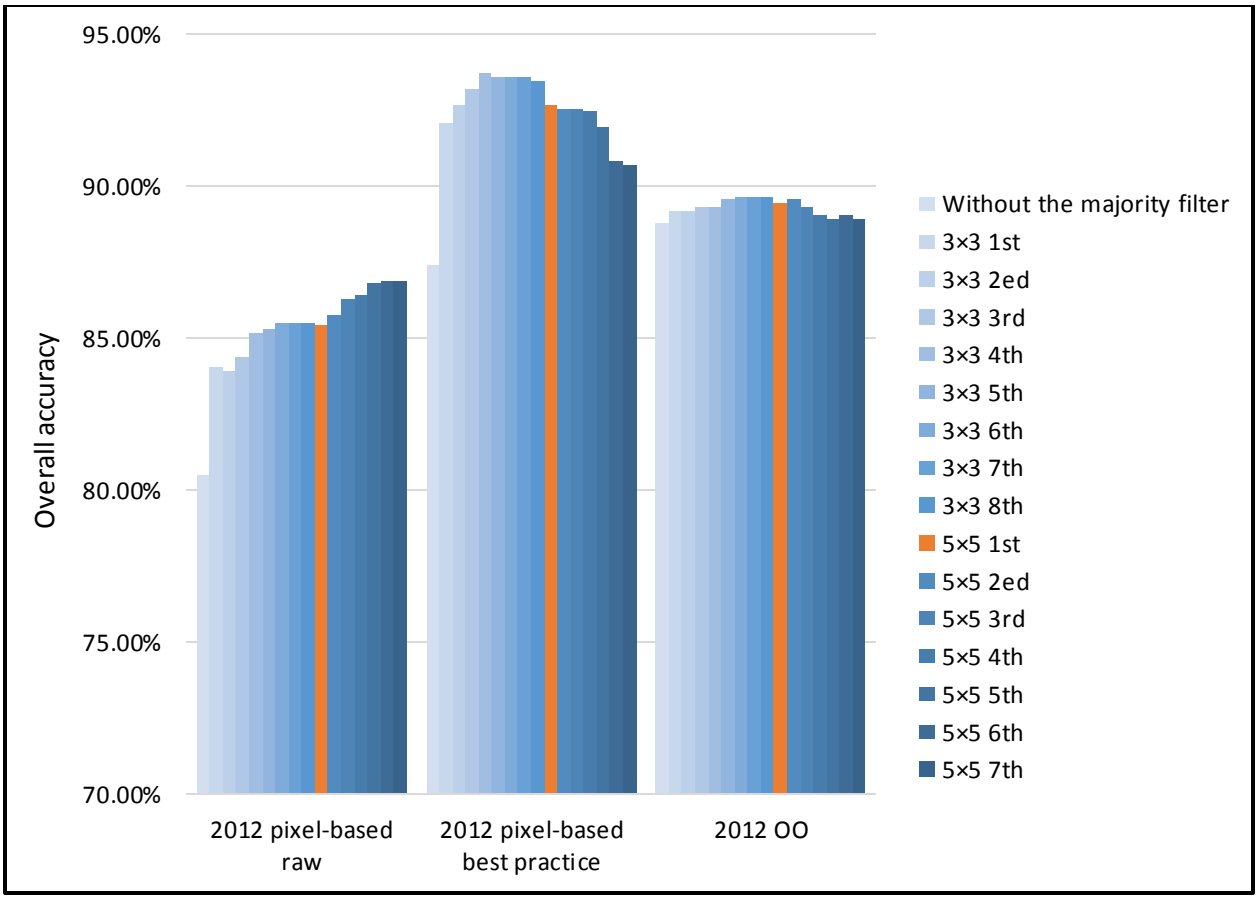

Figure 5.7 Influence of the iterative majority filtering procedure on different 2012 classifications

Figure 5.8 shows a comparison between the original and the filtered classifications based on a subset of the image. In spite of a few remaining "salt and pepper" patches in the forest, most of the misclassified pixels scattered in the classified map were removed by the iterative majority filtering procedure, which makes the output map resemble more a real world scenario. In a sense, the filtered classification is comparable to the object classification performed on the same image, although it does not involve any segmentation of the image. In addition, the majority filter is considered less likely to introduce classification errors independent of those already in the classified maps. On the other hand, it is incapable of correcting any classification error other than those related with the "salt and pepper" effect. In light of this idea, the accuracy of a filtered classification is considered largely subject to the quality of the original classification. If two

classified maps with comparable levels of "salt and pepper" effect were compared, the rank between the two classifications should not change after the application of any majority filter, which accounts for the consistent performance discrepancy between the two pixel-based classifications regardless of the use of the majority filter from the 2004 to the 2012 image. Interestingly, the fact that the performance of the object-based classification group was surpassed by the best pixel-based group could also be explained by this theory: since the 2012 object-based classification suffers much less from the "salt and pepper" effect than the pixel-based classification, the pixel-based classification benefits more from the iterative majority filtering operation.

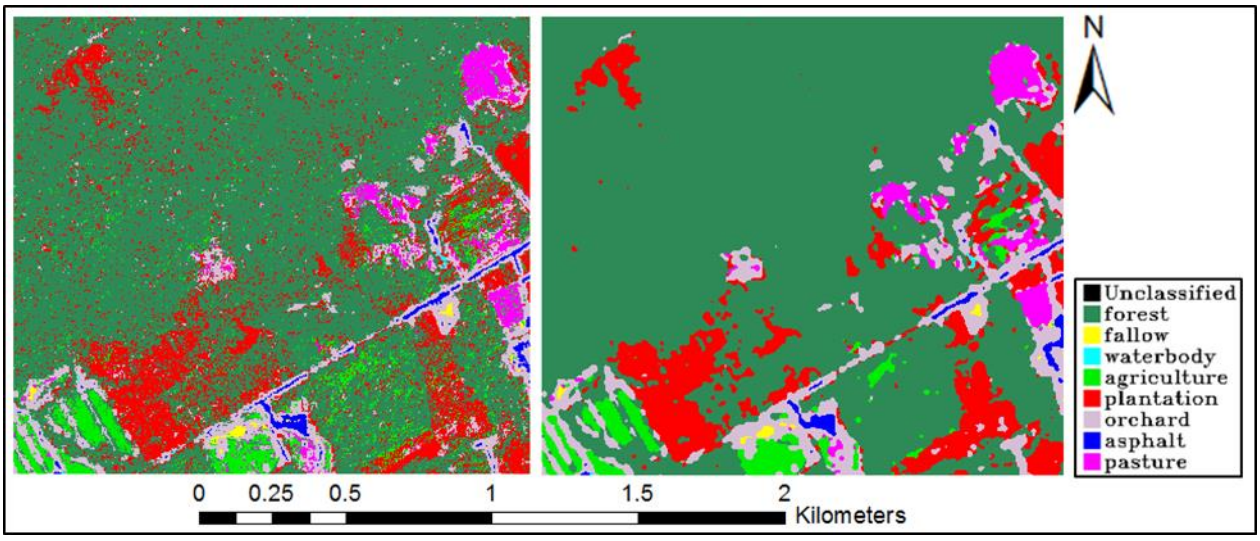

(a) Best pixel-based classification (b) Best filtered classification

Figure 5.8 Comparison between the original and filtered 2012 classifications

5.2 Change/no change discrimination

5.2.1 Change/no change maps based on original image features

As the source of qualitative change information to be derived in this study, the three change descriptor features are presented in Figure 5.9, including CVA change magnitude, NDVI

difference, and absolute NDVI difference image. Compared with the other two image features, CVA change magnitude shows more variations within the forest stands, where minimal land cover change was observed based on visual interpretation of the multitemporal IKONOS imagery. This is mainly due to the contribution of all of the four multispectral bands to the composition of CVA change magnitude: the dynamics of soil background characteristics or fluctuations from other sources could be highlighted as change just as likely as vegetation related changes. Considering the objective of detecting land cover changes in this study, these spectral variations in the forest stands are more noise than useful information. In the CVA change magnitude and absolute NDVI difference image, the relatively dark areas represent the ones that are relatively stable over the period of investigation, while the grey tone in the NDVI difference image represents unchanged areas, since the positive and negative changes are differentiated. According to the visual assessment of the three image features, the two images associated with NDVI are more sensitive to vegetation related changes than CVA change magnitude, which is deemed an advantage against the CVA change magnitude, given the dominance of vegetation in the study area.

As can be seen from Figure 5.10, the binary change/no change map derived from CVA change magnitude suffers more from the "salt and pepper" effect than the other two classifications, which are mainly introduced by the noise present in the forest in the original change magnitude image. With the only difference being the representation of NDVI difference image, the classifications associated with the 2-class and 3-class implementation of NDVI are very similar, and the minor discrepancies between these two classified maps are only noticeable at large scales. The distribution of changed areas in the change/no change maps is mainly concentrated in the southeastern corner of the scene, with the majority of them representing the

transition from fallow land to agricultural fields. According to the accuracy scores listed in Table 5.9, the overall accuracies for the classification based on CVA change magnitude, 2-class NDVI difference image, and 3-class NDVI difference image are respectively 87.5%, 89.6%, and 91.3%, and the corresponding kappa coefficients are 0.75, 0.79, and 0.83 respectively. Therefore, the 3-class implementation of NDVI difference is considered as the most appropriate among all three features used for depicting land cover changes in this study, while the CVA magnitude yields the worst performance in the binary change/no change classification, despite the fact that all the three classifications have acceptably good accuracy.

Figure 5.11 shows a more detailed example of the three change/no change classifications based on a subset of the scene, where the regions of interest are highlighted in red, blue, and yellow rectangles. According to the visual interpretation of the multitemporal IKONOS imagery, the area highlighted in the red box went through the transition from fallow to agriculture during the period of investigation. In addition, it is worth noting that this changed feature is extracted in a relatively compact fashion by the classification based on the 3-class implementation of NDVI difference image, while it is not well delineated in the other two classified maps, which implies that the other two image features are less sensitive to vegetation related changes with a relatively small magnitude.

Similar performance discrepancy can also be found in the area highlighted by the blue rectangle in Figure 5.11. The NDVI difference image is able to classify the entire block as changed land with minor "salt and pepper" effect, while only limited portion of the block is identified as changed land in the classification based on the absolute NDVI difference image. By contrast, this entire block is misclassified as unchanged in the classification based on CVA change magnitude, owing to the relatively small change magnitude in the feature space

determined by all four multispectral bands of the multitemporal IKONOS imagery. The superior performance of the 3-class implementation of NDVI difference image can be attributed to its separation of positive and negative change in NDVI, which may not have the same magnitude. Since the other two classifications only take the magnitude of change into account, the determination of the hyperplane in the multidimensional feature space defined by SVM might be confused by the training samples containing changes with various magnitudes, thus leading to less accurate differentiation between changed and unchanged pixels.

The area highlighted by the yellow rectangle illustrates another interesting example of inconsistent performance of the three classifications. According to the false color composite images in Figure 5.11, this area was converted from fallow to pasture over the time span from 2004 to 2012. Instead of providing a less accurate extraction of the changed block as in the previous two examples, the classification based on CVA change magnitude successfully categorized this block into the changed group, while the other two classifications barely managed to detect the area with relatively abundant vegetation cover in the 2012 image as changed land. Since the field program for this study was mainly guided by the 2004 IKONOS image (the only image available before the field data collection window), which does not feature much pasture coverage, field inspection was not conducted in pasture area. Therefore, near-range observation of the local landscape is not available regarding spatial distribution of plants and their spectral profiles. It is suspected that the spatial heterogeneity of restoration sites might be related with the varying growth stages and health status of the plants or different vegetation species present in the site, which results in spectral change not only in the "red edge" region characterized by NDVI, but also the green and blue band of the spectrum. If this is a typical example of pasture, NDVI will be less adequate for detecting emerging pasture land over time. Instead, CVA change

magnitude or other indices focusing on the green and blue band of the spectrum may be more suitable for mapping the transition from fallow to pasture.

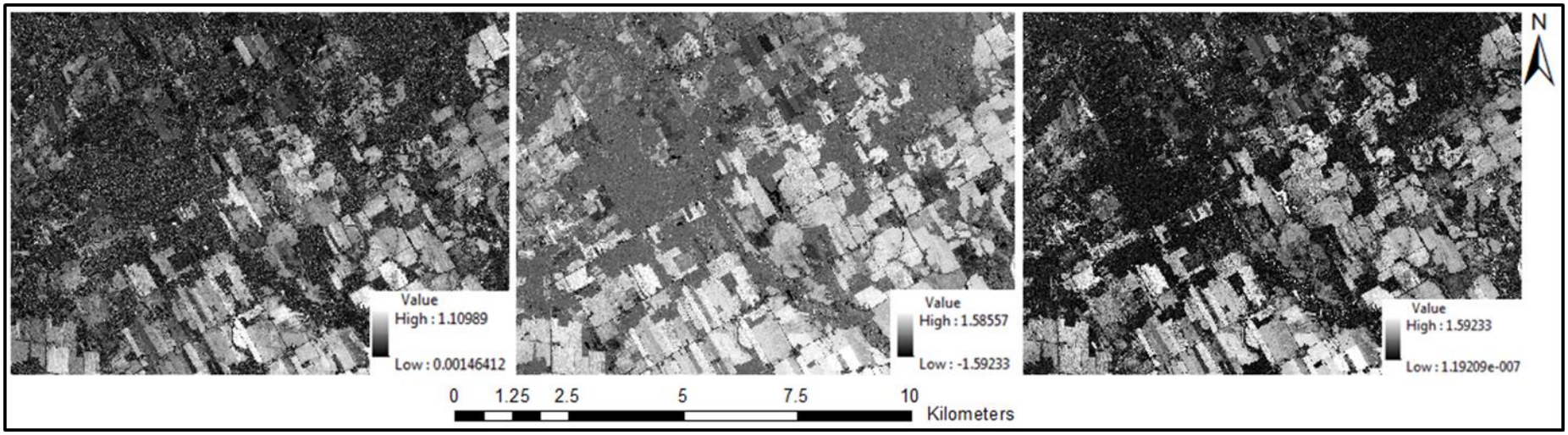

(a) CVA change magnitude image (b) NDVI difference image (c) Absolute NDVI difference image

Figure 5.9 Individual image features used for change/no change discrimination

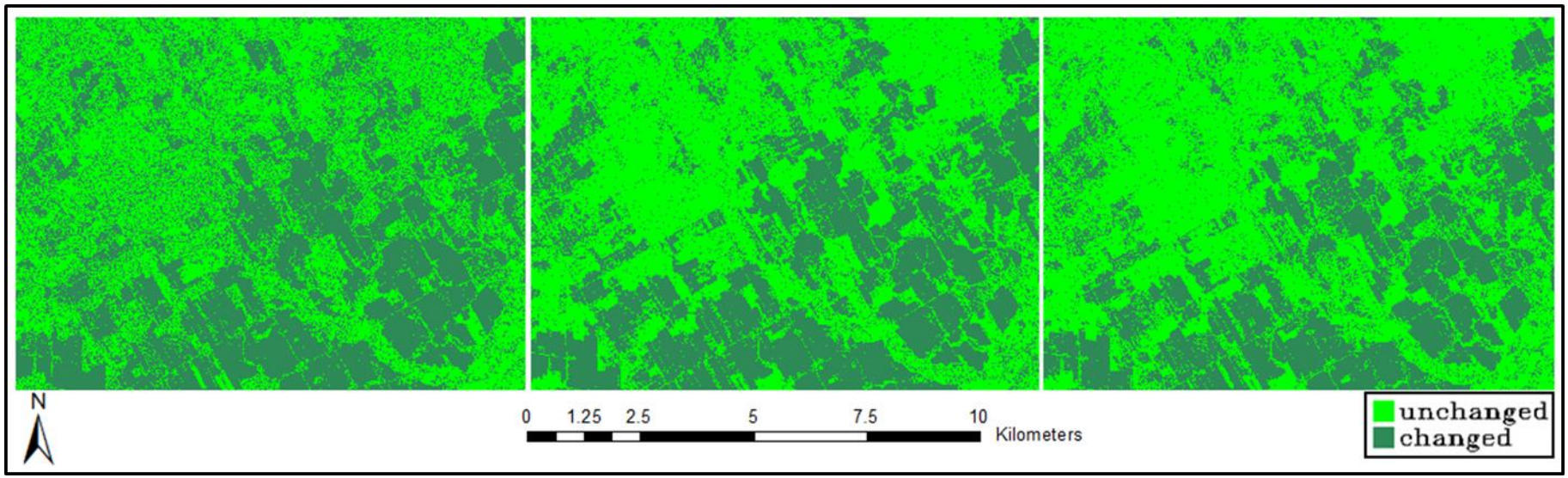

(a) CVA change magnitude classification (b) NDVI difference classification (c) Absolute NDVI difference classification

Figure 5.10 Binary change/no change maps derived without the application of any spatial filter

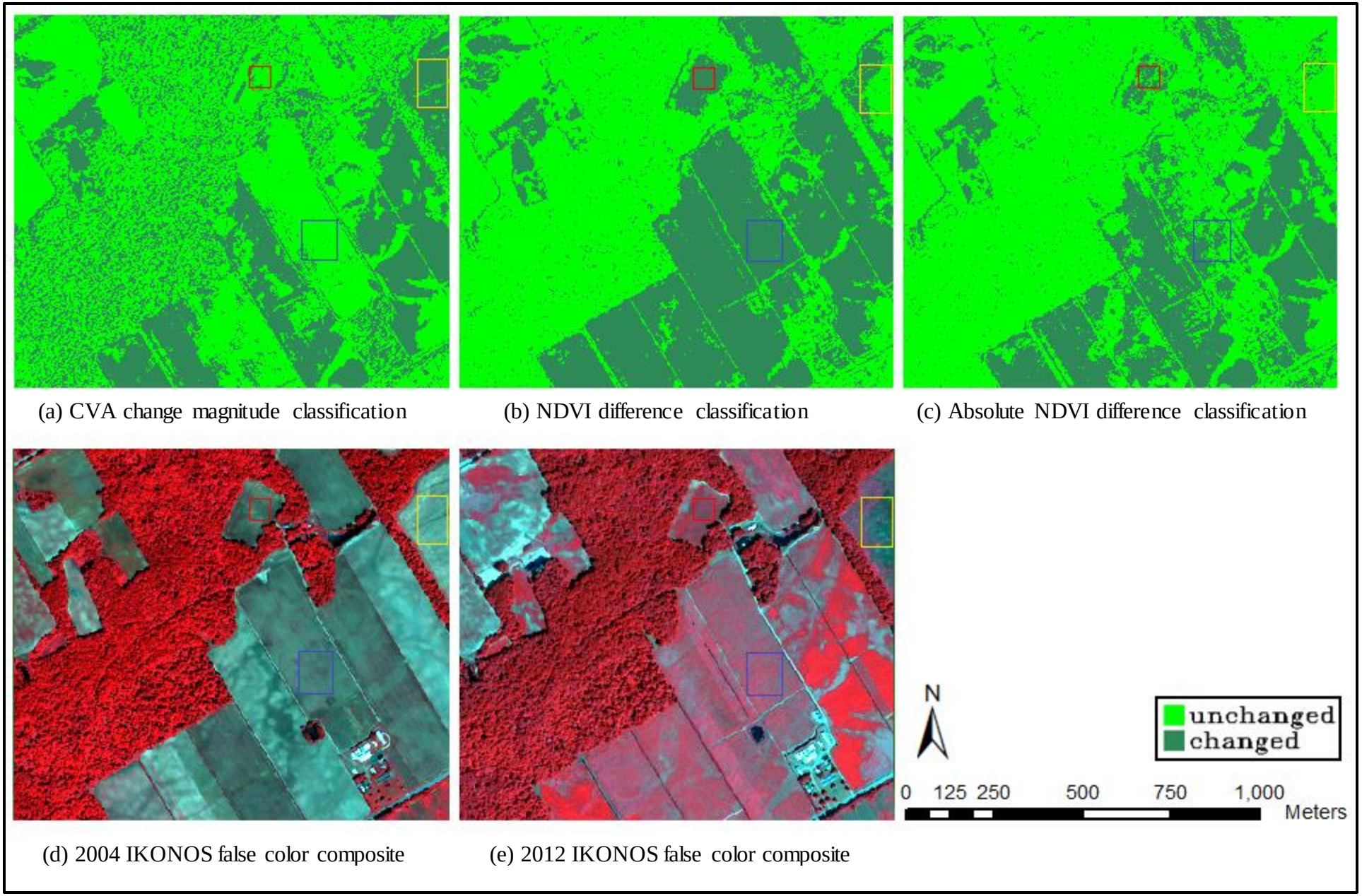

Figure 5.11 Comparison of change/no change classifications based on three different image features

5.2.2 Change/no change maps based on the Getis image features

In order to examine the influence of the Getis statistic on the individual image features used for change detection, histograms were derived for each image before and after the application of the Getis statistic, and are presented in Figure 5.12. Based on the spectral signature of the training samples collected for change/no change classification, the peak centered around 0.5 in the histogram associated with the original NDVI difference image corresponds to positive changes in NDVI, while the peak on its left represents the unchanged pixels. Due to the much smaller proportion of pixels related with negative NDVI change compared with those related with unchanged and positive change, they reside on the left tail of the histogram and are not distinguishable from the histogram itself. As a result, it would be relatively difficult to identify negative change based on an unsupervised clustering technique without the presence of apparent clusters associated with negative NDVI change. By contrast, the 3-class implementation of image differencing is capable of imposing different thresholds for positive and negative changes based on independent training samples, thus accounting for the potential systematic difference between the magnitude of positive and negative changes. In addition, the asymmetric distribution of the NDVI difference image prohibits the employment of the conventional thresholding approach based on the mean and standard deviation of the distribution. Thus, the supervised approach adopted in this study is considered suitable for the current application.

As the Getis statistic with various window sizes is applied to the original NDVI difference image, higher levels of separation between the two peaks are observed according to their relative distance on the value axis, implying that the changed pixels are increasingly separable from the unchanged ones. In addition, the range of the filtered images has a growing trend with the increase of window size ranging from three by three to nine by nine, which also suggests

improved separability between unchanged and changed pixels, including NDVI positive change and negative change. Compared with the regular Getis images, the maximum Getis image contains the least number of pixels with negative Getis values, since pixels with one or more positive Getis values among the Getis images based on different window sizes will be assigned a positive Getis value according to the definition of the maximum Getis statistic. Furthermore, the pixels associated with the negative NDVI change are likely to be moved closer to the origin of the distribution, thus making them less separable from the unchanged pixels. In addition, divergence of the Getis values associated with positive change is observed in the maximum Getis image, which may result in reduced accuracy for change/no change discrimination. As for the extreme Getis statistic proposed in this study, it has the most unique distribution among all the derivatives of the NDVI difference image, due to the discontinuity at the origin of the histogram. This discontinuity is mainly caused by the movement of pixels towards the tails of the distribution, as per definition of the extreme Getis statistic. The pixels located near the origin of the distribution represent areas whose overall local NDVI difference values are close to zero, suggesting that they underwent minimal change from 2004 to 2012. Therefore, the extreme Getis statistic is considered promising for improving the separability between changed and unchanged pixels in the context of change detection.

The absolute NDVI difference feature negates the possibility of separating negative from positive changes, which is the opposite case of the NDVI difference image. Considering its unique relationship with the NDVI difference image, the secondary peak in its histogram can be attributed to positive change, which is located approximately at the same position as its counterpart in the NDVI difference image with a value of 0.5. Since the count of pixels with the same magnitude are added together in the histogram of absolute NDVI difference image, the sag

between the two peaks respectively representing unchanged and positive change is less obvious than that from the distribution of the NDVI difference feature. Accordingly, the possibility of misclassifying these pixels near the sag is increased, which might be the reason for the performance discrepancy between classifications derived from the NDVI difference and absolute NDVI difference images. As can be seen from the histograms in the second row of Figure 5.12, the application of the Getis statistic is capable of improving the separability between the two peaks in the distribution of the absolute NDVI difference image, which represent changed and unchanged areas respectively. Similarly to the case with the NDVI difference image, the continuity of the distribution of the extreme Getis image for the absolute NDVI difference feature is broken at the origin of the histogram.

As can be seen from the histograms in the third row of Figure 5.12, the distribution of the CVA change magnitude has a distinct shape compared with the other two groups discussed above. In addition to the primary peak corresponding to unchanged pixels, the large number of positive NDVI change pixels appearing as the secondary peak in the other two image features are barely noticeable in the histogram of CVA change magnitude. This can be explained by the equal weight of four multispectral bands in the formulation of the change magnitude, which highlights not only land cover changes sensitive to NDVI but also other types of changes. Therefore, it is relatively difficult to differentiate changed from unchanged pixels based on visual interpretation of the histogram. On the other hand, the application of the Getis statistic is able to improve the separability between these two classes, which can be seen from the distribution of the Getis change magnitude images.

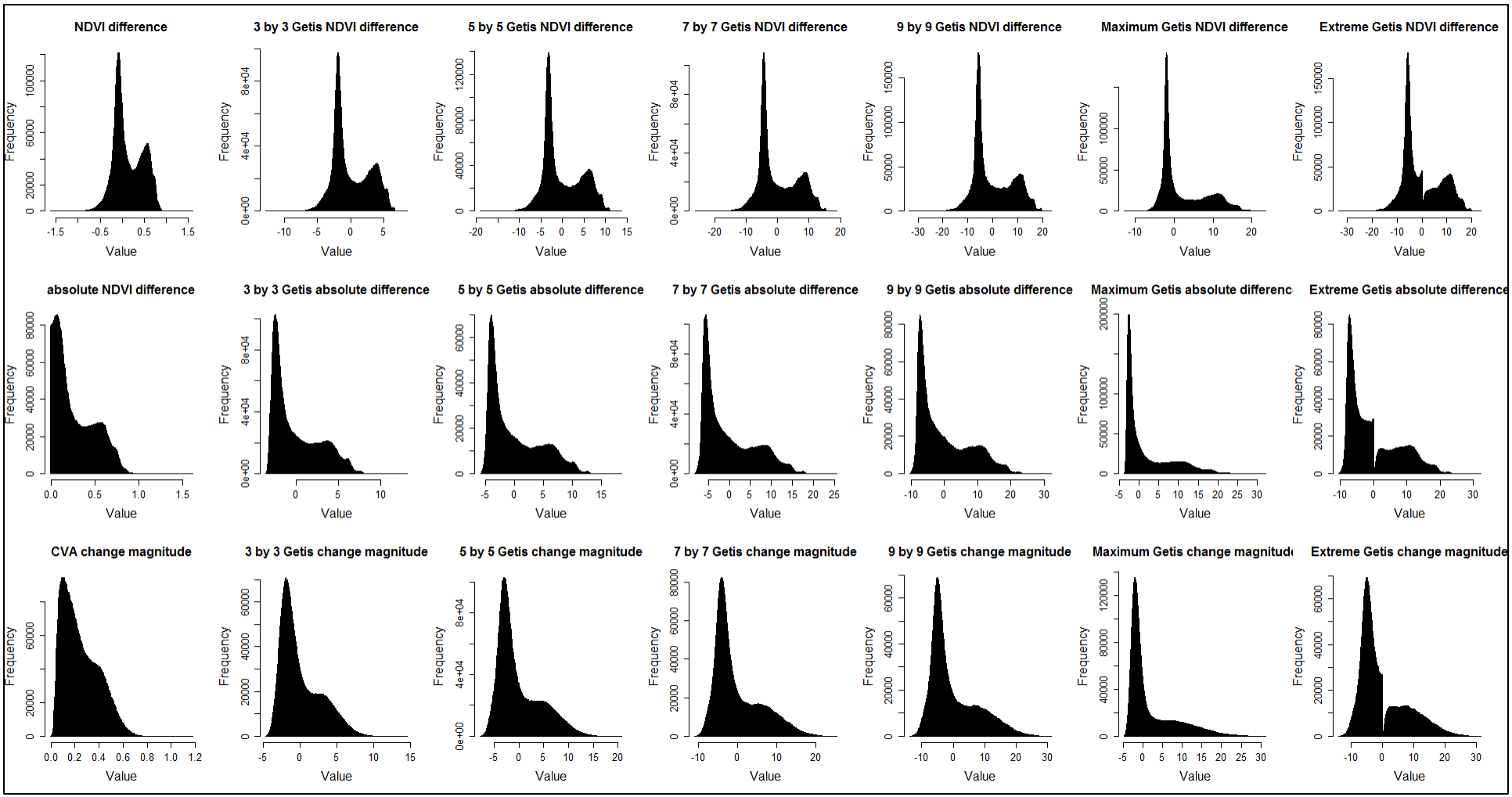

Figure 5.12 Histograms of various image features used for change/no change discrimination

Table 5.9 presents the accuracy scores for the binary change/no change maps derived from various change descriptor images, with the highest accuracy scores within each feature group highlighted in bold. The most accurate classification from the CVA change magnitude group is based on the Getis image derived from a three by three moving window, with an overall accuracy of 89.2% and a kappa coefficient of 0.78. Compared with the original classification based on CVA change magnitude, the filtered image is able to improve the overall accuracy by 1.7% and the kappa coefficient by 0.03. Denoted by its overall accuracy of 91.7% and kappa coefficient of 0.83, the classification based on the extreme Getis image features the highest accuracy within the 2-class NDVI difference image group, which improves the overall accuracy of the original 2-class NDVI classification by 2.1% and the kappa coefficient by 0.04 respectively. The highest overall accuracy among all the classifications in Table 5.9 is 92.9%, and the corresponding kappa coefficient is 0.86, which are achieved by the 3-class NDVI difference image with a five by five Getis filter applied. Compared to the overall accuracy of 91.3% and kappa coefficient of 0.83 associated with the original classification in the 3-class NDVI difference feature group, the application of the Getis statistic is capable of improving the quality of the classified map to a certain degree.

As an attempt to systematically examine the effect of the Getis statistic on supervised change detection based on SVM, the overall accuracy of the individual change/no change maps are presented in Figure 5.13, which makes the accuracy scores more interpretable. Among the three feature groups, the CVA change magnitude group has the lowest accuracy, while the 3-class NDVI difference group boasts the highest accuracy, despite the fluctuation of accuracy scores within each group. Interestingly, the application of the Getis statistic does not change the performance ranks between these three image groups, given that the average accuracy of the

classifications within each group is used as an indicator of their overall performance to take account of the effect of the Getis filters. This observation is similar to the one associated with the influence of the iterative majority filtering procedure discussed in the previous section, which suggests that the benefit of the majority filter is dependent on the performance of the original classification. In the case of the Getis statistic, its effect on the change/no change discrimination is also considered subject to the usefulness of the image feature and the capability of the classifier of choice, thus serving the purpose of an enhancement technique.

Since the best classifications from each image group are not of the same origin, it is difficult to determine the optimal window size for the Getis statistic to make the strongest contribution to change detection. However, it is worth noting that the classification based on the extreme Getis feature ranks the first in the 2-class NDVI difference group and the second in the 3-class NDVI difference group. Therefore, it is considered promising for automatically selecting the optimal spatial scale for maximizing the spatial homogeneity of the classification, which would contribute to the improvement of classification accuracy. The fact that the extreme Getis image ranks only the fifth in the CVA change magnitude group may be caused by the relatively poor discrimination power of the change magnitude compared with the other two features. Given that CVA change magnitude is less sensitive to certain types of change in the study area, it is less likely for the Getis statistic to correct classification errors associated with this deficiency of the change magnitude. In other words, there is no optimal spatial scale that would facilitate the accurate differentiation between changed and unchanged pixels without an effective change descriptor. Therefore, the extreme Getis statistic is not very useful in the case of CVA change magnitude. In light of this observation, a benchmark approach is advisable for selecting an appropriate change descriptor for change detection, which would benefit the most from the

employment of the Getis statistic as a spatial filter. In order to obtain more insight into the application of a Getis statistic in the context of change detection, more experiments should be conducted in different physical environments, with remote sensing imagery featuring various spatial resolutions, and based on assorted change indicators as well as thresholding approaches.

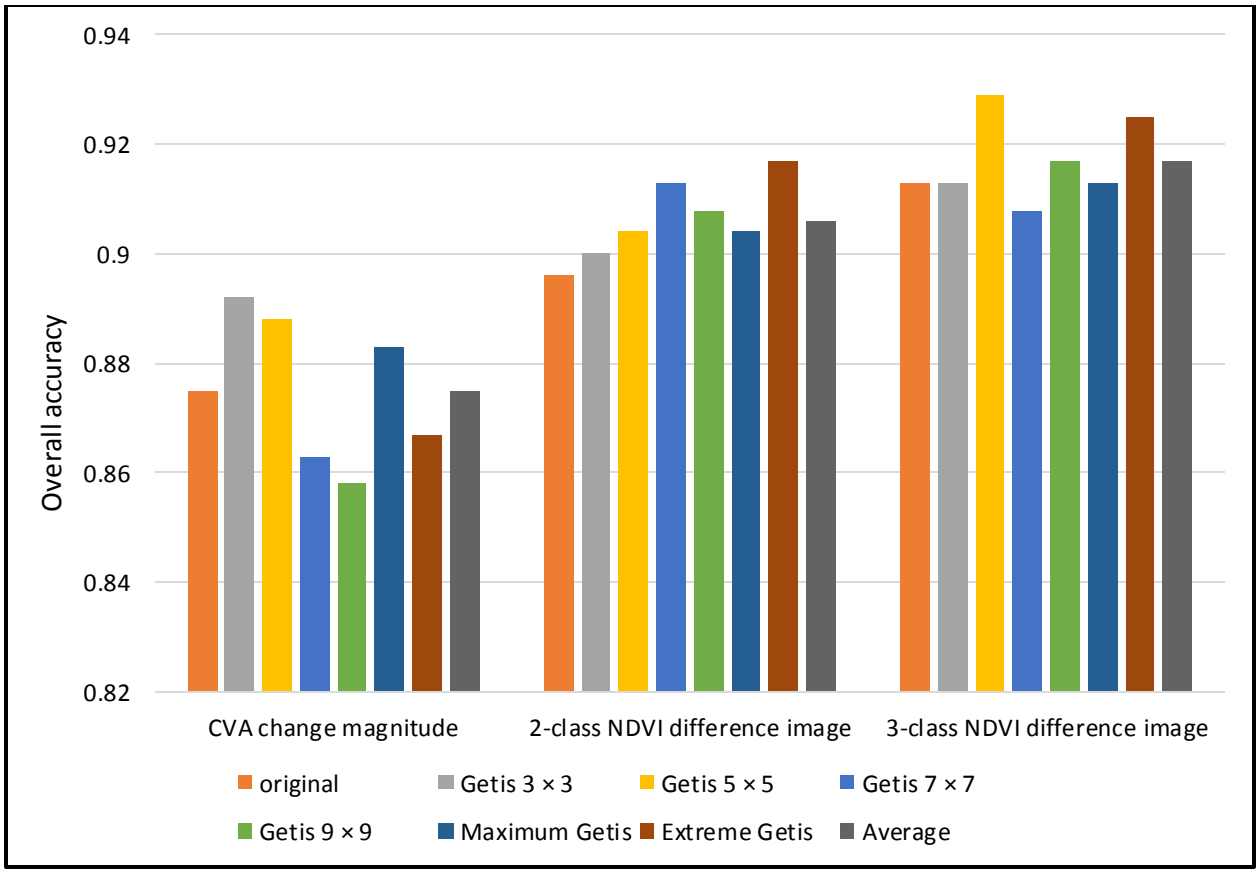

Figure 5.13 Performance comparison between all the change/no change classifications

Table 5.9 Quality of the individual change/no change maps

Accuracy scores	CVA change magnitude			2-class NDVI difference image			3-class NDVI difference image		
	Overall accuracy	Kappa coefficient	Rank	Overall accuracy	Kappa coefficient	Rank	Overall accuracy	Kappa coefficient	Rank
original	87.5%	0.75	4	89.6%	0.79	7	91.3%	0.83	4
Getis 3×3	**89.2%**	**0.78**	**1**	90.0%	0.80	6	91.3%	0.83	4
Getis 5×5	88.8%	0.78	2	90.4%	0.81	4	**92.9%**	**0.86**	**1**
Getis 7×7	86.3%	0.73	6	91.3%	0.83	2	90.8%	0.82	7
Getis 9×9	85.8%	0.72	7	90.8%	0.82	3	91.7%	0.83	3
Maximum Getis	88.3%	0.77	3	90.4%	0.81	4	91.3%	0.83	4
Extreme Getis	86.7%	0.73	5	**91.7%**	**0.83**	**1**	92.5%	0.85	2
Average	87.5%	0.75	NA	90.6%	0.81	NA	91.7%	0.84	NA

The classifications with the highest accuracy within each feature group (bottom row) are compared with the ones produced without the application of the Getis statistic (top row) in Figure 5.14. Owing to the local spatial autocorrelation information captured in the Getis images, the "salt and pepper" effect in each classification was reduced to a certain extent after its deployment, which is consistent with the improved accuracy scores listed in Table 5.9. That being said, "speckles" labeled as changed land are still present in the forest stands depicted in the classification based on the Getis change magnitude, which are identified as unchanged through visual examination of the multitemporal imagery. On the contrary, the other two classifications derived from the Getis statistic are more accurate and informative, with changed land clearly depicted in the map. Similar to the comparison between the original classifications based on the 2-class and 3-class implementation of NDVI differencing, the corresponding classifications with the application of the Getis statistic show great resemblance in terms of the location of the changed areas, despite some minor differences noticeable only at large scales.

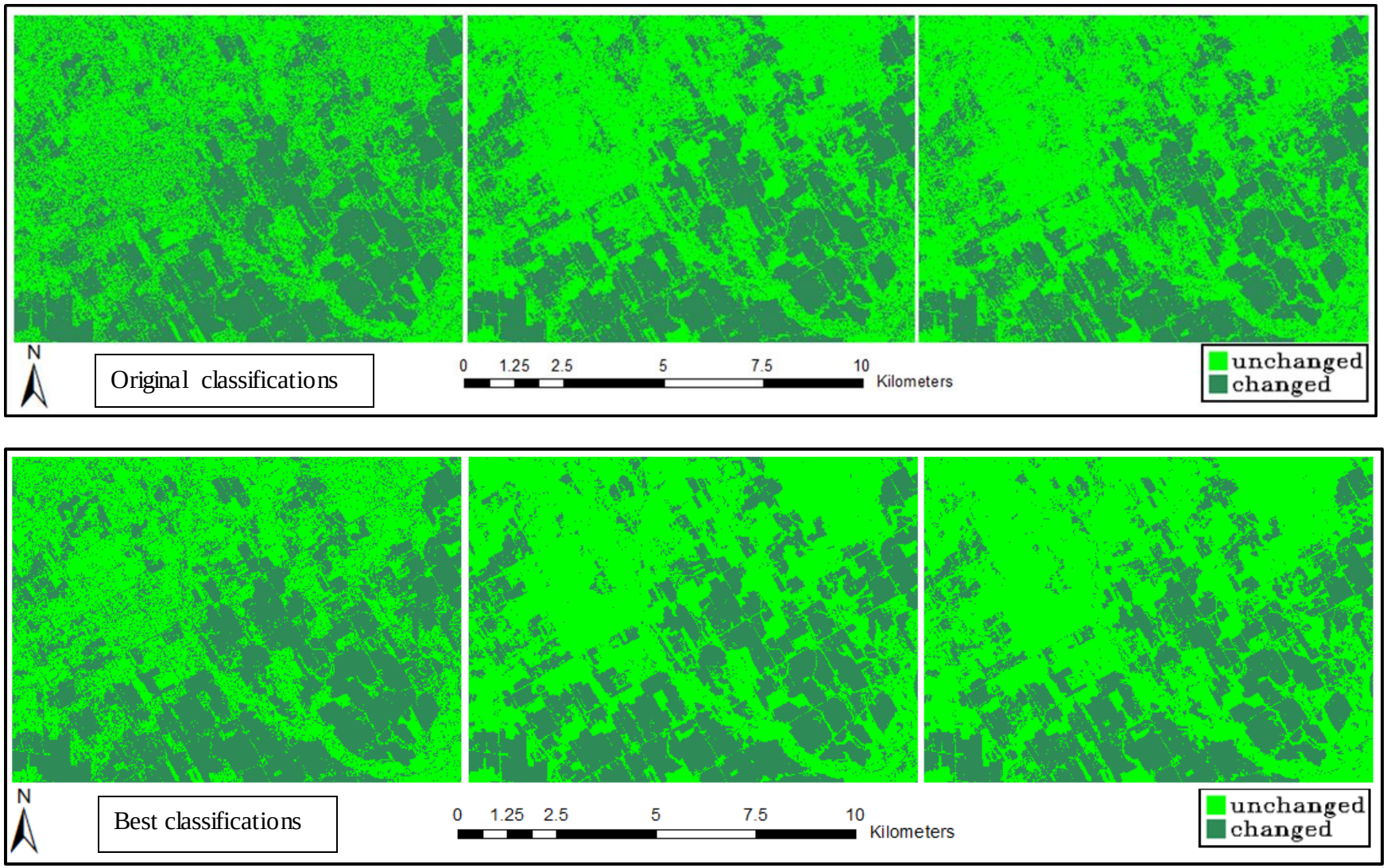

(a) CVA change magnitude group (b) NDVI difference group (c) Absolute NDVI difference group

Figure 5.14 Comparison of binary change/no change maps before and after the application of the Getis statistic

Figure 5.15 provides a detailed example of how the use of the Getis statistic influences the classification results. In the classification based on CVA change magnitude, the misclassification of part of an unchanged forest stand as changed land is potentially caused by the change of soil moisture level or varying growth stages of the trees, which does not qualify as land cover change. It is worth noting that the spatially adjacent misclassified "salt and pepper" in the original classification are aggregated as "speckles" in the Getis classification, since they are presented as changed "hotspots" in the Getis change magnitude image. Due to the fact that these changes are essentially "false alarms", the application of the Getis statistic does not contribute to more accurate detection of land cover changes in this case, which relates to the relatively weak performance of the Getis images in the CVA change magnitude group, especially those associated with larger window sizes. In other words, the Getis image capable of maximizing local clustering effects would lead to particularly weak performance of the classification, since the "false alarms" are highlighted. Therefore, the effectiveness and uncertainties of change descriptors should be fully examined when change detection techniques that utilize local spatial autocorrelation characteristics are employed.

Since the extreme Getis statistic is considered as a potential method for automatically selecting the spatial scale related to the maximum level of local spatial association, its implication for change detection is analyzed systematically by comparing it to the Getis classification with a window size of five by five, the Getis classification with a window size of nine by nine, and the original binary change/no change classification. It should be noted that all these classifications are derived from the 3-class implementation of NDVI difference feature, since it is more accurate than the other two features according to visual assessment of the classified maps and the accuracy scores derived from confusion matrix. As can be seen from

Figure 5.16, the original classification suffers from the "salt and pepper" effect present in the forest, orchard, as well as fallow class. On the contrary, it is greatly reduced in the three classifications which take advantage of the Getis statistic.

Unlike the two classifications on its right, the classification corresponding to the Getis image with five by five moving window identified some changes in the middle of the orchard (highlighted by the yellow rectangle). However, they are deemed not of much interest to the present study, since these "changes" are mainly caused by variation of the soil background, which does not qualify as land cover change. Therefore, this classification does not perform as well as the other two candidates, despite its highest overall accuracy listed in Table 5.9. In addition, the hedgerow highlighted in blue rectangle is correctly classified as unchanged in the original 3-class NDVI difference classification and the extreme Getis classification, yet this feature is not properly mapped in the other two classifications. To be precise, the hedgerow is merged into the background as changed in the 9×9 Getis classification, while this feature is discontinued in the 5×5 Getis classification, which implies that a moving window with the size of five by five is beyond the range of local spatial association in this case. Therefore, the extreme Getis image is proven to be a feature that is able to capture the maximum level of spatial association automatically across the study area. Essentially, this property of the extreme Getis statistic can be interpreted as a continuity preserving characteristic, which contributes to more accurate mapping of the linear features in the image.

The feature highlighted by the red rectangle shows an example of such characteristic: the channel that went through the transition from vegetated to bare soil is extracted in a continuous fashion in the two classifications on the bottom left of corner of Figure 5.16, while it is discontinued in the classified map derived from the nine by nine Getis image. Although this

channel is misclassified as unchanged, it is mainly due to the classification process itself, since the channel is of cohesive negative Getis values in the extreme Getis image, which relates to negative change in NDVI. If negative change samples had been collected at this site, it is very likely that this feature would be classified correctly. Considering the presentation of this channel in the original 3-class NDVI difference classification, its width has decreased over time, which explains the changed areas surrounded by two strips of unchanged pixels. This complication might also be a factor that has compromised the performance of the Getis statistic in this case.

After careful examination of the classified maps derived from the previous analysis, the extreme Getis classification is considered the most accurate in representation of actual features, although its overall accuracy statistic ranks the second among all the classifications. Its lower overall accuracy than the 5×5 Getis classification may be a result of the defect of the current accuracy assessment approach based on confusion matrix, which does not fully assess the homogeneity of the classified maps. As a matter of fact, a certain technical advancement, be it an enhancement method, a classifier, or a specific workflow, is difficult to improve the allocation of all the pixels in the classification of a particular nature. In other words, the improvement in certain areas within a classified map could potentially induce misclassification in other subsets of the map. Therefore, it is entirely possible that the higher overall accuracy of the 5×5 Getis classification is obtained by chance, subject to the selected testing samples. In addition, it is very likely that the spatial extent determined by the five by five moving window coincides with the extent of local spatial association associated with the dominant land cover types in this study, which would account for the impressive performance of the classification derived from the five by five Getis image. By contrast, the usefulness of the extreme Getis image lies in its capability

of automatically presenting a filtered image in accordance with the maximum level of local spatial autocorrelation across the image of interest.

This characteristic of the Getis image could potentially benefit change detection studies employing different remotely sensing imagery in various environments without having to rely on a benchmark approach, which necessitates the examination of change/no change maps based on change descriptor images with assorted window sizes to locate the most accurate classification. In other words, the use of the extreme Getis statistic is able to secure a relatively accurate classification among all the classifications performed on the Getis images with various window sizes. Essentially, the Getis statistic is comparable to the majority filter, since they are both associated with a kernel of certain size. Without a detailed variogram analysis for each type of cover in the image, no priori knowledge is available regarding the range of spatial autocorrelation effect for these classes. Due to its capability of automatically applying the optimal scale for spatial aggregation, the extreme Getis classification is deemed more efficient than the iterative majority filtering procedure used earlier in this study, and it would certainly be worthwhile to apply it on other images or in a different environment to obtain a better understanding of its performance.

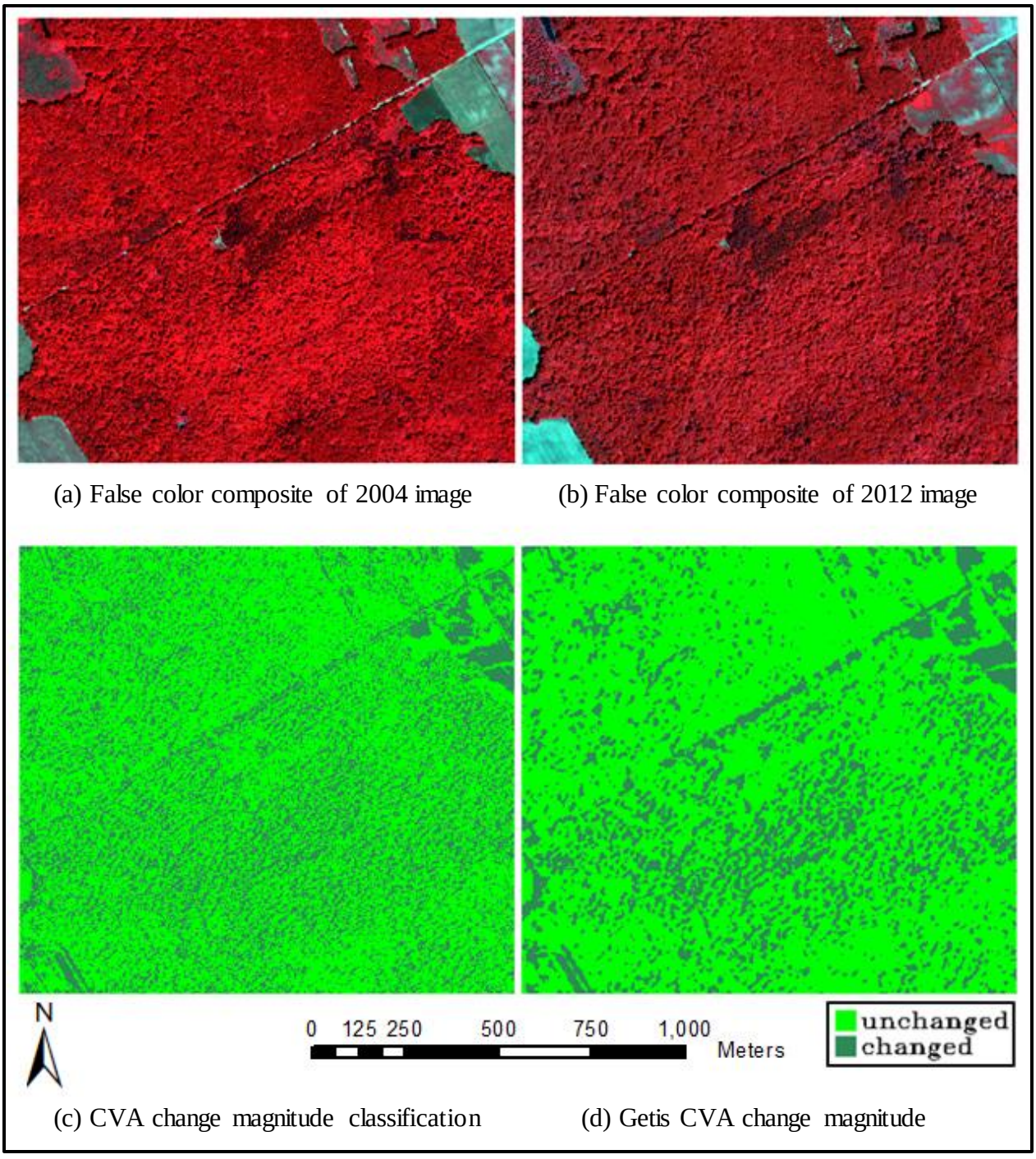

(a) False color composite of 2004 image (b) False color composite of 2012 image

(c) CVA change magnitude classification (d) Getis CVA change magnitude

Figure 5.15 Illustration of the effect of the Getis statistic on change/no change discrimination

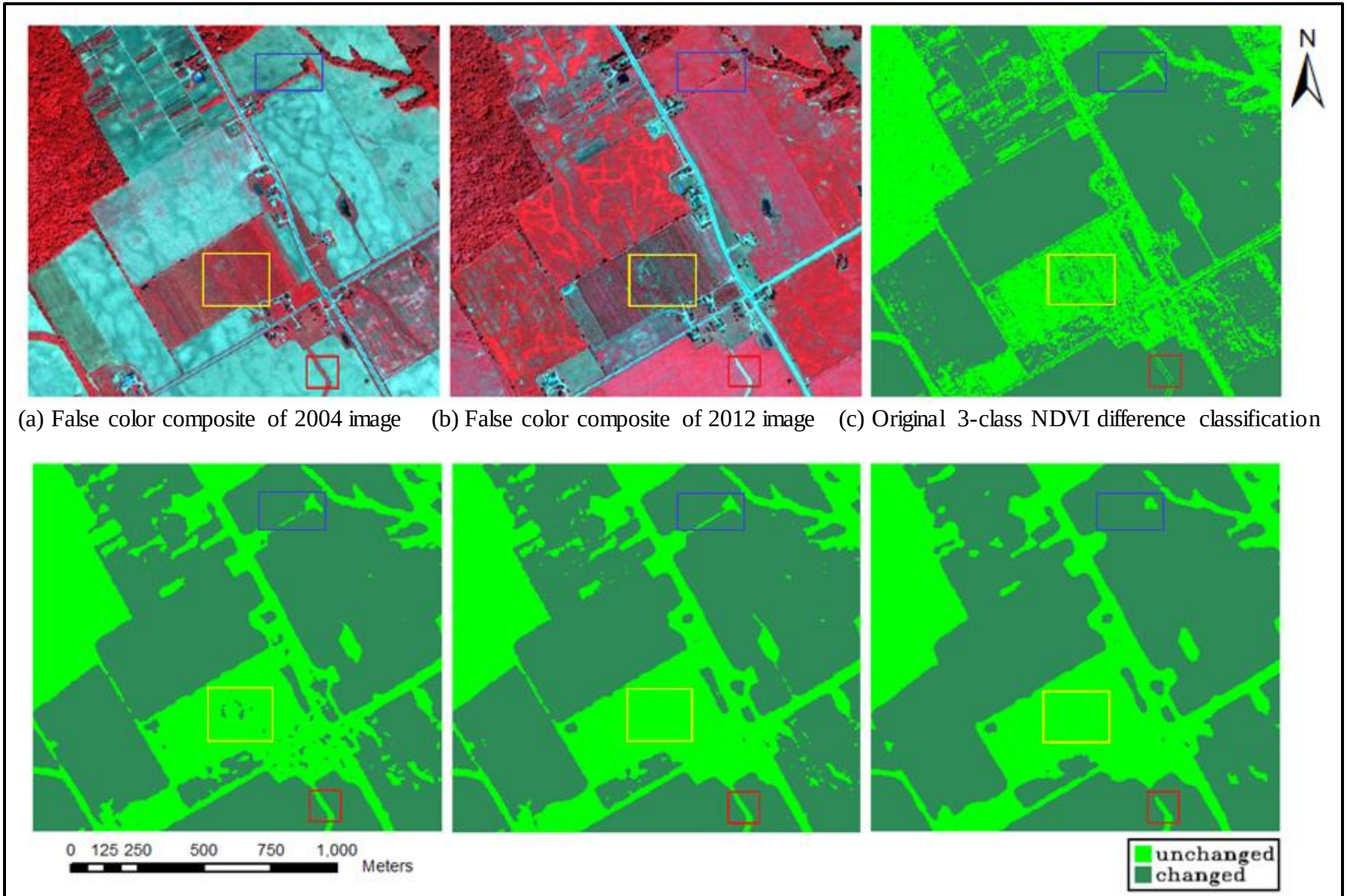

(a) False color composite of 2004 image (b) False color composite of 2012 image (c) Original 3-class NDVI difference classification

(d) Getis classification based on 5×5 window (e) Extreme Getis classification (f) Getis classification based on 9×9 window

Figure 5.16 Assessment of the effect of the extreme Getis statistic on change/no change classification

According to the discussion above, the extreme Getis image is considered of better quality than its peer derived from the five by five Getis image. Therefore, it will be compared to the various change/no change maps based on post-classification comparison approach as the best practice from the change/no change discrimination phase of the workflow. Figure 5.17 presents this best change/no change map in detail, which contains 60.6% of unchanged and 39.4% of changed areas. It is worth noting that stable linear features surrounded by changed areas are well depicted in this map, such as local roads and hedgerows, separating the changed lands as isolated patches. This unique characteristic of the map could potentially contribute to the segmentation of the classified map for further processing, which may benefit the extraction of quantitative change information for this study. Considering the identification of most wetland areas as unchanged, it circumvents the poor classification accuracy of the wetlands very well, which is induced by great intra-class spectral variability. Based on the visual interpretation of the multitemporal IKONOS imagery, the change/no change discrimination in the wetlands is deemed generally accurate. Therefore, the use of this change/no change map could facilitate the change type categorization phase of this study, since it is immune to potential errors emerging from post-classification comparison approach caused by inconsistent classifications of the 2004 and 2012 image.

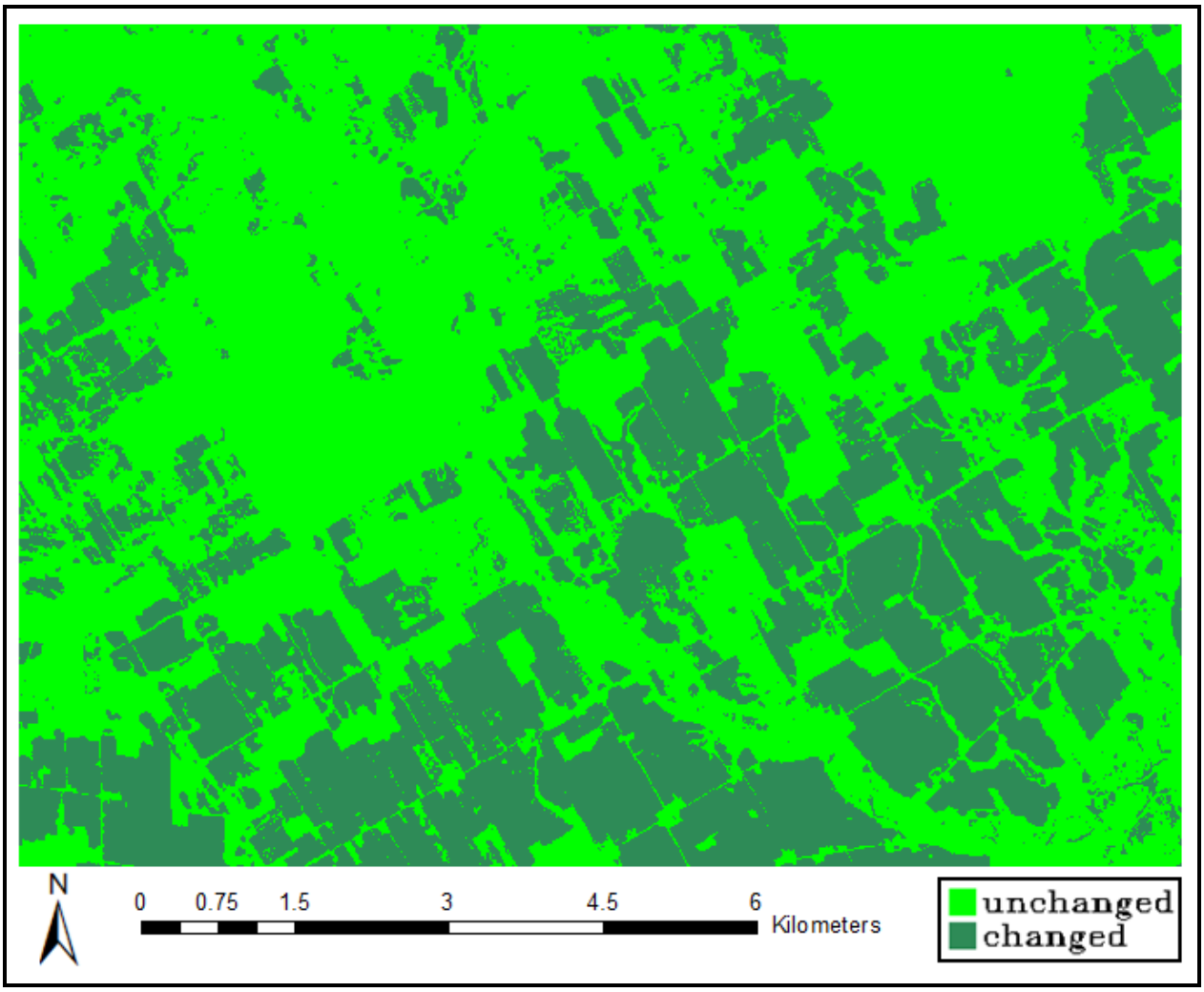

Figure 5.17 The best map derived from the change/no change discrimination analysis

5.3 Post-classification comparison

Prior to the extraction and analysis of quantitative change information using the post-classification comparison approach, the performance of the individual pairs of classifications subject to the post-classification comparison is examined. In Table 5.10 we summarize the accuracy scores of the single date classifications as well as the binary change/no change maps derived from the corresponding post-classification comparisons, where the accuracy scores associated with the most accurate change/no change classification are highlighted in bold. Despite the high accuracy of the single date object-based classifications, they suffer from relatively poor performance at the post-classification comparison stage, indicated by the highest overall accuracy of 79.2% and kappa coefficient of 0.58 among all the change/no change maps related with object-based classification. On the contrary, the pixel-based classifications boast comparatively higher performance in the post-classification comparison: all the change/no change maps determined by pixel-based classifications feature higher accuracy scores than the ones related with object classifications.

It should be noted that object-based classifications tend to overlook trivial fluctuations of spectral, textural, and spatial characteristics present at large scales, which contributes to the homogeneous presentation of the classified maps and relatively high classification accuracy at times. As a matter of fact, the segmentation parameters in object-based classifications play an irreplaceable role in determining the level of omission of these details, which may have differing influence on landscapes with distinctive characteristics. If two object-based classifications subject to post-classification comparison did not have an identical level of abstraction, changes would likely to emerge from the inconsistent mapping of the same heterogeneous object in post-classification comparison. In other words, the change/no change maps derived from object-based

classifications have the tendency to overestimate the extent of change, resulting in higher misclassification rates than the case with pixel-based classifications. Furthermore, it is highly possible that the abstraction in the individual object-based classifications could lead to the omission of significant land cover changes with relatively limited spatial extent, such as the loss of green corridors.

The column listing the product of the overall accuracy scores for the 2004 and 2012 classification aims to shed some light on the relationship between the quality of the individual classified maps and that of the change detection product derived from post-classification comparison. Owing to the high accuracy scores of the object-based classifications and their relatively poor performance in producing change/no change maps, the product of the individual overall accuracy scores exceed the accuracy of the change/no change map in each case that involves object-based classification. On the contrary, the binary change/no change maps based on pixel-based classifications feature higher overall accuracy than the product of the individual accuracy scores associated with the single date classifications. Therefore, it is suspected that the overall accuracy of the change/no change maps derived from post-classification comparison approach has the central tendency to fall into the range of 70 percent to 90 percent, regardless of the quality of the individual classifications. The reliability of the accuracy measures retrieved from confusion matrix may be improved by incorporating more testing samples, yet it is also possible that the accuracy of the binary change/no change maps does not fully represent the quality of the post-classification comparison. After all, a confusion matrix that entails every possible type of changed and unchanged class would be able to provide a more comprehensive assessment of the situation, if time and resources permitted.

In addition, it is found that the employment of textural features benefits not only the single date pixel-based classifications but also their derivatives in post-classification comparison phase, since the two classification pairs with the input of texture features have slightly higher accuracy scores than their counterparts that solely rely on spectral information. Furthermore, the adoption of the iterative majority filtering procedure was proven effective at the post-classification comparison stage, with the only exception of the best pixel-based classification pair, which has an overall accuracy of 85.0% and a kappa coefficient of 0.70 regardless of the application of the majority filter. In order to determine a pair more suitable for categorizing land cover changes, the change/no change maps associated with these two classification pairs are visually evaluated.

Table 5.10 Accuracy scores pertaining to the post-classification comparisons

Accuracy scores	2004 classification		2012 classification		Product of 2004 and 2012 overall accuracy	Post-classification comparison	
	Overall accuracy	Kappa coefficient	Overall accuracy	Kappa coefficient		Overall accuracy	Kappa coefficient
Best individual	91.2%	0.90	93.7%	0.93	85.5% >	79.2%	0.58
Best OO	91.2%	0.90	89.7%	0.88	81.8% >	75.8%	0.52
Unfiltered OO	90.6%	0.89	88.8%	0.87	80.5% >	74.6%	0.49
Best pixel	88.0%	0.86	93.7%	0.93	82.5% <	**85.0%**	**0.70**
Unfiltered best pixel	84.6%	0.82	87.4%	0.86	73.9% <	**85.0%**	**0.70**
Best raw	82.9%	0.80	86.9%	0.85	72.0% <	84.6%	0.69
Unfiltered raw	79.0%	0.76	80.5%	0.78	63.6% <	83.3%	0.67

According to Figure 5.18, the map based on unfiltered classifications exhibits a certain level of “salt and pepper” effect, while the other map derived from filtered classifications is able to present the changed and unchanged areas in a more compact fashion. The black rectangle in

Figure 5.18 highlights an instance of false change detected by the post-classification comparison approach. In spite of the varying tones of the area surrounding the creek in the two false color composite images, it is considered unchanged since it does not qualify as land cover change of a clear nature. This false alarm illustrates an intrinsic drawback of post-classification comparison approach. Figure 5.19 shows the two unfiltered pixel-based classifications subject to post-classification comparison as well as the extreme Getis classification for the same area. As can be seen from the top left corner of Figure 5.19, the area highlighted by the black box covers pixels identified as forest, plantation, pasture and agricultural fields in the 2004 classification. Although the identical set of classes can be found in the same area in the 2012 classification, they do not follow the same spatial distribution as the 2004 map, which is quite questionable. Unsurprisingly, the area is identified as changed due to the unmatching class memberships of the pixels within it. By contrast, this area is correctly categorized as unchanged in the extreme Getis classification, as the best practice derived from the change/no change discrimination phase of this study. Since it essentially analyzes spectral change in the multitemporal imagery, rather than attempting to extract information from the two images independently, the confusion between various land cover classes in the single image classification scenario is effectively avoided.

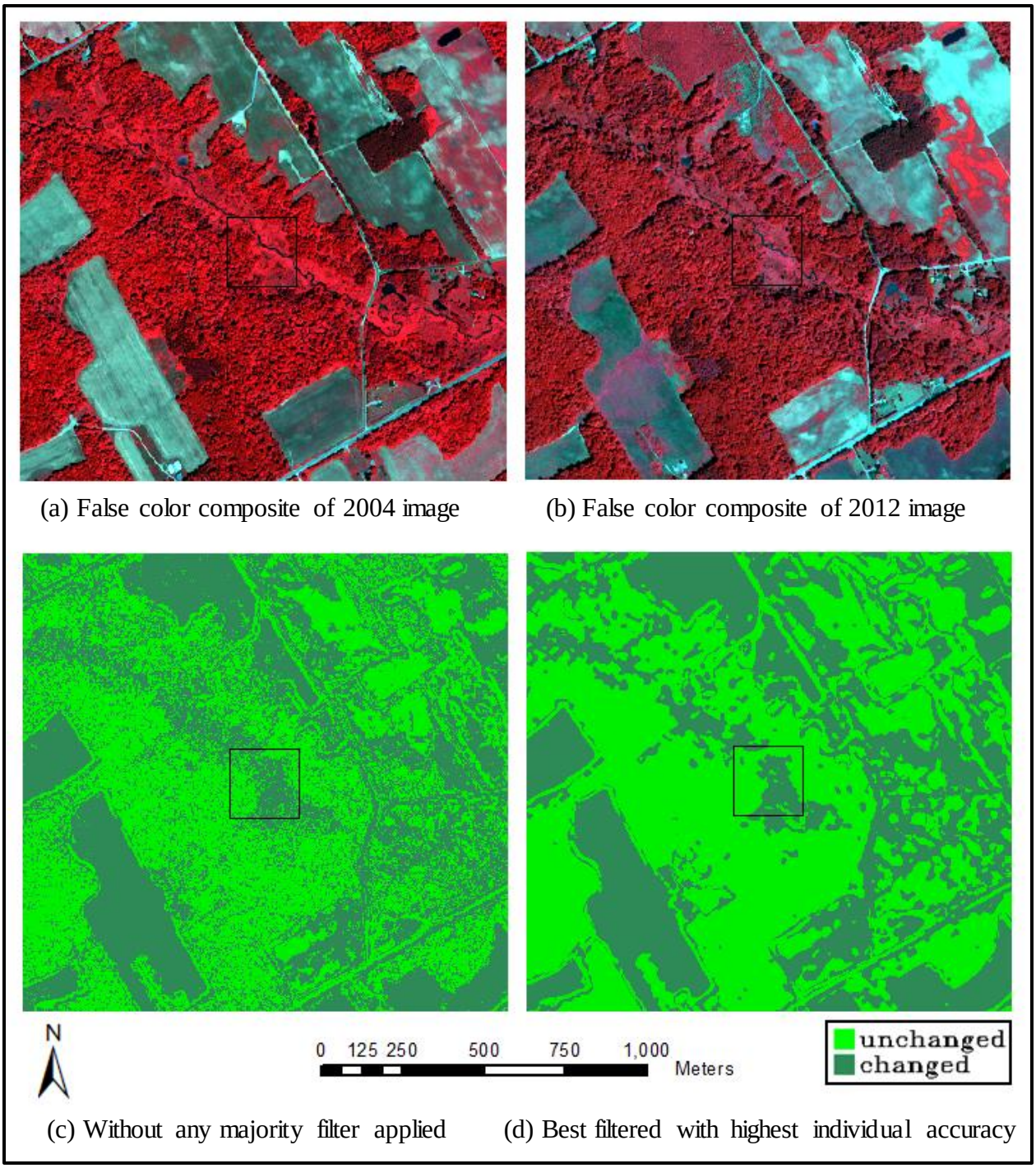

(a) False color composite of 2004 image (b) False color composite of 2012 image

(c) Without any majority filter applied (d) Best filtered with highest individual accuracy

Figure 5.18 Change/no change maps derived from different classification pairs

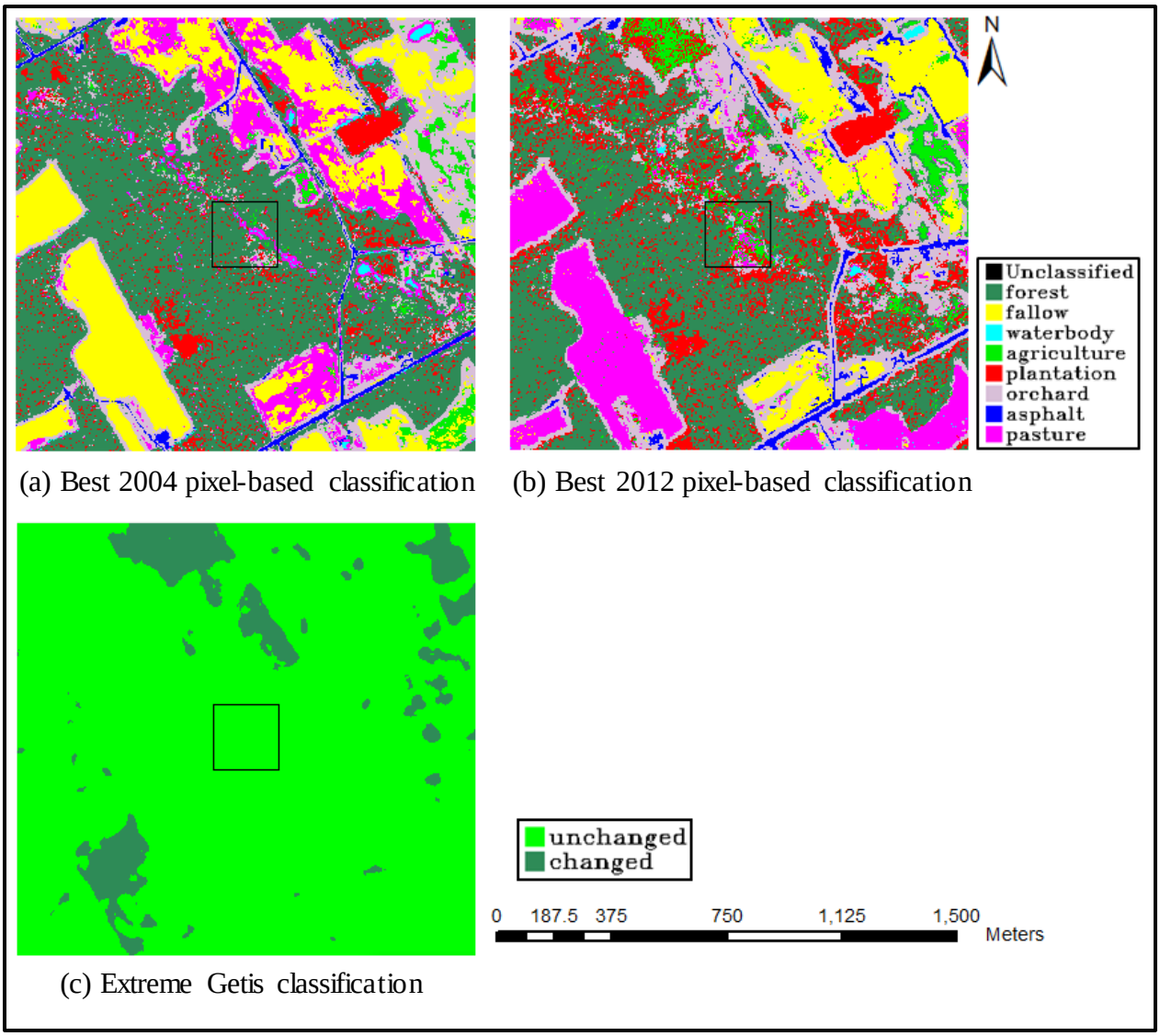

(a) Best 2004 pixel-based classification (b) Best 2012 pixel-based classification

(c) Extreme Getis classification

Figure 5.19 Illustration of the intrinsic drawback of the post-classification comparison approach

In light of the more homogeneous presentation of the binary change/no change map based on filtered classifications than its unfiltered counterpart through post-classification comparison, it will result in relatively compact patches of changed land in the land cover change map delivered as a final product from this study. Therefore, it was considered the best practice among all the change/no change maps derived from the post-classification comparison approach, despite the tied accuracy scores. Compared with the extreme Getis classification, boasting an overall accuracy of 92.5% and a kappa coefficient of 0.85, the accuracy scores of even the best

change/no change map based on post-classification comparison is surpassed: its overall accuracy and kappa coefficient is lower by 7.5% and 0.15 respectively. As a result, it is justified to use the changed areas from the extreme Getis classification as a mask to confine the geographic scope within which the change type categorization will be conducted.

Upon in-depth analysis of the transition matrix associated with the classification pair previously considered as the best practice, an area of approximately 5.4 square kilometer within the change mask was found to be converted from other types of cover to orchard, which is unlikely to be the reality within this time frame. After visual assessment of the "increased orchard coverage" in the change map, it is deemed as a result of the overestimation of orchard cover in the 2012 classification. More specifically, agricultural fields with greater spatial heterogeneity, potentially caused by the presence of drainage channels or cultivation ridges, tend to be misclassified as orchard in both the 2004 and 2012 image. This is essentially a side effect of incorporating texture features into the input feature set for SVM classification, since areas with relatively high level of intra-class spectral variability would be confused with orchard. The phenological difference between the two IKONOS images results in much more extensive coverage of agricultural fields in the 2012 image than the 2004 image, which means a larger number of pixels are misclassified as orchard in the 2012 image. Since this problem cannot be effectively solved by the introduction of the change mask, the classification pair consisting of best individual pixel-based classifications is no longer deemed appropriate for extracting quantitative information for this study.

Accordingly, the criteria for selecting the best post-classification comparison results were rationalized using a series of heuristic rules stated as follows:

Rule #1: Since changed class does not have to be pure, low user's accuracy for the changed class is acceptable.

Rule #2: Since unchanged class does not have to be pure, low user's accuracy for the unchanged class is acceptable.

Rule #3: Since strong capability of allocating changed pixels is desired, high producer's accuracy of the changed class is preferred.

Rule #4: Since the ability of allocating unchanged pixels is not critical, low producer's accuracy of the unchanged class is fine.

It should be noted that these rules are established on condition of the reliance on the change mask generated by the extreme Getis classification, such that the only responsibility for the post-classification comparison analysis is to derive the most accurate and reliable "from to" information within the mask. Therefore, the producer's accuracy of the changed class is of the most importance to the determination of the best classification pair to be used in conjunction with the change mask. Table 5.11 summarizes the detailed accuracy scores of the change/no change maps derived from post-classification comparison approach, where the highest producer's accuracy of the changed class is highlighted in bold. Considering the "salt and pepper" effect associated with the unfiltered classification pair utilizing texture input as well as its tendency of overestimating the coverage of orchard, the filtered classification pair based on raw multispectral bands of IKONOS is deemed more appropriate for the subsequent analysis, although they both feature a producer's accuracy of 98.3% of the changed class. Since all the classification pairs have similar producer's accuracy, a larger number of testing samples are desirable for more reliable accuracy assessment of the change/no change maps.

According to the class statistics of the binary map obtained from the best classification pair in the post-classification comparison group, nearly 60.4% of the study area is categorized as changed. By contrast, the extreme Getis classification is able to refine the changed area down to around 39.4% of the study area. According to the results obtained from post-classification comparison, roughly 1.4% of the study area is found to be unchanged within the change mask. In other words, approximately 3.6% of the pixels identified as changed in the extreme Getis classification have identical class membership in the 2004 and 2012 classifications. This discrepancy is mainly caused by the distinctive approaches taken by using these two streams of techniques towards the objective of detecting land cover changes, which is acceptable considering its limited percentage.

Table 5.11 Detailed accuracy scores of the post-classification comparisons

Accuracy scores	Changed		Unchanged	
	User's accuracy	Producer's accuracy	User's accuracy	Producer's accuracy
Best individual	72.2%	95.0%	92.7%	63.3%
Best OO	68.2%	96.7%	94.3%	55.0%
Unfiltered OO	67.1%	96.7%	94.0%	52.5%
Best pixel	78.4%	96.7%	95.7%	73.3%
Unfiltered best pixel	77.6%	**98.3%**	97.7%	71.7%
Best raw	77.1%	**98.3%**	97.7%	70.8%
Unfiltered raw	76.3%	96.7%	95.5%	70.0%

5.4 Land cover change interpretation

Summary statistics regarding the land cover changes found within the change mask is presented in the form of change matrix in Table 5.12. The diagonal elements in this table represent the number of pixels/area that had identical class membership in 2004 and 2012, while the off-diagonal elements are associated with land cover changes, with the column and row indicating the initial and final state of the cover respectively. Figures under the column entitled "Row total" stand for the total number of pixels/area for each type of land cover in 2004, while the figures in the row called "Column total" denote the total number of pixels/area for each type of land cover in 2012. The number of pixels/area that altered their membership from each class in the initial state is given in the row named "Class changes", which does not account for the population changing into the corresponding land cover classes. To supplement, the "Total gain/loss" column depicts the overall gain or loss of coverage for each class, which takes both the "incoming" and "outgoing" pixels/area into consideration.

As can be seen from Table 5.12, the coverage of fallow land has decreased by roughly 31 km^2 (84% of the fallow coverage in the 2004 image or 34% of the entire study area), mostly replaced by agricultural fields, which is consistent with the findings based on visual assessment of the multitemporal remote sensing imagery. On the other hand, the approximately 1 km^2 (3% of the fallow coverage in the 2004 image or 1% of the entire study area) of change from fallow to forest is mainly due to misclassification of agricultural fields as forest, since they possess extremely similar spectral signatures in certain cases, depending on factors such as the type of crop and soil moisture, etc. In addition, the spectral similarities between agricultural fields, orchard, and pasture has led to misclassification of these classes in either the 2004 or 2012 image, resulting in the estimated drop of pasture and orchard coverage with relatively large

magnitude, which actually have stable or even increasing coverage. Therefore, visual assessment of the change maps should be conducted in conjunction with the interpretation of summary statistics in the transition matrix, so as to put them into perspectives.

As an attempt to illustrate the potential of the proposed methodology, a few examples of land cover changes that are effectively detected and categorized are given below. Due to the large number of possible land cover transitions present in the study area, the change maps are shown in such a fashion that only changes with the same origin or outcome are shown in one display. For example, Figure 5.20 presents a subset of the map showing transitions from fallow to other classes. The green areas in this map delineate the change from fallow to agricultural fields, while the areas in pink represent the change from fallow to pasture. It should be noted that the black area denoted as unclassified in the legend means it does not cover any change originating from fallow, be it unchanged or changes of other classes. As can be seen from this map, there are a few black areas surrounded by pink, which are not successfully detected as change from fallow to pasture due to the spectral similarity between fallow land and pasture without abundant vegetation cover. In addition, the areas misclassified as change from fallow to orchard in this map are caused by the presence of a highly vegetated strip of land in the 2012 image, whose spectral signature is similar to that of orchard.

Despite the false estimation of increased forest cover resulting from misclassification, a few instances of deforestation can be identified from the change map, and Figure 5.21 shows one of them. More specifically, a patch of forest was converted into agricultural fields, fallow land, water body, and plantation, although the classification of water body and plantation is more likely to be the result of the shadow-casting edge of the adjacent forest stand. By contrast, some reforestation activities can be spotted from the change map as well, and one example of such is

shown in Figure 5.22, delineating pasture and fallow land changing to forest. Although the pasture shown in this map is more likely to be an agricultural field and that the trees are still in a relatively early stage of growth, it is considered as a sign of reforestation. It should be noted that the area to the northwestern corner of this patch is categorized as orchard in the 2012 classification due to the more sparsely spaced trees. Therefore, it is not shown in this map, since only areas with the outcome of forest are included in it. Figure 5.23 presents an interesting example of urban expansion. Due to the spectral heterogeneity of what appears to be an agricultural field in the 2004 image, it is categorized as orchard, fallow or agricultural field in the corresponding classification, which explains the relatively complex composition of the change map.

Table 5.12 Land cover change matrix

Land cover transitions		Initial state (2004) Expressed in Pixel count (area in Square Km)								
		Forest	Fallow	Water body	Agriculture	Plantation	Orchard	Asphalt	Pasture	Row total
Final State (2012)	Forest	820 (0.013)	66662 (1.067)	544 (0.009)	1459 (0.023)	1630 (0.026)	1450 (0.023)	118 (0.002)	3937 (0.063)	76620 (1.226)
	Fallow	1254 (0.020)	61299 (0.981)	717 (0.011)	19009 (0.304)	584 (0.009)	12710 (0.203)	491 (0.008)	5106 (0.082)	101170 (1.619)
	Water body	941 (0.015)	270 (0.004)	4205 (0.067)	4994 (0.080)	1102 (0.018)	925 (0.015)	17 (0.000)	1088 (0.017)	13542 (0.217)
	Agriculture	648 (0.010)	1880467 (30.087)	4765 (0.076)	12791 (0.205)	1106 (0.018)	39270 (0.628)	4280 (0.068)	64885 (1.038)	2008212 (32.131)
	Plantation	673 (0.011)	4947 (0.079)	3059 (0.049)	358 (0.006)	1036 (0.017)	432 (0.007)	1 (0.000)	1808 (0.029)	12314 (0.197)
	Orchard	0 (0.000)	9533 (0.153)	2642 (0.042)	123 (0.002)	360 (0.006)	70 (0.001)	1 (0.000)	3222 (0.052)	15951 (0.255)
	Asphalt	34 (0.001)	1050 (0.017)	27 (0.000)	1024 (0.016)	50 (0.001)	951 (0.015)	53 (0.001)	889 (0.014)	4078 (0.065)
	Pasture	431 (0.007)	37915 (0.607)	1147 (0.018)	3750 (0.060)	86 (0.001)	1414 (0.023)	94 (0.002)	2919 (0.047)	47756 (0.764)
	Column total	4801 (0.077)	2062143 (32.994)	17106 (0.274)	43508 (0.696)	5954 (0.095)	57222 (0.916)	5055 (0.081)	83854 (1.342)	
	Class changes	3981 (0.064)	2000844 (32.014)	12901 (0.206)	30717 (0.491)	4918 (0.079)	57152 (0.914)	5002 (0.080)	80935 (1.295)	
	Total gain/loss	71819 (1.149)	-1960973 (-31.376)	-3564 (-0.057)	1964704 (31.435)	6360 (0.102)	-41271 (-0.660)	-977 (-0.016)	-36098 (-0.578)	

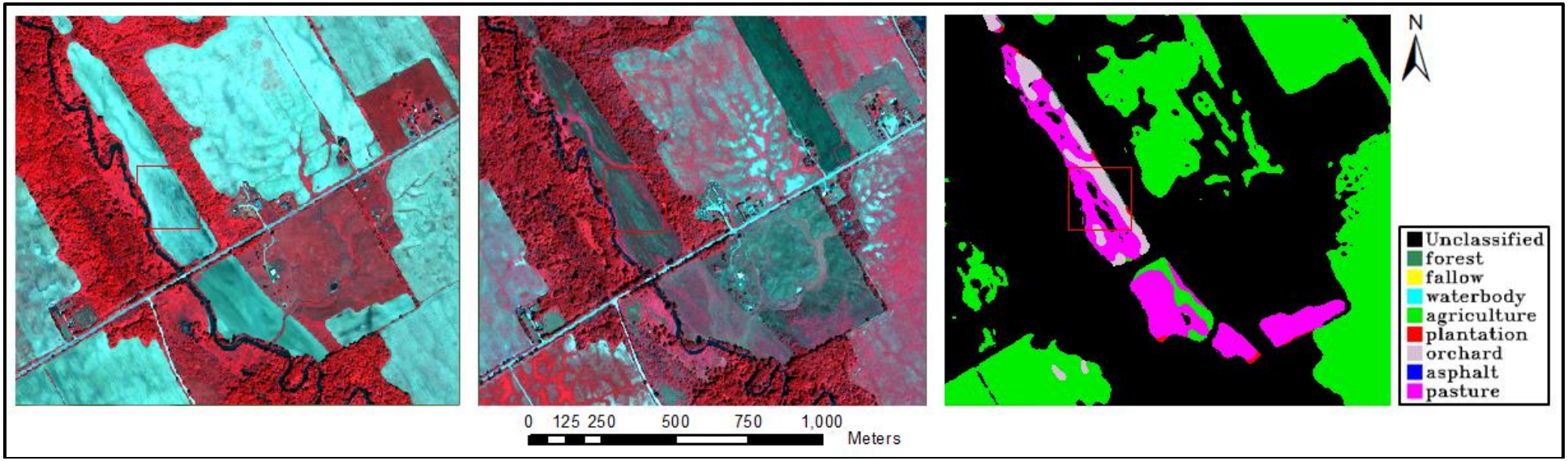

(a) False color composite of 2004 image (b) False color composite of 2012 image (c) Transition from fallow land

Figure 5.20 Change originating from fallow identified in the change detection analysis

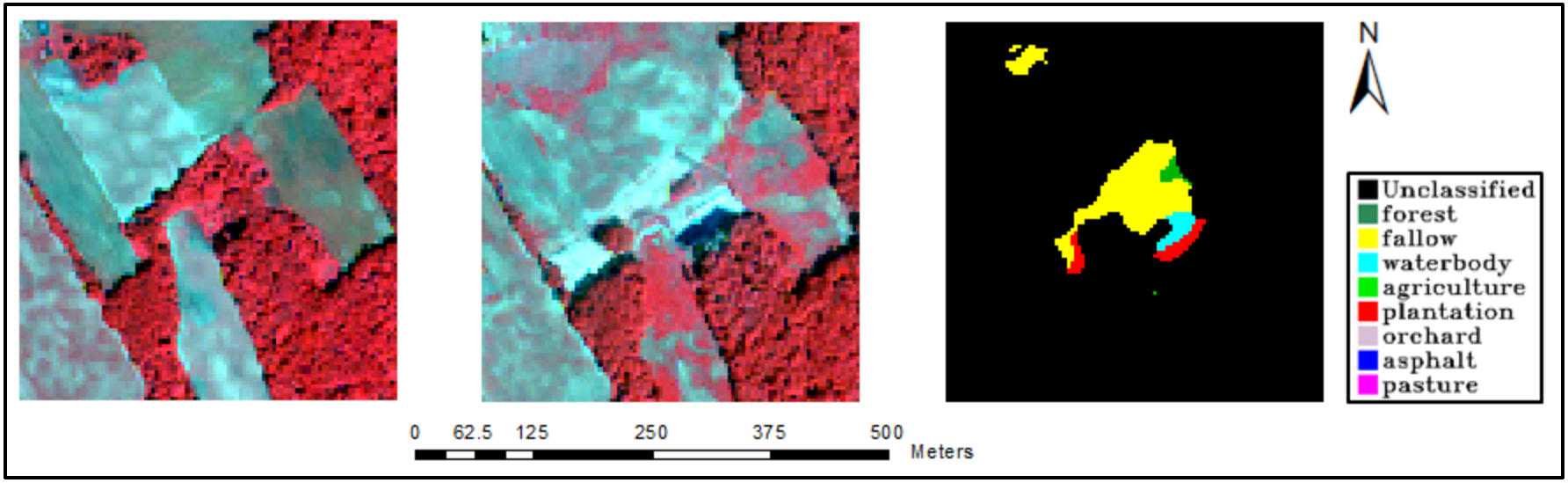

(a) False color composite of 2004 image (b) False color composite of 2012 image (c) Transition from forest

Figure 5.21 Forest loss identified in the change detection analysis

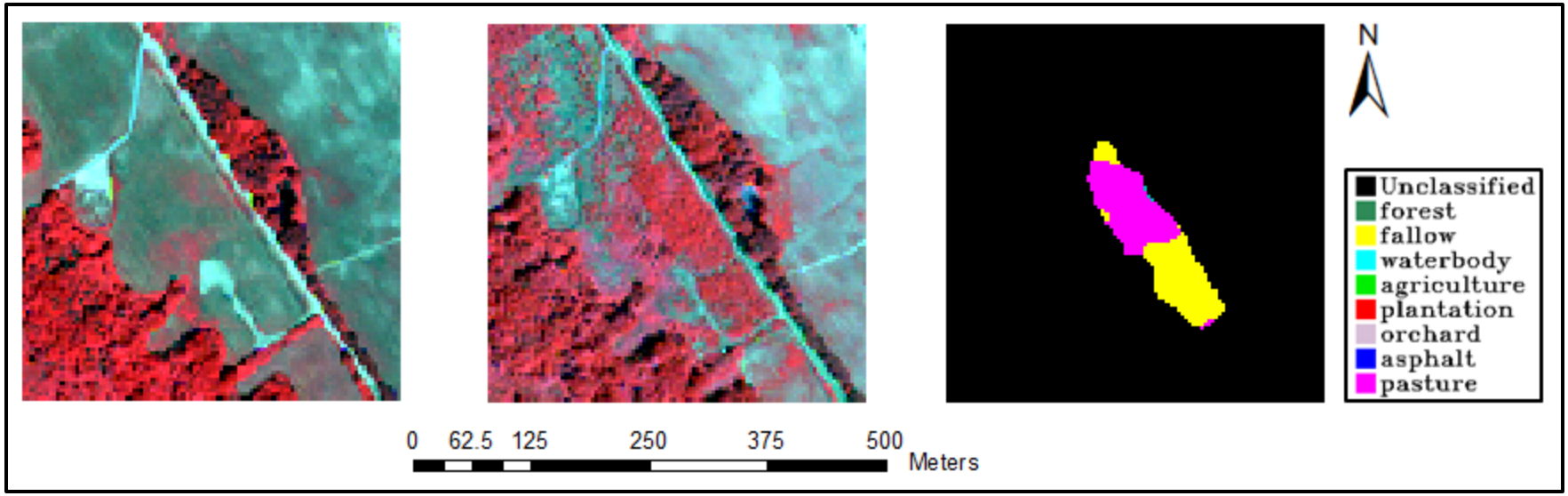

(a) False color composite of 2004 image (b) False color composite of 2012 image (c) Transition to forest

Figure 5.22 A sign of reforestation detected in the change detection analysis

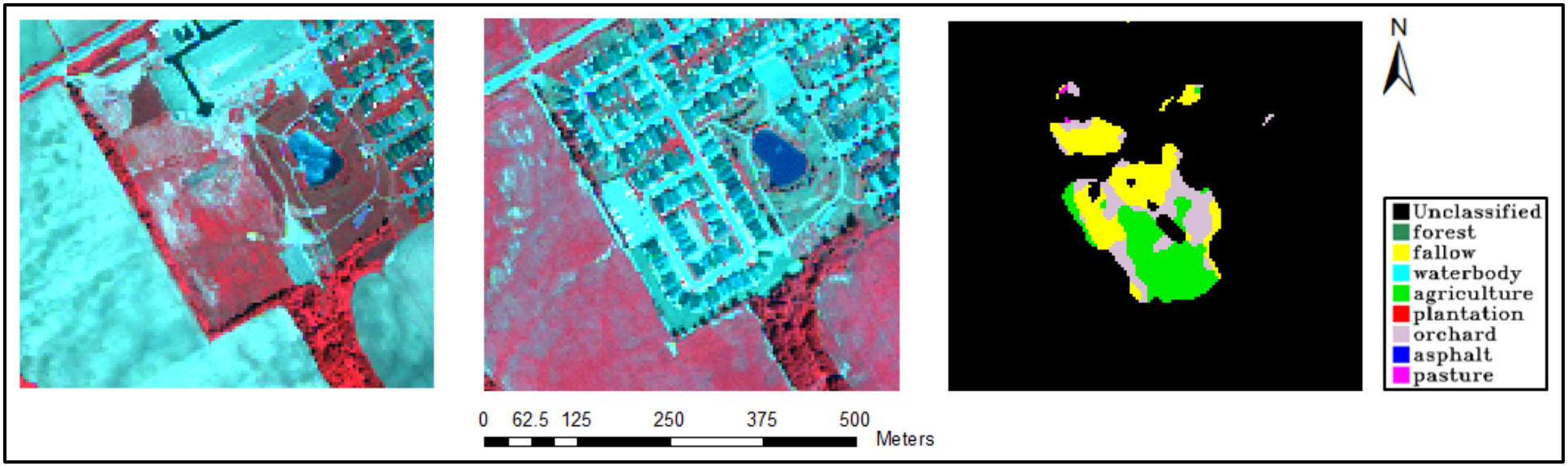

(a) False color composite of 2004 image (b) False color composite of 2012 image (c) Transition to residential area

Figure 5.23 Expansion of residential area discovered in the change detection analysis

In order to improve the interpretability of the change maps derived from the post-classification comparison approach, a few alternative strategies can be adopted. To start with, improved single date image classifications should be pursued, although proportional improvement of the post-classification comparison results might not be observed in accordance. In addition, vectorization of the extreme Getis classification could be used to generate image objects within which homogeneous changed patches are extracted, determined by the dominating class membership in the individual objects. Depending on the complexity of the class composition in each image object, a rule based classifier can be devised to assign the membership of the individual image objects according to summary statistics such as majority, variation, and percentages, even regardless of the allocation made by the extreme Getis classification. However, the quality of the image objects derived from the extreme Getis classification should be carefully examined, in order to ensure the accuracy of the subsequent analysis. Otherwise, objects covering multiple changed areas of different natures would seriously bias the change map.

Furthermore, it is relatively difficult to quantitatively assess the accuracy of the change map produced by post-classification comparison, no matter whether the above mentioned methods are employed, since there are simply too many categories in the change map. As a matter of fact, environmental conservation groups or planners may not be concerned with all kinds of land cover change available from the transition matrix, which sum up to 56 in this case: some are not of interest to them; others may not even be realistic, such as transition from residential to forest. Therefore, it would be reasonable to make use of the change angle components of CVA in a supervised manner based on a few predetermined types of change. This approach has the potential for reducing the errors induced by misclassifications in a typical land cover

classification. Due to the relatively small number of classes in the change map, accuracy assessment can be conducted in a similar fashion as land cover classification, using the confusion matrix. As a result, the results presented in the change map would be more clearly interpretable, with associated accuracy scores estimated based on a desired confidence interval. Alternatively, land cover classification for the multitemporal remote sensing imagery could be performed within the change mask determined by the extreme Getis classification, thus reducing the number of pixels that need to be classified. Accordingly, the problems related to intra-class variability can be alleviated, which may contribute to more accurate individual classifications than those produced in this study, even if the same classifier with the exact parameterization and input feature set is employed.

Chapter 6

Conclusions

In order to detect and categorize land cover changes in a typical rural environment in southern Ontario, which covers one of the 38 Carolinian signature sites, a hybrid change detection methodology is proposed in this study. After the multitemporal IKONOS images used in this study were coregistered and radiometrically rectified, both pixel-based and object-based classifications were performed to categorize the individual images into eight classes, where additional input features and majority filters were employed to improve the classified maps. In addition, CVA change magnitude and NDVI were used as two change indicators aimed at differentiating changed from unchanged pixels in the study area based on SVM classification. The influence of separating positive from negative changes on change/no change classification was also examined within the framework of NDVI differencing. After the Getis statistic was applied to the change descriptor images as a spatial filter, the extreme Getis classification was selected as the best practice for the change/no change discrimination analysis and was used to generate a change mask, serving the purpose of confining the geographic scope where quantitative change information is extracted. Furthermore, the usefulness of the classification pairs subject to post-classification comparison was systematically examined on the basis of a series of heuristic rules, thus ensuring the accuracy and interpretability of the change maps derived from this study.

Based on accuracy scores reported from the confusion matrix and visual interpretation of the change/no change maps produced by various change detection techniques, NDVI differencing used in conjunction with SVM classifier is considered to be the most effective method for detecting land cover changes in the study area, especially in the case of its 3-class

implementation. Compared with the results obtained from CVA change magnitude, the more accurate change/no change classifications derived from NDVI difference features prove that NDVI is a generally more efficient and sensitive change indicator than the CVA change magnitude, due to the dominance of vegetated land in the Big Creek area. Nevertheless, CVA change magnitude is able to detect changes underrepresented by NDVI, such as the development of pasture. Despite the similar results retrieved from the 2-class and 3-class implementation of NDVI differencing method, improvement, albeit with a relatively limited magnitude, was found with the application of the 3-class implementation of NDVI differencing, due to its isolation of positive and negative change in the classification.

In addition, the employment of the Getis statistic is able to improve the separability between changed and unchanged pixels by manipulating their distribution in the feature space determined by the individual change descriptors. As a result, the Getis classifications exhibit certain levels of improvement compared with those based on original change descriptors. The improvement lies not only in the higher accuracy scores, but also the increased overall homogeneity of the change/no change maps, which represents the reality better than the classifications suffering from a serious "salt and pepper" effect. Furthermore, the extreme Getis statistic is capable of presenting the change descriptor images in a way that maximizes the local spatial association, which can be essentially considered as a mechanism which automatically selects the optimal scale for spatial filtering. Such a characteristic of the extreme Getis statistic also relates to its potential for preservation of linear features in the image, such as local roads and green corridors, thus contributing to the study of significant habitats, especially their connectivity in natural spaces.

As an attempt to obtain more insight into the performance of the post-classification comparison approach, classification pairs derived from various sources are examined in terms of their potential for producing quality change/no change maps. Surprisingly, higher overall accuracy of the individual classifications does not necessarily lead to more accurate binary maps resulting from post-classification comparison, which is mainly affected by the intrinsic properties of the individual classifications. In particular, the varying classification units in pixel-based and object-based classifications tend to have distinctive implications in terms of the results of the post-classification comparison. Therefore, it is unadvisable to feed classified maps generated by different procedures to a post-classification comparison method, such as a pixel-based classification and an object-based classification. In addition, classifications based on inconsistent input feature sets may compromise the performance of the post-classification comparison approach, since they have distinctive misclassification tendencies.

Although the post-classification comparison is confined within the change mask determined by the best classification available in the change/no change discrimination phase of the workflow, the resulting transition matrix has a tangible margin of error, induced by misclassifications in either the 2004 or the 2012 classification. Therefore, visual assessment of the change maps has to be conducted in conjunction with the interpretation of the transition matrix. Apart from the extensive shift from fallow to agriculture across the entire study area, land cover changes in the Big Creek area are relatively limited in terms of coverage. In spite of the errors associated with the labeling of land cover changes, the change maps could enable the potential users to pinpoint the "hotspots" of change and help them reveal the nature of the change, with the aid of the visual assessment of the multitemporal remote sensing imagery. In other words, the qualitative change information derived from this study is more accurate and readily accessible than the quantitative

information, partially due to the much more demanding nature of the quantitative change analysis. In addition to the mapping practice itself for the Big Creek area, the main contribution of this study lies in the development of a change detection framework for a typical rural environment in southern Ontario with a relatively complex land cover configuration. Furthermore, the feasibility of using IKONOS imagery to identify key natural habitats was examined, from both single date mapping and change detection perspectives.

If the methodology proposed in this study were to be applied in a different environment with less complex land cover configuration, it is reasonable to expect improved performance at the change/no change discrimination level and the change type categorization stage as well, owing to the reduced number of classes in the classification scheme. That being said, it is strongly recommended that the characteristics of the study area should be fully understood and the priority information needs of the key interest groups well understood before the deployment of the change detection methodology by any interest group. More specifically, it is desirable that the classification scheme for each image be simplified to the greatest extent, since extra classes tend to induce misclassification errors, which would propagate to the deliverables of the change detection study. For example, orchard has an extremely limited coverage in the Big Creek area, which may not result in any meaningful land cover change statistics at all. However, incorporating it in the classification scheme reduced the accuracy of the single date classifications to a certain degree and compromised the interpretability of the change maps. If land cover classifications were only performed within the change mask as suggested in the discussion chapter, the change maps should experience a notable improvement.

In addition to the image processing point of view, the proposed methodology can also be improved from a resource utilization point of view. More specifically, the utility of the resources

(money, time, equipment, etc.) allocated for the field program should be maximized, such that the land cover change detection study can benefit the most from the field work. Despite the fact that spectral measurements made with a spectrometer are able to give the researchers an intimate understanding of the surface conditions of various land covers present in the study area, they are particularly time consuming compared with field reconnaissance based on human inspection and photography of the landscape under investigation. For the sake of consistent acquisition conditions between the satellite imagery and in situ spectral measurements, the field work was undertaken synchronously with the satellite overpass. Essentially, any cloudy day was avoided for the field trip based on the premise that any spectral profiles collected on a cloudy day would be as useless as a satellite image with excessive cloud coverage. As a matter of fact, field trips should not be necessarily linked to spectral measurements: human inspection alone could be very informative for understanding the local land cover configurations no matter whether it was conducted on a cloudy day or not. In light of this, it is suggested that field inspections be made regardless of the spectral measurements that may not make substantial contribution to the change detection analysis after all. Without the constraint requirements of in situ spectral measurements, relatively comprehensive understanding of the spatial distribution of various land cover classes would be available upon multiple field inspections.

On the other hand, the use of in situ spectral measurements for radiometric correction purposes require that the same set of sample sites be covered in the individual field trips, such that variability of the image acquisition conditions within the contracted time window of acquisition can be captured. As a matter of fact, the spectral profiles collected at any sample site depend upon a series of factors, such as time of the day, cloud coverage, soil moisture, etc. Furthermore, the disparity between the footprint of the satellite observation and that of the ASD

spectrometer makes the spectral signatures collected by the respective instrument less comparable than one may assume. Although this problem may be resolved by the employment of certain sampling strategies for the in situ spectral measurements, it is not very feasible in the field, considering the privately-owned nature of most of the agricultural fields in the Big Creek area. In addition, the spectral profiles can only be collected for certain sample sites, which mainly include pavement surface as well as fallow and agricultural fields. The other types of cover are less accessible based on the limited resources allocated for this study. Essentially, the potential contribution of the in situ spectral measurements is relatively limited for this particular study area: even if the spectral profiles acquired by an ASD spectrometer were comparable to those acquired by the imaging satellite, they would not directly benefit any specific radiometric correction procedure, due to the lack of deep water bodies as calibration targets in the study area.

Furthermore, the spectral measurements made in approximately the same time window as the satellite overpass would only represent the surface conditions within this specific period, should variations of the physical conditions within this time frame not be considered or sampled. Even if a rigorous radiometric correction procedure could be performed based on these in situ measurements, the correction would be less accurate for the historical image, since the assumption that the multitemporal remote sensing images are acquired under the same physical conditions may not be valid. Therefore, it is recommended that the field program be set out from a land cover point of view, which does not necessarily require quantitative spectral measurements. Consequently, more comprehensive understanding of the local land cover configurations could result from the more frequent and efficient in situ human inspections that are not strictly restricted by weather conditions. This would facilitate the design of the

classification scheme for the study area as well as the determination of training samples for the supervised approaches to be employed in the subsequent change detection analysis.

The land cover change analysis based on remote sensing imagery is essentially delivering a product similar to the development of software in the field of software engineering, which follows a classic life cycle, starting with requirements analysis and specification (Schach, 2002). This phase is deemed equally important in change detection analysis or the derivation of information based on remote sensing imagery at large. It focuses on the understanding of the basic needs of the client and put them into technical terms, such that the developers are able to reach an understanding with the client, with necessary revisions going back and forth. In the case of change detection analysis, it is of utmost importance for the analyst to understand the changes of interest to the potential users of the mapping product. In turn, it is the responsibility of the analyst to inform the users of the capability and limitations of the current remote sensing imagery and image processing techniques, thus the scope and feasibility of the project could be understood clearly. Despite the generally fixed concept of the individual change detection techniques, there is a high level of flexibility when it comes to their implementations. Therefore, the communication back and forth between the map users and the analyst would facilitate the determination of a series of tradeoffs required at various stages of the workflow. In this way, the strengths of the remote sensing imagery and techniques can be utilized and their weaknesses avoided.

References

Afify, H. A. (2011). Evaluation of change detection techniques for monitoring land-cover changes: A case study in new Burg El-Arab area. *Alexandria Engineering Journal*, *50*(2), 187-195.

Allen, T. R., & Kupfer, J. A., (2000). Application of spherical statistics to change vector analysis of Landsat data: Southern Appalachian spruce-fir forests. *Remote Sensing of Environment, 74*, 482–493.

Alphan, H., Doygun, H., & Unlukaplan, Y. I. (2009). Post-classification comparison of land cover using multitemporal Landsat and ASTER imagery: the case of Kahramanmaraş, Turkey. *Environmental monitoring and assessment*, *151*(1), 327–336.

Anselin, L. (1995). Local indicators of spatial association-LISA. *Geographical analysis*, *27*(2), 93–115.

Anys, H., Bannari, A., He, D. C., & Morin, D. (1994). "Texture analysis for the mapping of urban areas using airborne MEIS-II images," *Proceedings of the First International Airborne Remote Sensing Conference and Exhibition, Strasbourg, France*, Vol. 3, pp. 231-245.

Atkinson, P. M., & Lewis, P. (2000). Geostatistical classification for remote sensing: an introduction. *Computers & Geosciences*, *26*(4), 361-371.

Blaschke, T. (2010). Object-based image analysis for remote sensing. *ISPRS journal of photogrammetry and remote sensing*, *65*(1), 2-16.

Breiman, L. (2001). Random forests. *Machine learning*, *45*(1), 5-32.

Brooks, T. M., Mittermeier, R. A., Mittermeier, C. G., Da Fonseca, G. A., Rylands, A. B., Konstant, W. R., ... & Hilton-Taylor, C. (2002). Habitat loss and extinction in the hotspots of biodiversity. *Conservation biology*, *16*(4), 909-923.

Bruzzone, L. (2000). Automatic analysis of the difference image for unsupervised change detection. *IEEE Transactions on Geoscience and Remote Sensing*, *38*(3), 1171-1182.

Carolinian Canada Coalition. (2013a). Who We Are. Retrieved from http://caroliniancanada.ca/about

Carolinian Canada Coalition. (2013b). The 1984 Carolinian Canada Signature Sites. Retrieved from http://caroliniancanada.ca/legacy/CarolinianSites_1984CarolinianCanadaSites.htm

Carolinian Canada Coalition, (2013c). The Big Picture Network: Norfolk County. Retrieved from http://www.carolinian.org/BigPicture_Network_Norfolk.htm

Congalton, R. G., & Green, K. (2009). *Assessing the accuracy of remotely sensed data: principles and practices*. CRC press.

Chander, G., Markham, B. L., & Helder, D. L. (2009). Summary of current radiometric calibration coefficients for Landsat MSS, TM, ETM+, and EO-1 ALI sensors. *Remote sensing of environment*, *113*(5), 893-903.

Chen, J., Gong, P., He, C., Pu, R., & Shi, P. (2003). Land-use/land-cover change detection using improved change-vector analysis. *Photogrammetric Engineering and Remote Sensing*, *69*(4), 369-380.

Chen, G., Hay, G. J., Carvalho, L. M. T., & Wulder, M. A. (2012). Object-based change detection. *International Journal of Remote Sensing*, *33*(14), 4434–4457.

Chica-Olmo, M., & Abarca-Hernandez, F. (2000). Computing geostatistical image texture for remotely sensed data classification. *Computers & Geosciences*, *26*(4), 373–383.

Coppin, P., Jonckheere, I., Nackaerts, K., Muys, B., & Lambin, E. (2004). Review Article Digital change detection methods in ecosystem monitoring: a review. *International journal of remote sensing*, *25*(9), 1565–1596.

Cracknell, A. P. (1998). Review article Synergy in remote sensing-what's in a pixel? *International Journal of Remote Sensing*, *19*(11), 2025-2047.

Desclée, B., Bogaert, P., & Defourny, P. (2006). Forest change detection by statistical object-based method. *Remote Sensing of Environment*, *102*(1-2), 1-11.

Du, Y., Teillet, P. M., & Cihlar, J. (2002). Radiometric normalization of multitemporal high-resolution satellite images with quality control for land cover change detection. *Remote Sensing of Environment*, *82*, 123–134.

Elmore, A. J., Mustard, J. F., Manning, S. J., & Lobell, D. B. (2000). Quantifying vegetation change in semiarid environments: precision and accuracy of spectral mixture analysis and the normalized difference vegetation index. *Remote Sensing of Environment*, *73*(1), 87-102.

ENVI HELP, (2013). Applying Support Vector Machine Classification. Environment for Visualizing Images.

Exelis Visual Information Solutions. (2013a). Computing ROI Separability.

Exelis Visual Information Solutions. (2013b). IKONOS Calibration Utilities.

Exelis Visual Information Solutions. (2013c). Fast Line-of-sight Atmospheric Analysis of Spectral Hypercubes.

Exelis Visual Information Solutions. (2013d). Warping and Resampling.

Exelis Visual Information Solutions. (2013e). Texture Filter.

Exelis Visual Information Solutions. (2013f). Support Vector Machine.

Exelis Visual Information Solutions. (2013g). Feature Extraction with Rule-Based Classification.

Fu, K. S., & Mui, J. K. (1981). A survey on image segmentation. *Pattern recognition*, *13*(1), 3-16.

Fung, T., & LeDrew, E. F. (1987). Application of principal components analysis to change detection. *Photogrammetric Engineering and Remote Sensing*, *53*, 1649–1658.

Fung, T. (1990). An assessment of TM imagery for land cover change detection. *IEEE Transactions on Geoscience and Remote Sensing*, *28*, 681–684.

Gamba, P., Acqua, F. D., & Lisini, G. (2006). Change detection of multitemporal SAR data in urban areas combining feature-based and pixel-based techniques. *IEEE Transactions on Geoscience and Remote Sensing*, *44*(10), 2820-2827.

GeoEye. (2006). IKONOS imagery products guide. Retrieved from http://glcf.umd.edu/library/guide/IKONOS_Product_Guide_jan06.pdf

GeoEye. (2013). IKONOS imagery metadata.

Getis, A., & Ord, J. K. (1992). The analysis of spatial association by use of distance statistics. *Geographical Analysis*, *24*(3), 189-206.

Ginevan, M. E. (1979). Testing land-use map accuracy: another look. *Photogrammetric Engineering and Remote Sensing*, *45*(10), 1371-1377.

Gong, J., Sui, H., Ma, G., & Zhou, Q. (2008). A review of multi-temporal remote sensing data change detection algorithms. *The International Archives of the Photogrammetry, Remote Sensing and Spatial Information Sciences*, *XXXVII*(Part B7), 757-762.

Gong, P. (1993). Change detection using principal component analysis and fuzzy set theory. *Canadian Journal of Remote Sensing*, *19*(1), 22–29.

Gong, P., Xu, B. (2003). Remote sensing of forests over time: change types, methods, and opportunities, in Woulder M., Franklin S.E., Eds. Remote Sensing of Forest Environments: Concepts and Case Studies, Kluwer Press, Amsterdam, Netherlands. pp. 301-333.

Google Map. (2013). Map of North America. Retrieved from http://maps.google.ca/

Grossman, R. & Forrester, A. L. (2001). Exploring remote sensing through forestry applications. Canadian Space Agency. Retrieved from: http://www.csa.com/discoveryguides/remote/overview.php

Hall, O., & Hay, G. J. (2003). A multiscale object-specific approach to digital change detection. *International Journal of Applied Earth Observation and Geoinformation*, *4*(4), 311-327.

Haralick, R. M., Shanmugam, K., & Dinstein, I. (1973). Textural Features for Image Classification. *IEEE Transactions on Systems, Man, and Cybernetics*, *3*(6), 610–621.

Hay, G. J., Marceau, D. J., Dube, P., & Bouchard, A. (2001). A multiscale framework for landscape analysis: object-specific analysis and upscaling. *Landscape Ecology*, *16*(6), 471-490.

Healey, S. P., Cohen, W. B., Yang, Z., & Krankina, O. N. (2005). Comparison of Tasseled Cap-based Landsat data structures for use in forest disturbance detection. *Remote Sensing of Environment*, *97*(3), 301-310.

Horne, J. H. (2003). A tasseled cap transformation for IKONOS images. In *ASPRS 2003 Annual conference proceedings* (pp. 60-70).

Hsu, C. W., Chang, C. C., & Lin, C. J. (2010). A practical guide to support vector classification. National Taiwan University. Retrieved from http://ntu.csie.org/~cjlin/papers/guide/guide.pdf

Jalava, J. V., Sorrill, P. J., Henson, J., & Brodri, K., (2000). The big picture project: developing a natural heritage vision for Canada's southernmost ecological region.

Jin, Y.-Q., & Yan, F. (2004). Monitoring sandstorms and desertification in northern China using SSM/I data and Getis statistics. *International Journal of Remote Sensing*, *25*(11), 2053–2060.

Johnson, L., (2007). The natural treasures of Carolinian Canada. Carolinian Canada Coalition.

Justice, C.O. & Townshend, J.R.G. (1981). Integrating ground data with remote sensing. In J.R.G. Townshend (Ed) *Terrain Analysis and Remote Sensing*, George Allen and Unwin, London, 38-58.

Karpouzli, E., & Malthus, T. (2003). The empirical line method for the atmospheric correction of IKONOS imagery. *International Journal of Remote Sensing*, *24*(5), 1143-1150.

Karsh, M., MacIver, D. C., Fenech, A., & Auld, H. (2007). Climate-based predictions of forest biodiversity using Smithsonian's global earth observing network. Environment Canada. Retrieved from: http://publications.gc.ca/collections/collection_2012/ec/En57-41-8-2007-eng.pdf

Kartikeyan, B., Sarkar, A., & Majumder, K. L. (1998). A segmentation approach to classification of remote sensing imagery. *International Journal of Remote Sensing*, *19*(9), 1695-1709.

Keuchel, J., Naumann, S., Heiler, M., & Siegmund, A. (2003). Automatic land cover analysis for Tenerife by supervised classification using remotely sensed data. *Remote Sensing of Environment, 86*(4), 530-541.

Lambin, E. F., & Strahler, A. H. (1994). Change-vector analysis in multitemporal space: a tool to detect and categorize land-cover change processes using high temporal-resolution satellite data. *Remote Sensing of Environment*, *48*(2), 231-244.

LAND INFO Worldwide Mapping, LLC. (2013). High-Resolution Satellite Imagery. Retrieved from: http://www.landinfo.com/products_satellite.htm

LeDrew, E. F., Holden, H., Wulder, M. A., Derksen, C., & Newman, C. (2004). A spatial statistical operator applied to multidate satellite imagery for identification of coral reef stress. *Remote Sensing of Environment*, *91*(3), 271-279.

Li, X., & Strahler, A. H. (1992). Geometric-optical bidirectional reflectance modeling of the discrete crown vegetation canopy: Effect of crown shape and mutual shadowing. *IEEE Transactions on Geoscience and Remote Sensing*, *30*(2), 276-292.

Long Point Region Conservation Authority. (2008). Long Point Region Watershed Characterization Report. Retrieved from http://www.sourcewater.ca/swp_watersheds_longpoint/Characterization_summary_LPR.pdf

Lu, D., Mausel, P., Brondízio, E., & Moran, E. (2004). Change detection techniques. *International Journal of Remote Sensing*, *25*(12), 2365-2407.

Malila, W. A. (1980). Change vector analysis: an approach for detecting forest changes with Landsat. In *LARS Symposia* (p. 385).

McDermid, G. J., Franklin, S. E., & LeDrew, E. F. (2005). Remote sensing for large-area habitat mapping. *Progress in Physical Geography*, *29*(4), 449-474.

McFeeters, S. K. (1996). The use of the Normalized Difference Water Index (NDWI) in the delineation of open water features. *International journal of remote sensing*, *17*(7), 1425-1432.

Mountrakis, G., Im, J., & Ogole, C. (2011). Support vector machines in remote sensing: A review. *ISPRS Journal of Photogrammetry and Remote Sensing*, *66*(3), 247-259.

Nackaerts, K., Vaesen, K., Muys, B., & Coppin, P. (2005). Comparative performance of a modified change vector analysis in forest change detection. *International Journal of Remote Sensing, 26*, 839-852.

Newman, C. M., Knudby, A. J., & LeDrew, E. F. (2007). Assessing the effect of management zonation on live coral cover using multi-date IKONOS satellite imagery. *Journal of Applied Remote Sensing*, *1*.

Ontario Ministry of Natural Resources. (2013). Ecological Land Classification Primer. Retrieved from http://www.mnr.gov.on.ca/stdprodconsume/groups/lr/@mnr/@lueps/documents/document/264777.pdf

Ord, J. K., & Getis, A. (1995). Local spatial autocorrelation statistics: distributional issues and an application. *Geographical analysis*, *27*(4), 286–306.

Pal, M., & Mather, P. M. (2005). Support vector machines for classification in remote sensing. *International Journal of Remote Sensing*, *26*(5), 1007-1011.

Peddle, D. R., Teillet, P.M., & Wulder, M.A. (2003). Radiometric image processing, in Woulder M., Franklin S.E., Eds. *Remote Sensing of Forest Environments: Concepts and Case Studies*, Kluwer Press, Amsterdam, Netherlands. pp. 181-208.

Petit, C., Scudder, T., & Lambin, E. (2001). Quantifying processes of land-cover change by remote sensing: resettlement and rapid land-cover changes in south-eastern Zambia. *International Journal of Remote Sensing*, *22*(17), 3435-3456.

Piwowar, J. M., & Ledrew, E. F. (1995). Hypertemporal Analysis of Remotely Sensed Sea Ice Data. *Progress in Physical Geography*, *19*(2), 216-242.

Pu, R., Gong, P., Tian, Y., Miao, X., Carruthers, R. I., & Anderson, G. L. (2008). Using classification and NDVI differencing methods for monitoring sparse vegetation coverage: a case study of saltcedar in Nevada, USA. *International Journal of Remote Sensing*, *29*(14), 3987-4011.

Ridd, M. K., & Liu, J. (1998). A comparison of four algorithms for change detection in an urban environment. *Remote sensing of environment*, *63*(2), 95-100.

Rouse, J. W., Haas, R. H., Schell, J. A., Deering, D. W., & Harlan, J. C. (1974). Monitoring the vernal advancement and retrogradation (greenwave effect) of natural vegetation. *NASA/GSFC Final report*, Greenbelt, MD, USA.

Samadzadegan, F., Bigdeli, B., & Ramzi, P. (2010). A multiple classifier system for classification of LIDAR remote sensing data using multi-class SVM. In *Multiple Classifier Systems* (pp. 254-263). Springer Berlin Heidelberg.

Schach, S. R. (2002). Object-oriented and classical software engineering (Vol. 6). New York: McGraw-Hill.

Schott, J. R., Salvaggio, C., & Volchok, W. J. (1988). Radiometric scene normalization using pseudoinvariant features. *Remote Sensing of Environment*, *26*(1), 1-16.

Seixas, J. (2000). Assessing heterogeneity from remote sensing images: the case of desertification in southern Portugal. *International Journal of Remote Sensing*, *21*(13-14), 2645–2663.

Serra, P., Pons, X., & Sauri, D. (2003). Post-classification change detection with data from different sensors: Some accuracy considerations. *International Journal of Remote Sensing*, *24*(16), 3311-3340.

Singh, A. (1989). Review Article Digital change detection techniques using remotely-sensed data. *International Journal of Remote Sensing*, *10*(6), 989-1003.

Song, C., Woodcock, C., & Seto, K. (2001). Classification and change detection using Landsat TM data: when and how to correct atmospheric effects? *Remote Sensing of Environment*, *75*(2), 230–244.

Swain, P. H., & Davis, S. M. (Eds.). (1978), Remote Sensing: The Quantitative Approach. New York: McGraw-Hill.

Toutin, T. (2003). Geometric correction of remotely sensed images, in Woulder M., Franklin S.E., Eds. *Remote Sensing of Forest Environments: Concepts and Case Studies*, Kluwer Press, Amsterdam, Netherlands. pp. 143-180.

Walter, V. (2004). Object-based classification of remote sensing data for change detection. *ISPRS Journal of Photogrammetry and Remote Sensing*, *58*(3-4), 225-238.

Wang, F., & Xu, Y. J. (2010). Comparison of remote sensing change detection techniques for assessing hurricane damage to forests. *Environmental monitoring and assessment*, *162*(1-4), 311-326.

Weeks, J., Gadalla, M., Rashed, T., & Stanforth, J. (2000). Spatial variability in fertility in Menoufia, Egypt, assessed through the application of remote-sensing and GIS technologies. *Environment and Planning A*, *32*(1929), 695– 714.

Wulder, M., & Boots, B. (1998). Local spatial autocorrelation characteristics of remotely sensed imagery assessed with the Getis statistic. *International Journal of Remote Sensing, 19*(11), 2223–2231.

Wulder, M., & Boots, B. (2001). Local spatial autocorrelation characteristics of Landsat TM imagery of a managed forest area. *Canadian journal of remote sensing*, *27*(1), 67–75.

Wulder, M. A., Kurz, W. A., & Gillis, M. (2004). National level forest monitoring and modeling in Canada. *Progress in Planning, 61*(4), 365-381.

Wulder, M. A., White, J. C., Coops, N. C., Nelson, T., & Boots, B. (2007). Using local spatial autocorrelation to compare outputs from a forest growth model. *Ecological Modelling*, *209*(2-4), 264–276.

Yang, X., & Lo, C.P., (2000). Relative radiometric normalization performance for change detection from multi-date satellite images. *Photogrammetric Engineering and Remote Sensing, 66(8),* 967-980.

Yu, Q., Gong, P., Clinton, N., Biging, G., Kelly, M., & Schirokauer, D. (2006). Object-based detailed vegetation classification with airborne high spatial resolution remote sensing imagery. *Photogrammetric Engineering and Remote Sensing, 72*(7), 799-811.

Zeng, Y., Schaepman, M. E., Wu, B., Clevers, J. G., & Bregt, A. K. (2008). Scaling-based forest structural change detection using an inverted geometric-optical model in the Three Gorges region of China. *Remote Sensing of Environment, 112*(12), 4261-4271.

Glossary

Carolinian Canada Coalition (CCC): Currently a registered charity, CCC is a prominent Canadian ecoregional group that was initially founded in 1984. During years of operation, CCC has drawn on the synergy of various people, organizations and governments to protect the fragile yet significant Carolinian Life Zone and address related environmental issues through ongoing education, research, and coordination (Carolinian Canada Coalition, 2013a).

Ecological land classification (ELC): A classification system that divides the natural landscape into individual categories based on their ecological characteristics to facilitate scientific research and planning practices (Ontario Ministry of Natural Resources, 2013).

Global indicators of spatial association: They refer to a class of tests that examine the presence of spatial autocorrelation within a given spatial dataset. Based on a specific test score, such as global Moran's I, it can be determined whether the null hypothesis of absence of spatial autocorrelation within the dataset can be rejected or not within a desired confidence interval. If the null hypothesis is not rejected, it implies that the distribution of the variable of interest does not follow any spatial pattern (random distribution). Therefore, objects located near each other do not have more similar values than objects located further away, and there is no distance decay effect regarding the correlation of variables of interest (Anselin, 1995).

Grey Level Co-occurrence Matrix (GLCM): A distribution used to estimate the textural properties of an image derived from spatial kernel functions with a user-specified range. The deliverables of the GLCM approach are similar to that of the occurrence matrix, yet they are based on the co-occurrence matrix rather than the occurrence matrix. The occurrence matrix directly presents the values within the moving window, while the co-occurrence matrix keeps

track of the counts of the unique combinations of values in the joint moving windows with a predetermined spatial lag (Haralick, Shanmugam, & Dinstein, 1973).

IKONOS: The name of an optical imaging satellite launched in 1999 and also the multispectral sensor onboard this platform. It is the first commercial remote sensing imagery that reached the spatial resolution of one meter, and has been used for a variety of geospatial applications (LAND INFO Worldwide Mapping, LLC, 2013).

Local indicators of spatial association (LISA): Unlike global indicators of spatial association, which summarizes the spatial attributes of the entire study area with a single test score based on a specific measure, local indicators of spatial association (LISA) are a group of statistics that presents spatial association at a predefined local level based on moving windows. Global indicators of spatial association assume a universal trend over the entire region being studied regarding the spatial distribution of variables of interest (stationarity), which might not hold true under all circumstances. When this assumption is violated, LISA is able to provide details regarding the characteristics of spatial association at local level. Some of the popular statistics that fall into the category of LISA include local Moran's I, Getis Ord's Gi, and Geary's C (Anselin, 1995).

Local spatial autocorrelation: The variation of spatial patterns of geospatial variables on a local scale. It is an important topic in the field of spatial analysis, especially if local spatial dependence is an obstacle or of interest (Ord & Getis, 1995).

Maximum Getis Distance (MGD): A variable derived from the Getis image stack that indicates the maximum range of local spatial association. It is determined by selection of the window size that leads to the maximum Getis value for each pixel in the image under investigation (LeDrew, Holden, Wulder, Derksen, & Newman, 2004).

Normalized Difference Water Index (NDWI): A spectral index that uses the green and near-infrared channel of a multispectral imagery to stress the presence of water content or level of moisture on the earth surface. It can be used as a stand-alone index in image analysis or an input feature in statistical pattern recognition programs (McFeeters, 1996).

Object-based Image Analysis (OBIA): An image processing technique that performs segmentation of the imagery before the required image analysis is conducted. The segmentation procedure aims to group spatially adjacent pixels in an image into individual objects according to their spectral, spatial, and textural characteristics, such that the following analysis of the image will be targeted at the individual image objects, rather than pixels as in the case with conventional pixel-based image analysis (Blaschke, 2010).

Occurrence matrix: An analytical approach aimed at deriving texture measures from a moving window with a predetermined size. Some of its deliverables include data range, mean, variance, and entropy, etc. It is a widely used method in the remote sensing community for incorporating textural information into the analysis (Anys et al., 1994).

Point Spread Function (PSF): A function that quantitatively characterizes the spatial distribution and weighting of the electromagnetic signal counted towards a single digital number (DN) in a certain type of remote sensing imagery. It provides complementary information about the accuracy of remote sensing measurements from a spatial point of view, in addition to spatial resolution (Cracknell, 1998).

Spatial stationarity: A scenario where a stationary relationship between geospatial variables holds true across the entire area of investigation. It is the premise of the employment of global indicators of spatial association (Anselin, 1995).

The extreme Getis image: An image feature optimized for maximum spectral separation in the context of change detection. Its formulation is similar to that of the maximum Getis image, yet the pixels representing positive and negative changes are "pushed" towards the opposite ends of the distribution, instead of in the same direction as in the case of the maximum Getis image.

The Getis image stack: A group of Getis images calculated on the basis of varying window sizes. The statistics of the multiple Getis images included in the Getis image stack, such as the maximum magnitude, may contribute to the extraction of certain objects or phenomena of interest from remote sensing imagery.

The Getis statistic: It refers to a particular type of LISA, which presents local clusters of spatial dependence to its user. In the context of remote sensing applications, the implementation that is commonly used is the standardized version of the Getis statistic, such that a high Getis value represents a cluster of pixels with high values, whereas a low Getis value represents a cluster of pixels with low values. Medium-range Getis values may result from a cluster of pixels with medium values or a group of scattered pixels whose mean is in the medium range (Getis & Ord, 1992).

The maximum Getis image: The image feature formed by extracting the maximum Getis values across the Getis image stack. It emphasizes the maximum level of local spatial autocorrelation, and is associated with the maximum Getis distance (LeDrew, Holden, Wulder, Derksen, & Newman, 2004).